Photocurrent Enhancement in InGaP/GaAs Thin-film Multi-junction Solar Cells by Light Trapping using Colloidal Lithography

（コロイダルリソグラフィを利用した光閉じ込めによる InGaP/GaAs 薄膜多接合太陽電池の光電流増大）

QUAN Shengjiang
ケン　ショウコウ

37-186991

Supervisor: Prof. Sugiyama Masakazu
Department of Electrical Engineering and Information Systems
Graduate School of Engineering, The University of Tokyo

Master Thesis

September, 2020

Acknowledgment

I wish to express my deepest gratitude to who supported me during my master period.

I would like to pay my special regards to Prof. Yoshiaki NAKANO and Prof. Masakazu SUGIYAMA for giving me the opportunity to study in our laboratory at The University of Tokyo. I wish to express my deepest gratitude to Prof. Masakazu SUGIYAMA who taught me how to complete a scientific research project including not only experimental design and data analysis but also how to present my research accomplishments in academic conferences and seminars.

I am indebted to Dr. Kentarou WATANABE and Dr. Hassanet SODABANLU who never tires of instructing me and giving me suggestions and help once in need. Dr. Kentarou WATANABE takes months teaching me in person the fabrication processes of solar cell devices. Each day, Dr. Kentarou WATANABE works day and night for the development of our laboratory. I admire his professional dedication from my heart.

And I would like to recognize the invaluable assistance that my parents provided during my study. Studying overseas, I am not able to fulfill obligations as a family member. But they are always on my side, giving me support in my daily life and encourage me for greater achievements.

Finally, thanks to my friends WANG Yuhang from Beijing Jiaotong University, Li Pengxu&LIU Tengyu from Chinese Academy of Sciences and ZHENG Jiapeng from Technical University of Munich. You help me a lot when I am in trouble, facing the problems with me and giving me the precious encourages. Wish you all have a bright future.

I wish to thank all the people whose assistance was a milestone in the completion of this project.

QUAN Shengjiang

Abstract

The application of light trapping in III-V solar cells is considered unnecessary for its intrinsically high absorption coefficient. But the high cost of III-V materials is definitely a huge barrier preventing it from large scale commercial use. To compress the total thickness of III-V solar cells while maintain its performance at a still relatively high level for better cost-effectiveness, in this project, an InGaP/GaAs thin-film multi-junction solar cell whose photocurrent is enhanced by colloidal lithography is designed, fabricated and tested. The thicknesses of InGaP and GaAs PV active layers under current matching are firstly calculated through a mathematical model, the performance of the colloidal lithography based texture is initially tested by ray optics simulation and finite element simulation under electromagnetic field and its practical performance is measured in subsequent experiment.

Contents

1 Introduction **1**

1 Solar energy 2

1.1 Solar radiation and photon energy 2

1.2 Current status of solar photovoltaic 3

2 Basic principle of solar cell 4

2.1 Photon absorption 4

2.2 Recombination 4

3 III-V semiconductor and multijunction solar cell 6

3.1 Absorption coefficient 6

3.2 Indirect and direct band gap 6

3.3 Photon recycling 7

3.4 Lattice match and multijunction solar cell 9

3.5 Inverted lattice match growth 10

4 Light trapping 11

5 Colloidal lithography 12

6 Inductively coupled plasma reactive-ion etching ICP-RIE 13

7 Previous work 14

8 Research objective and outline 15

2 Thickness calculation of two sub-cells in InGaP/GaAs solar cell **16**

1 Light absorption model 16

2 Simulation and result 19

3 Texture fabrication by colloidal lithography **26**

1 Colloidal mask 26

1.1 Sedimentation 28

1.2 Vertical aggregation 28

1.3 Spin coating 30

2 Surface hydrophilic treatment 31

2.1 Surface treatment by water 32

2.2 Surface treatment by ethanol 34

2.3 Surface treatment by hydrogen peroxide 35

3 ICP-RIE 36

4 Optical performance simulation **38**

1 Ray optics simulation 38

2 Electromagnetic wave simulation 42

2.1 Methodology 43

2.2 Gaussian distribution 44

2.3 Simulation model 44

2.4 Simulation result 44

5 Fabrication of the InGaP/GaAs multi-junction solar cell **53**

1 Layer transfer 54

2 Reflectance measurement 55

3 Output characteristic 56

6 Summary **57**

Reference **61**

Appendix I – Figures **62**

Appendix II – Source code **67**

List of Figures

1.1 Estimated Renewable Energy Share of Global Electricity Production, End-2018 1

1.2 Solar spectrum from wavelength of 250 nm to 2500 nm 2

1.3 Solar PV Global Capacity and Annual Additions, 2008-2018 3

1.4 A typical band diagram of a solar cell 5

1.5 Three Types of Recombination 5

1.6 Absorption coefficient of several materials 6

1.7 Energy vs. crystal momentum for a semiconductor with an indirect and direct band gap 7

1.8 Schematic of radiative recombination and reabsorption process 8

1.9 Bandgaps and lattice constants for typical semiconductors and their alloys . 9

1.10 Structure and spectral irradiance of a multijunction solar 10

1.11 Inverted lattice match growth 11

1.12 A diagram of how light trapping works 12

1.13 Fabrication process of rear side texture using colloidal lithography. 12

1.14 A typical ICP-RIE system 13

2.1 Schematic cross sections of N-junction solar cells with textured and flat rear surface 18

2.2 Absorptivity Simulation result of InGaP/GaAs solar cells with rear texture, mirror and substrate 20

2.3 J_{sc} for substrate, flat and textured rear surface at current matching 21

2.4 J_{sc} of a subcell vs the thickness of another subcell in an InGaP/GaAs dual-junction solar cell 22

2.5 Short circuit current J_{sc} at current matching vs. length of top InGaP and bottom GaAs subcells in an InGaP/GaAs dual-junction solar cell 23

2.6 Requisite L_1 and L_2 under current matching 24

2.7 Absorptivity simulation result of InGaP/GaAs dual-junction solar cells with rear texture (solid), mirror (dots) and substrate (dashed) at current-matching subcell thickness combination 25

3.1 Schematic of etching probability and texture morphology after etching when a single layer colloidal mask is coated on sample surface 27

3.2 Dumbbells crystallize in confinement 29

3.3 Schematic of etching probability and texture morphology after etching when a multi layer colloidal mask is coated on sample surface 30

3.4 Schematic illustration of possible phenomena that occurred during three-step spin-coating method of SiO_2 particles 32

3.5 Schematic representation of the silica gel surface. 32

3.6 Surface treatment in water for 24 hours 33

3.7 Surface treatment in 99.5% ethanol for 3, 6 and 24 hours 34

3.8 Surface treatment in 30% hydrogen peroxide for 3, 6, 12 and 24 hours . . . 35

3.9 SEM picture of texture structure with SiO_2 particles 36

3.10 An aerial view of texture structure after removing SiO_2 colloidal mask . . . 37

3.11 A cross section view of the boundary between the area covered and not covered by SiO_2 colloidal mask 37

4.1 3D model extracted from SEM image 39

4.2 Two parallel incident lights are reflected by the inner surface of texture unit 40

4.3 3D model of flat cell and texture cell 41

4.4 Initial status of (a) flat and (b) texture cells under grating light source 42

4.5 Initial status of (a) flat and (b) texture cells under natural light source 42

4.6 Measurement of escaped lights 43

4.7 An electromagnetic field satisfying Gaussian distribution with amplitude of 360 V/m is applied on the testee. 45

4.8 A flat and four texture cells with 15, 25, 35 and 17 random texture units . . 46

4.9 Distribution of Electromagnetic field module with wavelength 400nm . . . 48

4.10 Distribution of Electromagnetic field module with wavelength 700nm . . . 49

4.11 Distribution of Electromagnetic field module with wavelength 1000nm . . . 50

4.12 A line segment is drawn to calculate the flux of upward component of electromagnetic field 50

4.13 Electric field module (V/m) of the electromagnetic wave that has been reflected back by the top and rear surface of solar cells from 100 nm to 1000 nm wavelength 51

4.14 Three components contribute to the interference 51

4.15 Peaks distribution from 100 to 1000 nm 52

5.1 Layer structure of the inverted lattice match InGaP/GaAs two junction solar cell sample grown by MOVPE 53

5.2 Cross-sectional structure of the InGaP/GaAs two junction cell 54

5.3 The reflectance of cells together with that in the electromagnetic simulation 55

5.4 I−V characteristics under AM 1.5G illumination for a flat cell (black) and several texture cells treated by hydrogen peroxide for 3 (red) , 6 (blue) , 12 (purple) and 24 (green) hours. 56

App.1 The side view of a single texture units 62

App.2 The side and bottom view of texture cell 63

App.3 3D plot of flat and texture cells under grating light source 64

App.4 3D plot of flat and texture cells under natural light source 65

App.5 Layers of solar cell in interference simulation 66

List of Tables

2.1 Requisite L_2 and total thickness at current matching of fixed L_1 24

4.1 Table of light escape under grating light source in flat and texture solar cells. 39

4.2 Table of light escape under natural light source in flat and texture solar cells. 41

4.3 Reflectance R_s on the interface between air and GaAs contact layer under wavelength of 400, 700 and 1000 nm. 45

4.4 Reflectance R_s on the interface between GaAs contact layer and InGaP top cell under wavelength of 400, 700 and 1000 nm. 47

Chapter 1

Introduction

1.5 billion kilometers away from the earth, nuclear fusion is on going and releasing plenty of energy from the sun in the form of solar radiation. At the point of earth, such solar radiation, acting as lifeline for all creatures on our planet so as to human civilization, is received by intensity of $1361W/m^2$, which is indicated from satellite observation [1].

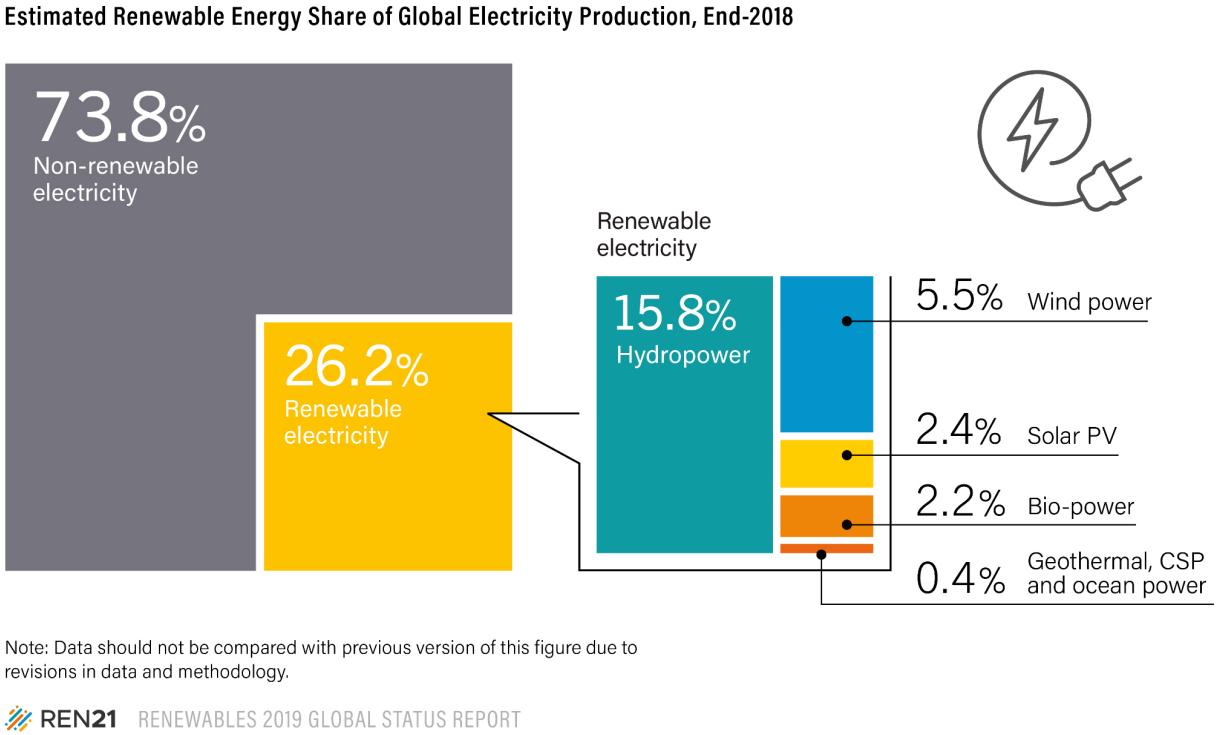

Figure 1.1: Estimated Renewable Energy Share of Global Electricity Production, End-2018 [2].

Figure 1.1 illustrates the share of global electricity production until the end of 2018. Almost three quarters of electricity comes from non-renewable energy, fossil fuel mostly. Among a quarter of renewable electricity share, solar PV occupies only 10 percent. The market data reflects those problems in the research of solar PV – intrinsic instability due to rotation of the earth, pervasive low-efficiency and thereupon its cost effectiveness.

1 Solar energy

1.1 Solar radiation and photon energy

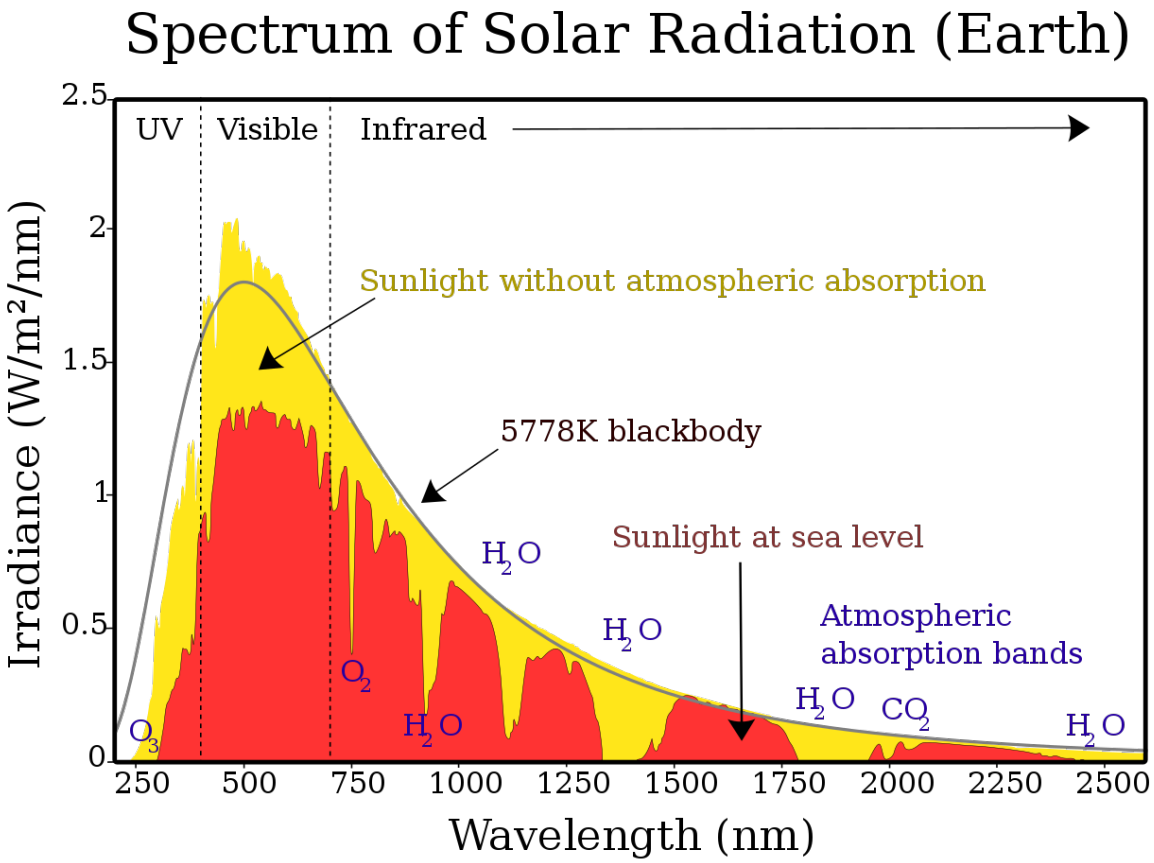

Figure 1.2: Solar spectrum from wavelength of 250 nm to 2500 nm [3]. The spectrum at sea level, in space and that of blackbody is denoted by red, yellow area and black line, respectively. The absorptive effect of components in atmosphere like O3, O2, H2O and CO2 gives rise to the difference between sunlight spectrum in space (yellow area) and at sea level (red area).

The solar radiation is described in the form of spectrum as shown in Figure 1.2. Extreme UV and X-rays, at the left side of the figure, compose only a small part of total output power from the sun. The spectrum of solar radiation in space is similar with that of a black body at temperature of 5778K. The difference between solar spectrum in space and at the sea level comes from the absorption of matters in atmosphere for instance O_2, CO_2 and H_2O.

The energy of sun light is carried by photons, which is given by

$$E = \frac{hc}{\lambda}, \tag{1.1}$$

where h is Planck constant, c denotes for the speed of light and λ is the wavelength of photon.

For convenience, Equation (1.1) is generally written as

$$E(eV) = \frac{1240}{\lambda(nm)}. \tag{1.2}$$

1.2 Current status of solar photovoltaic

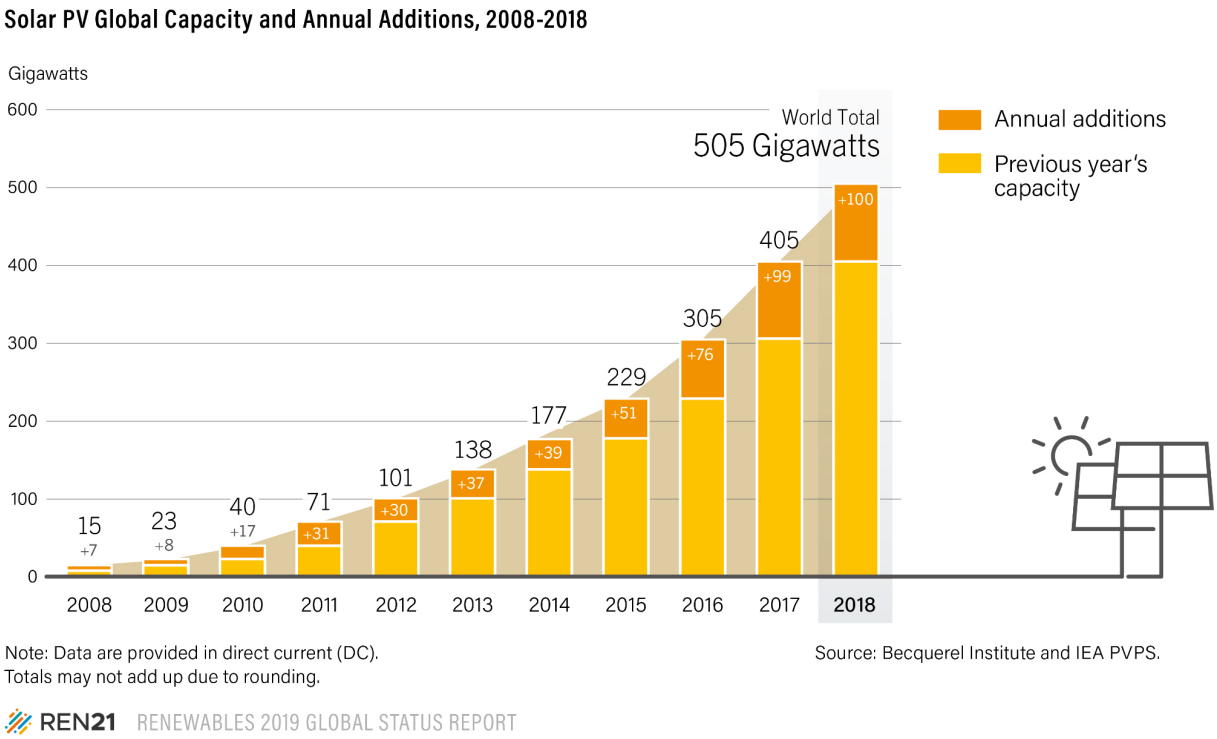

Figure 1.3: Solar PV Global Capacity and Annual Additions, 2008-2018 [2]. The PV capacity of each year is consist of two parts – previous year's capacity (yellow part) pluses annual additions (orange part).

In the year of 2018, cumulative capacity increased approximately 25% to at least 505 gigawatts compare to that of the year 2017. And this is also for the first time annual addition reaches 100 gigawatts. With the development of researches in photovoltaic field in the past decade, the solar PV global capacity increases from 15 gigawatts 2008 to 505 gigawatts 2018 Figure 1.3, increasing by 42% per year on average.

Regardless of the single-digit development pace of the worldwide market in 2018, sunlight based PV has become the world's quickest developing vitality innovation, with gigawatt-scale showcases in an expanding number of nations [4]. Interest for sun oriented PV is spreading and extending as it turns into the most serious alternative for power age in a developing number of business sectors –for private and business applications and progressively for utility activities – even without representing the outside expenses of petroleum derivatives [5].

2 Basic principle of solar cell

By photovoltaic effect, a solar cell convert the energy of light directly into electricity. Such conversion process including the following steps:

1. Absorb incident light, generating electron-hole pairs;
2. Light generated electrons and holes diffuse to opposite direction;
3. Extract those carriers to external load.

2.1 Photon absorption

Defined as band gap, it refers to the region from top of valence band and bottom of conduction band, where no electronic states can exist. An electron is only allowed to exist within valence or conduction band, or move directly from one of those band to the other.

When a photon with enough energy incidents into a solar cell, an electron in valence band would be excited to conduction band, generating an electron-hole pair. Once excited an electron can either dissipate the energy as heat and return to its orbital or travel through the cell until it reaches an electrode. Current flows through the material to cancel the potential and this electricity is captured Figure 1.4.

2.2 Recombination

Generally, recombination process is classified by the region where such recombination occurs in solar cell devices. Two main areas of recombination lies in the surface area and bulk area which are corresponding to surface and bulk recombination.

Divided by mechanism of recombination, three major recombination process is on going within solar cell devices – radiative recombination, Auger recombination and SRH(Shockley-Read-Hall) recombination. In radiative recombination, which dominates in direct bandgap semiconductors, an electron from the conduction band directly combines with a hole in the valence band and releases a photon; and the emitted photon has an energy similar to the band gap and is therefore only weakly absorbed such that it can exit the piece of semiconductor. Auger Recombination involves three carriers. An electron and a hole recombine, but rather than emitting the energy as heat or as a photon, the energy is given to a third carrier, an electron in the conduction band. This electron then thermalizes back down to the conduction band edge [7]. SRH recombination is a two-step process: An electron (or hole) is trapped by an energy state in the forbidden region which is introduced through defects in the crystal lattice. These defects can either be unintentionally introduced or deliberately added to the material, for example in doping the material; and if a hole (or an electron) moves up to the same energy state before the electron is thermally re-emitted into the conduction band, then it recombines [8, 9].

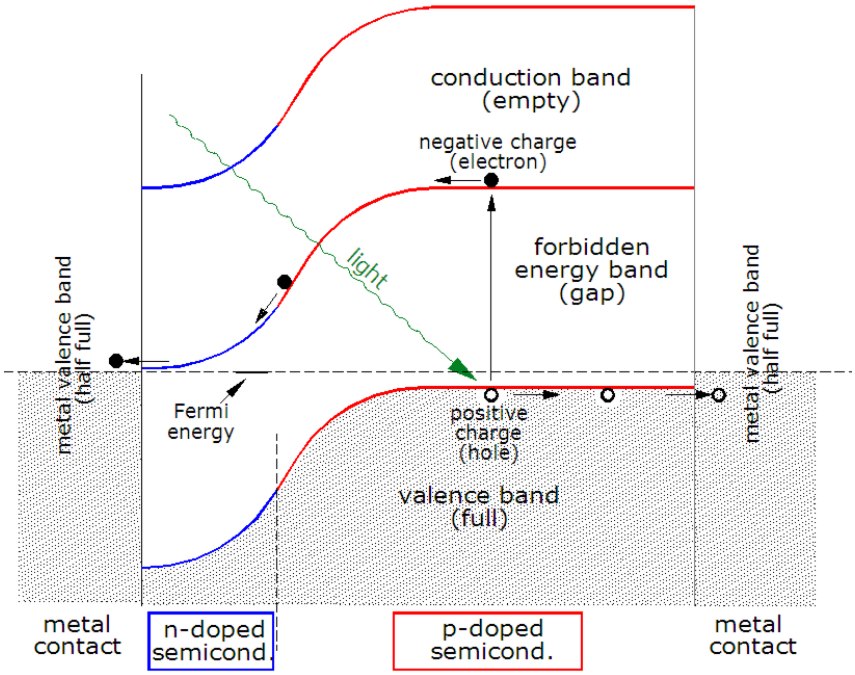

Figure 1.4: A typical band diagram of a solar cell [6]. From left to right side, this diagram is divided into four parts – metal contact, n-doped semiconductor, p-doped semiconductor and another metal contact. The valence band, at the top of which an incident light marked in green generates a electron-hole pair, is filled by shade. Solid and hollow circle denote for electron and hole, respectively. Their diffuse movement direction is illustrated by the black arrow.

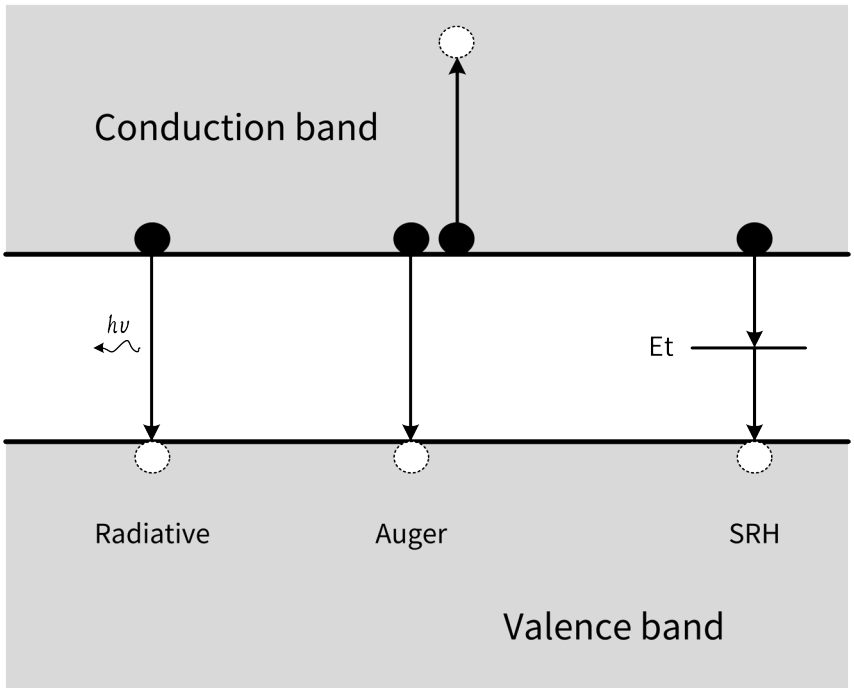

Figure 1.5: Three Types of Recombination. From left to right are radiative recombination, auger recombination and SRH recombination, respectively. Valence and conduction band are filled with shade, between which is the band gap. Black and white circle respectively represent for electron and hole. There are a recombination generated photon denotes by hv and an extra energy state denotes by Et.

3 III-V semiconductor and multijunction solar cell

3.1 Absorption coefficient

Defined as the absorption of light per unit length in a medium, absorption coefficient determines how far into a material light of a particular wavelength can penetrate before it is absorbed. The incident light is barely absorbed in a too-thin medium with low absorption coefficient. Absorption coefficient depends on not only the material itself but also the wavelength of incident light since the incident photon with energy lower than medium band gap can never excite an electron from valence band into conduction band. This is also the reason why each absorption coefficient has a discontinuous point as shown in Figure 1.6.

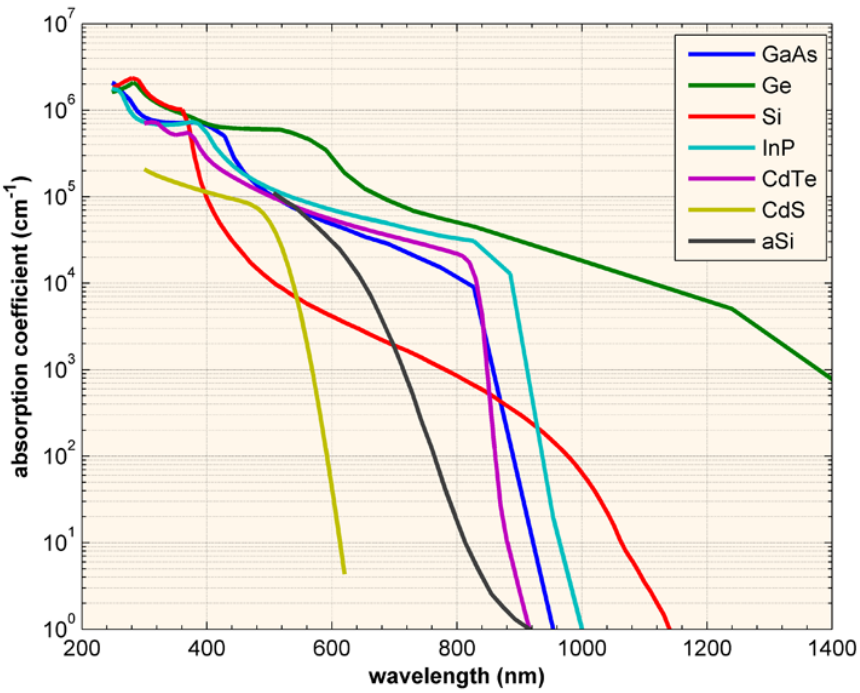

Figure 1.6: Absorption coefficient of several materials.

3.2 Indirect and direct band gap

A semiconductor which has a vertically aligned conduction and valence band is called direct band gap semiconductor. A photon would be absorbed if an empty state in the conduction band is available for which the energy and momentum of the incident photon equals that of an electron in the valence band minus that in the conduction band. Photons have little momentum relative of their energy since they travel at the speed of light. The electron therefore makes an almost vertical transition on the E-k diagram Figure 1.7(b). While for an indirect band gap semiconductor Figure 1.7(a), the conduction band is not vertically aligned to the valence band unless a phonon gives its fatal help. [10]

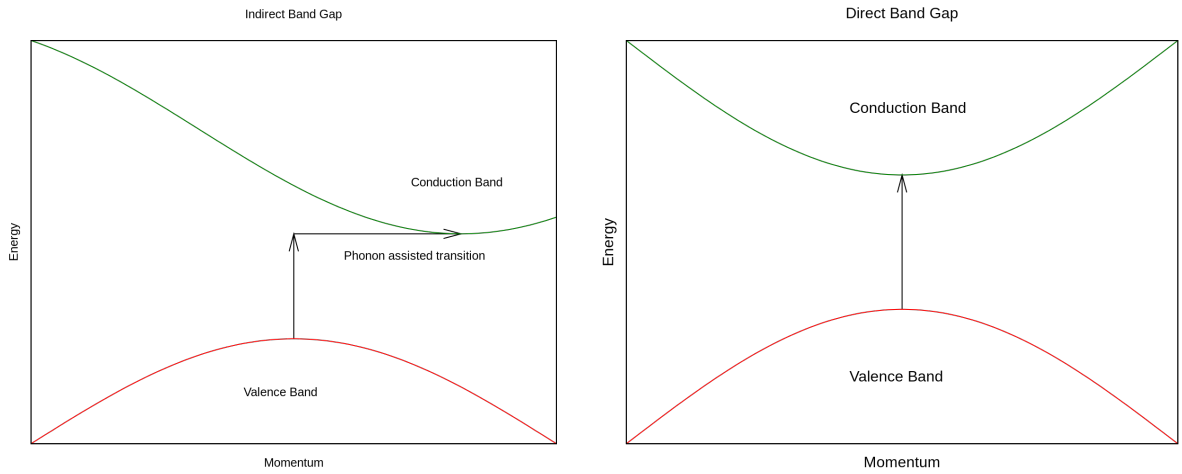

(a) Indirect band gap (b) Direct band gap

Figure 1.7: Energy vs. crystal momentum for a semiconductor with an indirect (a) and direct (b) band gap [11]. An electron cannot shift from the highest-energy state in the valence band (red) to the lowest-energy state in the conduction band (green) without a change in momentum [11]. Here, almost all of the energy comes from a photon (vertical arrow), while almost all of the momentum comes from a phonon (horizontal arrow) [11].

Therefore a simply interaction of an incident photon with an electron in the valence band will not provide the correct energy and momentum corresponding to that of an empty state in the conduction band. As a result absorption of light requires the help of another particle, namely a photon. Since , i.e a particle associated with lattice vibrations, has a relatively low velocity close to the speed of sound in the material, it has a small energy and large momentum compared to that of a photon. Conservation of both energy and momentum can therefore be obtained in the absorption process if a phonon is created or an existing phonon participates. [10]

3.3 Photon recycling

Radiative recombination, where an electron from the conduction band and a hole from valence band annihilate emitting a photon whose energy is likely to be equal with band gap, can be negligible in indirect band gap semiconductor materials like Silicon but can never be forgotten in direct band gap materials, for instance III–V materials.

Reabsorption of radiative recombination generated photon can significantly diminish the effectiveness from radiative recombination in such III–V direct band gap materials. This phenomenon is referred to as ”photon recycling” Figure 1.8. [12] This is not possible in an indirect band gap semiconductor, as photons whose energy is just equal to band gap cannot carry crystal momentum.

Photon recycling directly confine radiation recombination loss and further enhanced a longer minority-carrier lifetime. The effect of recombination can be discussed in terms of minority-carrier lifetime due to the excitation independent of majority-carrier concentration. [13] For instance, in p-type material, the recombination rate could be written as

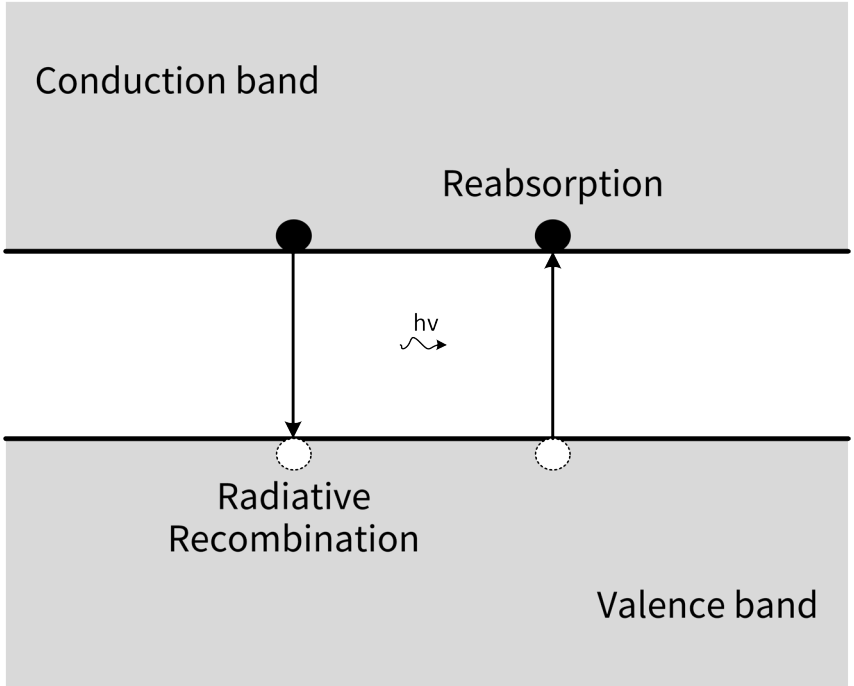

Figure 1.8: Schematic of radiative recombination and reabsorption process. The energy of photon is formulated by $h\nu$. An electron in conduction band recombines directly with a hole in valence band, generating a photon with energy hv. Later this recombination generated photon could be reabsorbed by an electron somewhere in the valence band, exciting this electron from valence band to conduction band and leaving a hole in the valence band.

$$U = \frac{1}{\tau_n}(n - n_0) \tag{1.3}$$

where n is minority-carrier density which mean electrons in this p-type material, n_0 is the intrinsic carrier density of electrons and τ_n is the minority-carrier (electron) lifetime which should be written as τ_p in n-type materials. The inverse of the lifetime—the rate constant—is a sum of the different contributions to the lifetime:

$$\frac{1}{\tau} = \frac{1}{\tau_{rad}} + \frac{1}{\tau_{Auger}} + \frac{1}{\tau_{SRH}} \tag{1.4}$$

where τ_{rad}, τ_{Auger} and τ_{SRH} denote for lifetime under radiative, Auger and SRH recombination. τ stands for τ_n or τ_p as appropriate. The reabsorption process effectively offsets the negative effects causing by radiative recombination in direct band gap III–V materials, for which the equivalent radiative recombination rate is suppressed. Equations (1.3) and (1.4) gives the consequence that a lower recombination rate leads to a longer minority-carrier lifetime, which further produce a substantial enhancement of open-circuit voltage.

3.4 Lattice match and multijunction solar cell

In a crystal lattice, the physical dimension of unit cells is called lattice constant, or lattice parameter. In three dimension space, each lattice has three lattice constants, referred as a, b and c generally. While in the case of cubic crystal structures, those three constants are equal and are referred to as a.

In semiconductor industry, lattice matching which means the matching of lattice structures between two divergent semiconductor materials enables changing of band gap in a continuous region without introducing a change in crystal structure. It is feasible to growth one semiconductor material on another which owns equal lattice constant, for instance, gallium arsenide, aluminium gallium arsenide, and aluminium arsenide which have almost equal lattice constants. In laboratory, MOVPE is one of the most frequently-used epitaxial method to fabricate solar cells. The characteristic of lattice match kick out the door of III–V multijunction solar cells Figure 1.9.

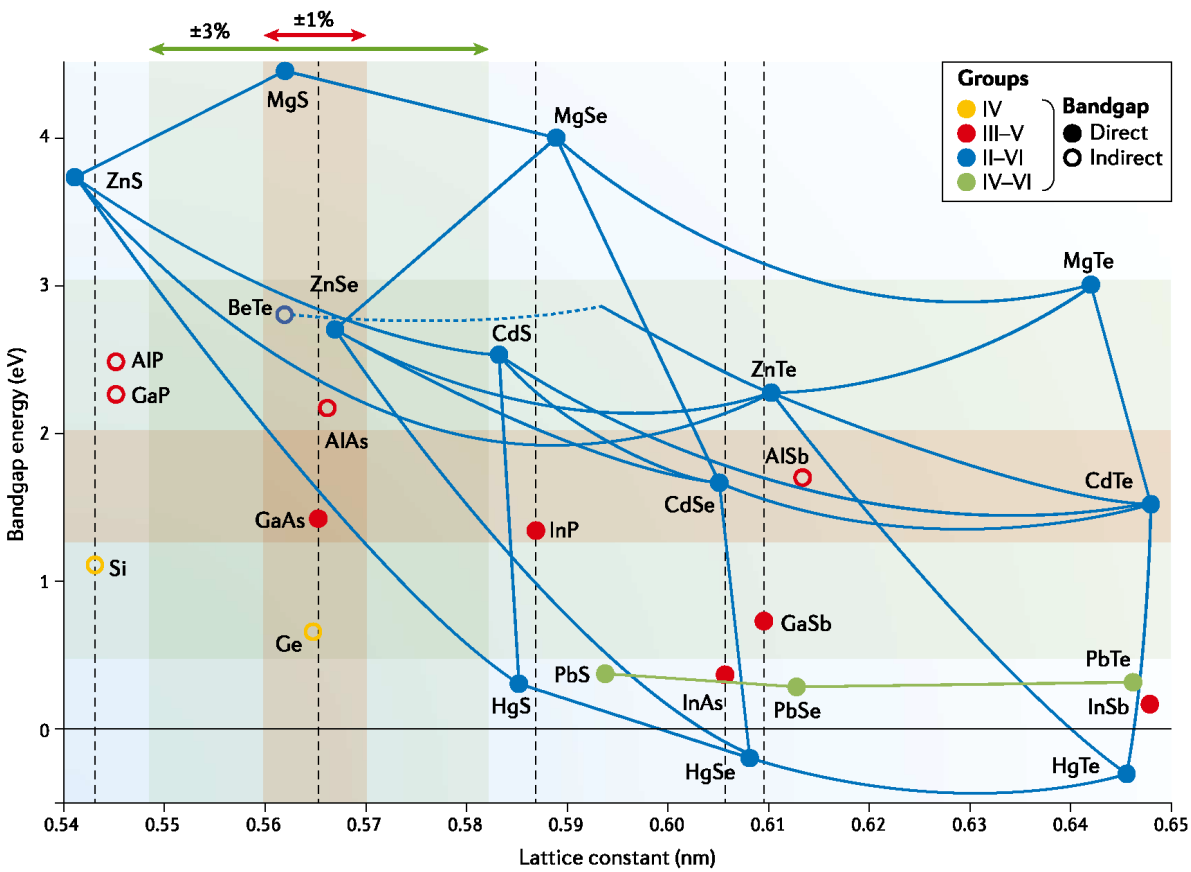

Figure 1.9: Bandgaps and lattice constants for typical semiconductors and their alloys. Filled and unfilled circles indicate, respectively, direct and indirect bandgap materials, and solid and dashed connecting lines indicate, respectively, direct and indirect alloys [14]. III–V alloys are marked in red. $In_0 \cdot 5\, Ga_0 \cdot 5\, P$, used in this project, is an alloy of InP/GaP and is supposed to locate on the dash line with band gap about 1.89 eV, lattice matching with GaAs.

In 1961, William Shockley and Hans-Joachim Queisser [15] proposed a theory (S-Q Limit) giving a maximum efficiency of 30% for a single p-n junction to collect power from the cell where the only loss mechanism is radiative recombination at optimum band gap 1.1 eV. For the aim of breaking the S-Q Limit, mission falls on multijunction solar cells. Figure 1.10 (a) shows a

typical structure of multijunction solar cells including three sub-cells – InGaP/InGaAs/Ge from the topmost sub-cell to the bottommost one, whose band gap should be a decreasing sequence – 1.86/1.40/0.65 eV – to enlarge its operation band gap as shown in Figure 1.10 (b). The tunnel junction between each subcells is of vital importance on the performance of the finished product. Tunnel junction is expected to act as non-rectifying ohmic contact between to adjacent subcells.

Between those sub-cells lies the tunnel junction (tunnel diode). For successful device operation, the TJ must form a low resistance path for carriers to travel between the p terminal of one subcell to the n terminal of an adjacent subcell. This low resistance path ensures a minimal voltage drop and hence a minimal impact on the overall solar cell efficiency. [16]

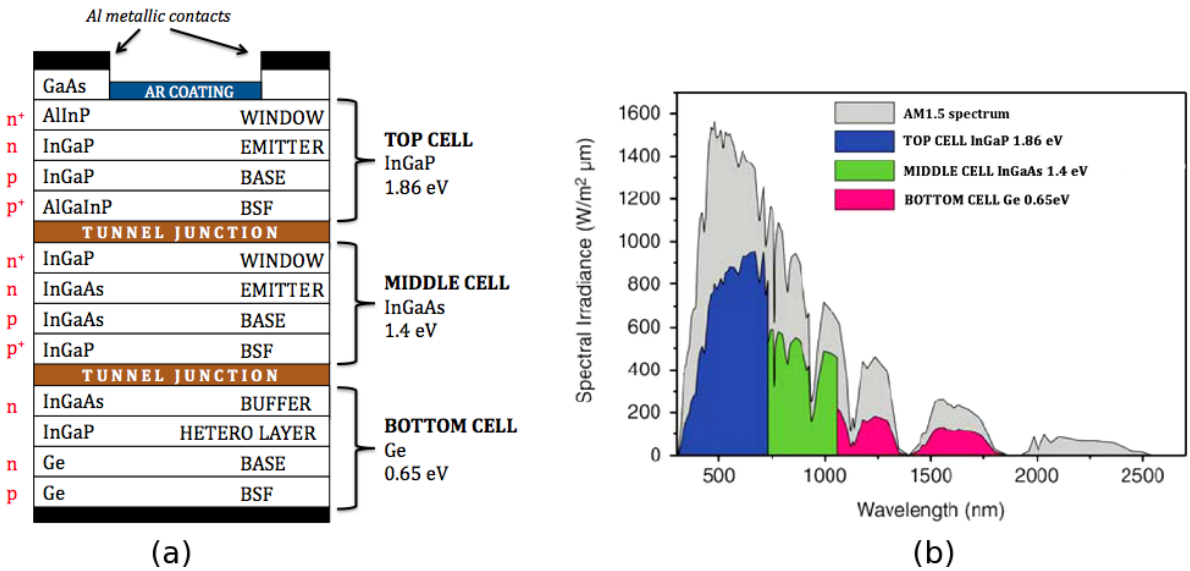

Figure 1.10: (a) The structure of an multijunction solar cell [17]. From up to down are metallic contacts as electrode, anti-reflection coating to prevent reflection, PV active layers and bottom contact. The PV active layer consist of three subcells – InGaP/InGaAs/Ge – and two tunnel junctions between them. (b) Graph of spectral irradiance E vs. wavelength λ over the AM1.5 solar spectrum [18]. The absorptive spectrum of top InGaP, middle InGaAs and bottom Ge subcells are marked in blue, green and red area, respectively, covering on the AM1.5 solar spectrum.

3.5 Inverted lattice match growth

For the convenience of operating on the rear surface to fabricate texture structure for light trapping, inverted lattice match growth is used to fabricate the designed multijunction solar cell. Figure 1.11 shows how an InGaP/GaAs two junction solar cell is grown inversely and transfer the active layer to a support layer. On a GaAs substrate, first an InGaP top cell and then a GaAs bottom cell are deposited by MOVPE (metalorganic vapour-phase epitaxy). Later after the operation on rear surface of this solar cell has finished, they are entirely transferred to a support layer (usually a silicon wafer), bonded tightly. This is called layer transfer. GaAs substrate is, after that, removed by for instance wet etching.

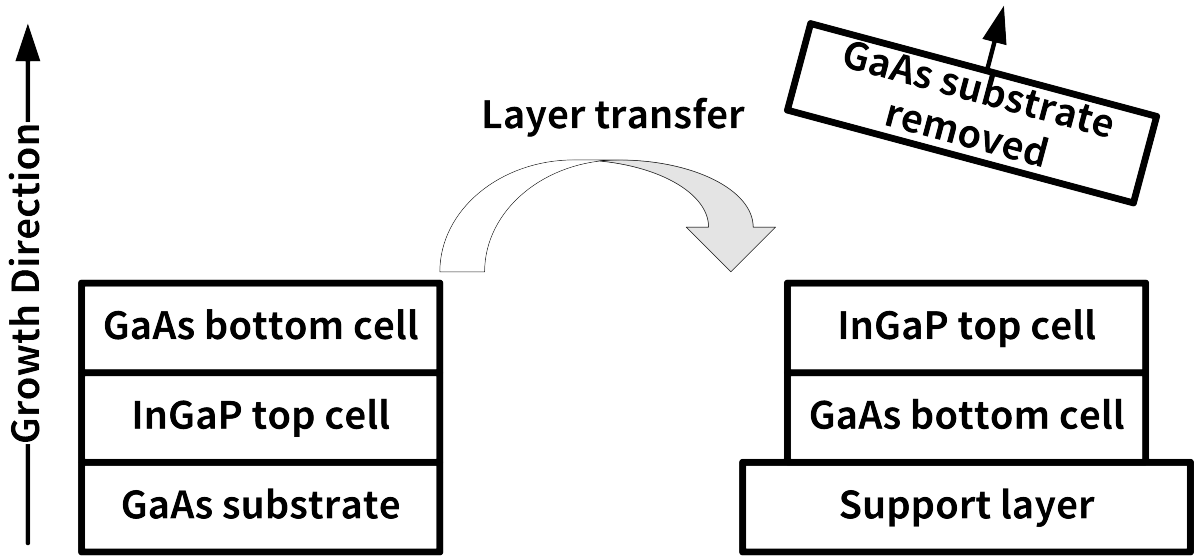

Figure 1.11: Inverted lattice match growth with its following layer transfer process. The epitaxial growth direction is upward as the direction of arrow on the left.

4 Light trapping

The fundamental goals of photon management are to reduce incident light reflection, improve absorption, and tailor the optical properties of a device for use in different types of energy conversion systems [19]. As a result, the short circuit current remains the same level with thicker conventional devices and on the other hand open circuit voltage is enhanced with the shrinking of device thickness, total cost of such devices is cut down due to the reduced material usage as well.For the aim of reducing recombination and optical losses, the concept of optical management or photon management has been proposed to enhance the power performance of solar cell devices. By doing so, the thickness of such devices would be compressed, while remaining the effective optical path length constantly.

To realize the above analyzed characteristics, researchers have experimented with approaches to capture the sunlight photon impinging on the device and forcing it to collaborate instead of being reflected away. This is done by changing the basic structure of solar cells, so that photons become trapped when they arrive in contact with the cell, thus providing a greater chance that they will be absorbed and converted into electrons. To this aim a light-trapping scheme introduction is mandatory [20].

Figure 1.12 illustrates the simple and basic principle of light trapping – refraction and reflection. The incident light perpendicularly reaches front surface of the solar cell, refracted initially by the textured front surface, divided into two sub-lights. They propagate in two different direction. They would be reflected back by the rear surface and for the second time reflected by the front surface. In this way, the incident light or photon is ”trapped” inside the cell, instead of escaping out of the cell from the bottom surface without being sufficiently absorbed.

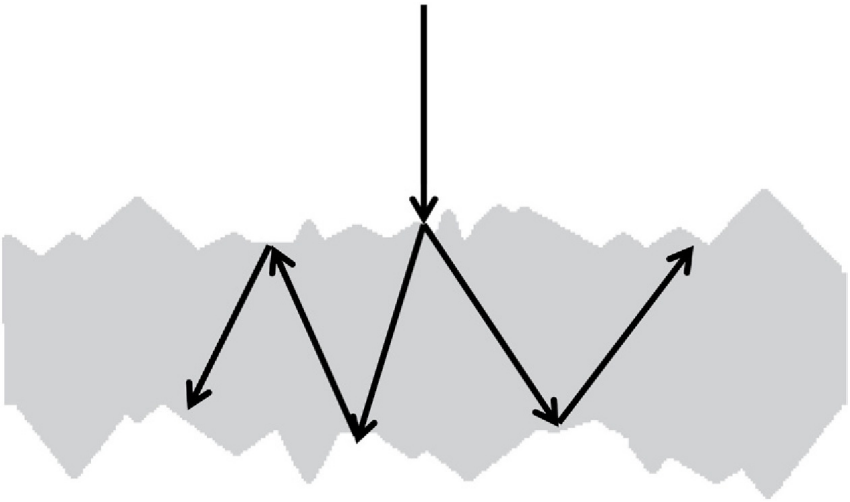

Figure 1.12: A diagram of how light trapping works. The grey area denotes for an arbitrary solar cell with uneven front and rear surfaces. And the white area is the outer space. A ray of light incident perpendicularly downward into the solar cell.

5 Colloidal lithography

A core part of this project is to fabricate a 3D texture structure on the rear side of the cell for light trapping, as described in Section 4. Colloidal lithography is a method that using colloid as mask to fabricate 3D nanostructure on a 2D surface. The main advantages of colloidal lithography are large area patterning, fast writing speed and low cost. The later two points are the most attractive characteristics in fabricating texture for light trapping in solar cells.

A typical fabrication process is illustrated in Figure 1.13. First, a layer of colloidal mask, 500 nm diameter silica here, is coated on the rear surface of the cell by spin coating to form a single layer mask. Second, use ICP-RIE to bombard rear surface. Under the action of electric field, reactants move straight down. Those reactants who, by coincidence, between two silica particles has the opportunity passing through the mask layer, reacting with GaAs contact layer directly and forming a groove texture.

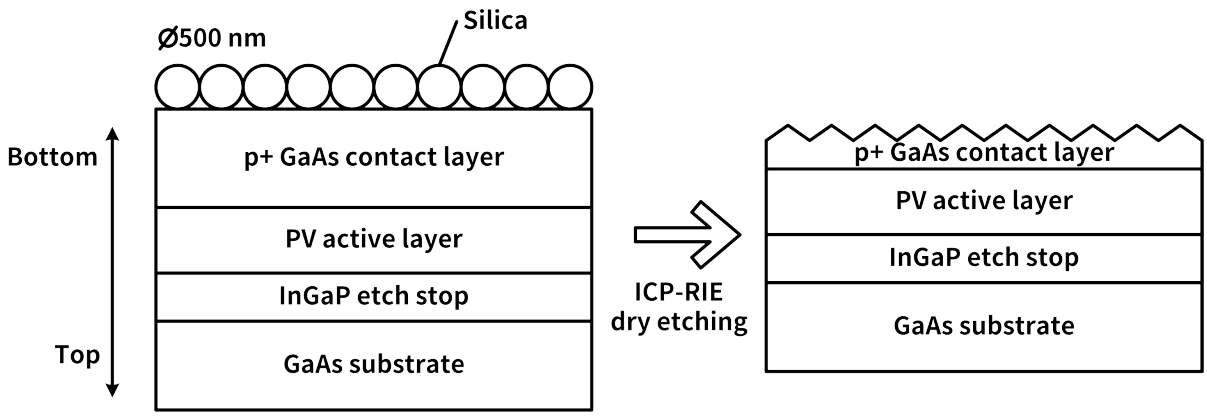

Figure 1.13: Fabrication process of rear side texture using colloidal lithography.

6 Inductively coupled plasma reactive-ion etching ICP-RIE

ICP-RIE etching is based on the use of an inductively coupled plasma source. The ICP source generates a high-density plasma due to inductive coupling between the RF antenna and the plasma. The antenna, located in the plasma generation region, creates an alternating RF magnetic field and induces RF electric fields, which energize electrons that participate in the ionization of gas molecules and atoms at low pressure. Due to the absence of an electric field near the reactor walls there is virtually no ion bombardment or erosion of the walls. [21]

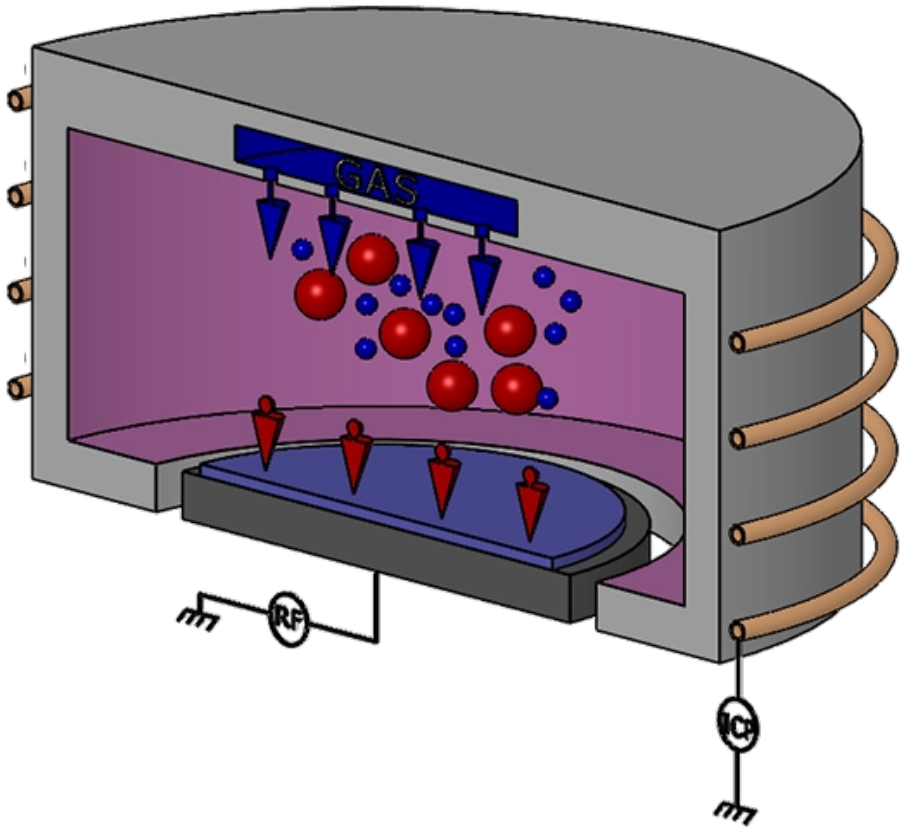

Figure 1.14: A typical ICP-RIE system [21]. A sample (purple) is placed at the center of support plate (black). The source gas (dark blue) carries high-energy ions (red), entering the chamber from the top entrance (dark blue arrow). Driven by the electric field, plasma ions move downward, reacting with the sample from its top surface (red arrow).

The key differentiation between ICP RIE and RIE is the separate ICP RF power source connected to the cathode that generates DC bias and attracts ions to the wafer. Thus, with ICP RIE technology it is possible to decouple ion current and ion energy applied to the wafer, enlarging the process window. Materials are etched with the use of a chemically reactive plasma under low pressure conditions, potentially combined with ion-induced etching. [21]

ICP-RIE can be used for rapid etching of a wide range of materials, including semiconductors, dielectrics, metals, and polymers. The available processes span from low damage ICP etch processes to the etching of hard materials. Process chemistries differ depending on the types of films to be etched. Those used in dielectric etch applications are typically fluorine-based.

Metal etch uses chlorine-based chemistries. Etch conditions can be adjusted and optimized by tuning the settings of many process parameters such as RF power, pressure, and gas flows. [21] Its etching depth is mainly controlled by its bias power (the magnitude of electric field) and reaction time.

7 Previous work

For the past decades, III-V solar cell has dominated among high efficiency solar cells [22] for their unique characteristic of large direct band gap and the ability of forming multi-junction solar cells [23]. The major problem preventing III-V solar cells from quantity production is the high cost of III-V materials. For the aim of cutting down total cost of III-V solar cells there are two ways mainly: one is to develop a cost-effective epitaxial growth method [24] and the other is to compress cell thickness to reduce material expenses. Light trapping, compressing cell thicknesses by increasing equivalent optical path length, helps on the later point [25]. It functions for the texture structure on the front or rear or both side of solar cell [26], stimulating scattering and as a result reducing reflection.

A. Gaucher et al. [27] reported an ultra-thin Si solar cell whose equivalent thickness is only $2.75\ \mu m$ with short-circuit current density of $25.3\ mA/cm^2$. N. Gupta and V. Janyani [28] proposed their light trapping enhanced GaAs thin film solar cell with 50 nm active layer thickness using 2-D Photonic Crystal Structures at Front Surface. In [29], the conversion efficiency measured under one-sun air mass 1.5 global illumination at room temperature can also be improved from 13.8% to 15.9%. Light trapping has been used for single junction III-V solar cells for years, but its application in multi-junction III-V solar cells is still blank.

Lin Zhu, Anurag Reddy and etc. [30] have proposed a model on InGaP/GaAs/InGaAs 3-junction solar cell to evaluate subcell photocurrents and the requisite thicknesses at current matching. This model gives an essential reference on how thin the III–V layer thicknesses in multijunction solar cells can be without a substantial sacrifice in the efficiency. This model assume an N junction solar cell, in which the energy-dependent absorption spectrum of each subcell is calculated based on the band gap theory. The short circuit current J is given as an integration of the absorption spectrum and solar spectrum. The final output current is constrained by the minimum value of each layer's short circuit current density due to the principle of current matching. Based on the result of short circuit current, the minimum thickness of each subcell can be estimated. And that is the cost-effective combination of those subcells. Explanation of this model is given in detail in Chapter 2, together with its application in this project.

So far, the III–V multijunction solar cells are thick enough to absorb incident light which performs quite well on refreshing efficiency ranking but awful on saving cost. To cut down unnecessary thickness of III–V multijunction solar cells and further reduce the cost, find the minimum necessary thickness of a III–V multijunction solar cell is the mission of this project. Combining with the research of Lin Zhu, Anurag Reddy and etc. [30], the feasibility and superiority of fabricate III–V multijunction solar cells in their minimum necessary thickness are demonstrated and proved.

8 Research objective and outline

In this study, an InGaP/GaAs two-junction solar cell enhanced by rear texture using colloidal lithography is proposed, fabricated and tested. In the left parts of this paper, the model of optimizing thickness is first introduced in Chapter 2, following by the fabrication of rear side texture based on colloidal lithography in Chapter 3. Optics ray and electromagnetic field simulations are build to test the performance of colloidal lithography based texture morphology Chapter 4. Finally, experimental results are demonstrated in Chapter 5.

Chapter 2

Thickness calculation of two sub-cells in InGaP/GaAs solar cell

1 Light absorption model

For a long time, there is one barrier on the way of industrialization of III–V based solar cells' cost-effectiveness. Two methods have already been proved to be feasible in the reduction of III–V solar cells' cost:

1. reduce the cost of source material during epitaxial growth by compressing every layer in a III–V solar cell;
2. develop a low-cost method of III–V crystal growth. Epitaxial lift-off (ELO) is one of this kind of methods.

Giving an algorithm of calculating the minimum thicknesses of each layer in a III–V solar cell while maintaining its output performance, this model focuses on the first point.

A schematic of N-junction solar cell with textured and flat rear surface is shown in Figure 2.1 (a) and (b) respectively. In Figure 2.1 (a), a perpendicular incident light goes through scattering and reflection by the bottom and top surface respectively with exit angle θ. Second scattering occurs on the rear surface of the cell with exit angle φ. For the third time, its exit angle turns to be ω on the rear surface, for which the optical path direction has been changed, avoiding the incident light escape out of the cell from top surface. By contrast in Figure 2.1 (b), the incident light with acute angle θ is reflected by both top and bottom surfaces for several times. Each time reflected, partial of the light escape out of the cell for its acute incident angle by refraction, which is definitely energy loss that reduces overall output performance.

Such textured rear surface is assumed as a perfect diffuse reflector (Lambertian scattering [31]) without outward transmission. An arbitrary subcell in Figure 2.1 is marked as subcell $i \in [1, N] \subset Z+$. E_{gi} stands for the band gap of material in subcell i and L_i denotes for the thickness of subcell i. T_i is defined as

$$T_i(\theta) = e^{-\frac{\alpha_i L_i}{\cos\theta}}, \tag{2.1}$$

is the light transitivity passing through subcell i with incident angle θ, where α_i is the absorption coefficient of subcell i. Here, the energy dependent absorption spectrum of arbitrary subcell i in N-junction solar cells is defined as $a_i(E)$,

$$a_i(E) = \begin{cases} a_{i1}, & & E & \geq E_{g1} \\ a_{i2}, & E_{g1} & >E & \geq E_{g2} \\ & \vdots & & \\ a_{ij}, & E_{gj-1} & >E & \geq E_{gj} \\ & \vdots & & \\ a_{ii}, & E_{gi-1} & >E & \geq E_{gi} \\ 0, & E_{gi} & >E & \end{cases} \tag{2.2}$$

in which $i \geq j > 1$. The absorptivity depended on photon energy is marked as $a_{ij}(E)$ and the subscript ij means the absorptivity in subcell i with photon energy between E_{gj} and E_{gj-1}.

For the N-junction solar cells with flat rear surface Figure 2.1(b), its a_{ij} is given by

$$a_{ij} = \frac{[1 - R_f(\theta)] \prod_{x=j}^{i} T_x(\theta)^{\frac{1-T_i(\theta)}{T_i(\theta)}} \left[1 + \prod_{x=j}^{N} T_x^2(\theta)\right]^{\frac{R_b(\theta)}{T_i(\theta)}}}{1 - \prod_{x=j}^{N} T_x^2(\theta) R_f(\theta) R_b(\theta)}, \quad 1 \leq j \leq i \leq N \tag{2.3}$$

where R_f and R_b are front and back surface reflectance respectively. In the flat case of the calculation, photon reabsorption and emission processes are neglected in each subcell and the incident light almost perpendicularly incident upon the top surface of the solar cell, for which an arbitrary incident angle for the total multi-layer reflection path is considered to be constant and set θ as 0. Take the total reflection into consideration, R_f is a function with photon energy of incident angle θ Equation (2.4).

$$R_f(\theta) = \begin{cases} R(E) & \theta < \theta_c \\ 1 & \theta \geq \theta_c \end{cases} \tag{2.4}$$

As for R_b, assume that it is 1 for perfect rear mirror and 0 for a perfect absorption substrate. The difference between flat and textured rear surface lies in that diffuse reflection or so called scattering occurs on the rear surface when an incident photon reaches the bottom surface. Reabsorption and recombination process are neglected in this model. As for the textured surface Figure 2.1(a), R_b is normalized by

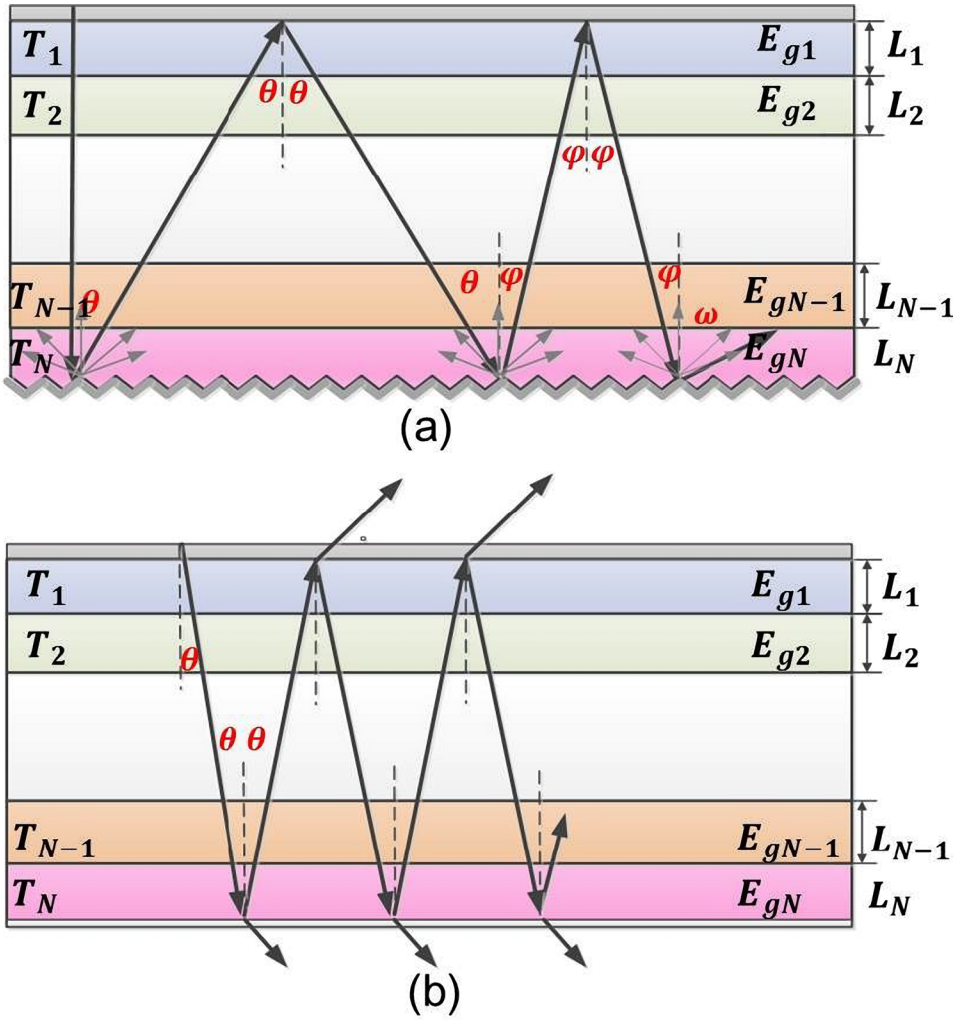

Figure 2.1: Schematic cross sections of N-junction solar cells (a) with textured rear reflector and (b) with flat rear surface [30]. E_g and L stands for the band gap and thickness of each subcell, respectively. T denotes for light transitivity. Each entry and exit angle is marked with θ, φ or ω.

$$R_b^{Tex} = \frac{\cos\theta}{\pi} \tag{2.5}$$

based on Lambert's emission law [32]. a_{ij} for multijunction solar cells with textured rear surface is formulated by

$$a_{ij} = [1 - R_f(0)] \frac{\prod_{x=j}^{i} T_x(0)}{T_i(0)} \left\{ 1 - T_i(0) + \prod_{x=i}^{N} T_x(0) \right.$$
$$\left. \times \frac{2\pi \int_0^{\frac{\pi}{2}} R_b^{Tex}(\theta) \prod_{x=i}^{N} T_x(\theta) \frac{1-T_i(\theta)}{T_i(\theta)} \left[1 + R_f(\theta) \frac{\prod_{x=j}^{i-1} T_x^2(\theta)}{T_i(\theta)} \right] \sin\theta d\theta}{1 - 2\pi \int_{\theta_c}^{\frac{\pi}{2}} R_b^{Tex}(\theta) R_f(\theta) \prod_{x=j}^{N} T_x^2(\theta) \sin\theta d\theta} \right\}, \quad 1 \le j \le i \le N \tag{2.6}$$

where $T_i(0)$ is the transitivity Equation (2.1) @ $\theta = 0$. With the simulated absorption spectrum $a_i(E)$, J_{sci} is given by

$$J_{sci} = q \int_0^{\infty} a_i(E) S(E) dE, \tag{2.7}$$

where i is arbitrary subcell i in N-junction solar cells, $S(E)$ denotes for solar spectrum and q stands for electron change [33]. In the following part, using the above analyzed model, in which $a_i(E)$ is defined by material parameters, reflectance $R(E)$ is measured from an anti-reflection coated practical solar cell. $a_i(E)$ and light generated photocurrents density of each subcell with thickness L_1 and L_2 respectively in InGaP/GaAs dual-junction solar cell is simulated. The band gap energy of InGaP and GaAs subcells are set as 1.89 eV and 1.41 eV, respectively.

2 Simulation and result

The test simulation is based on an InGaP (E_{g1}, 1.89 eV) /GaAs (E_{g2}, 1.44 eV) two junction solar cell with thickness L_1 and L_2. The result of simulated absorptivity has been shown in Figure 2.2 for three typical scale of two junction solar cells – (a) L_1=300 nm, L_2=110 nm, (b) L_1=500 nm, L_2=270 nm and (c) L_1=700 nm, L_2=630 nm, denoting for thin, medium and thick cell respectively. For the top InGaP subcell with larger band gap, the enhancement is quite obvious for thin and medium cells comparing with the thick cell in the energy range from 1.44 eV to 2.75 eV (Figure 2.2(a)) or 2.5 eV (Figures 2.2(b) and 2.2(c)), so as to that of bottom GaAs subcell. In the energy range larger than 2.75 eV (Figure 2.2(a)) or 2.5 eV (Figures 2.2(b) and 2.2(c)), the absorptivity change little for relatively larger absorption coefficient (Section 3.1). This indicates that it is the photons with relative low energy that benefit most from textured rear structure.

The results demonstrate that, comparing with rear mirror or absorptive substrate, rear texture significantly improves the bottom-subcell absorptivity and it also gives a positive influence on the top cell. For not only the top subcell but also bottom cell, the enhancement is conspicuous in thin cells, which is supposed to be the main application scenarios of textured rear structure. The application of such texture rear structure is not that necessary in a thick enough solar cell since it already has high probability to absorb most of incident photons before they reach the rear surface. With the same layer thickness, cells with textured rear surface always own the highest absorptivity among all of those three kinds of solar cells, demonstrating the potential of rear surface texture to enhance performance of III–V multijunction solar cells.J_{sc}, which is supposed to be the minimum among J_{sc1} and J_{sc2} because of current matching, are predicted as 12.7, 14.0 and 15.0 mA/cm^2 in textured rear surface solar cells. And J_{sc} for mirror and substrate rear surface are 2.5, 3.0, 3.8 mA/cm^2 and 1.3, 1.5, 1.9 mA/cm^2 respectively.

Figure 2.3 gives the J_{sc} for InGaP/GaAs two junction solar cells with substrate, flat mirror and textured rear surface. The green surface stands for light generated short circuit current by the top subcell (InGaP) J_{sc1}, and red surface represents that of the bottom subcell (GaAs) J_{sc2}. The thickness of top InGaP subcell L_1 is fixed to 300, 500 and 700 nm for the aim of comparing the requisite total thicknesses of three kinds of solar cells at current matching. On average, the

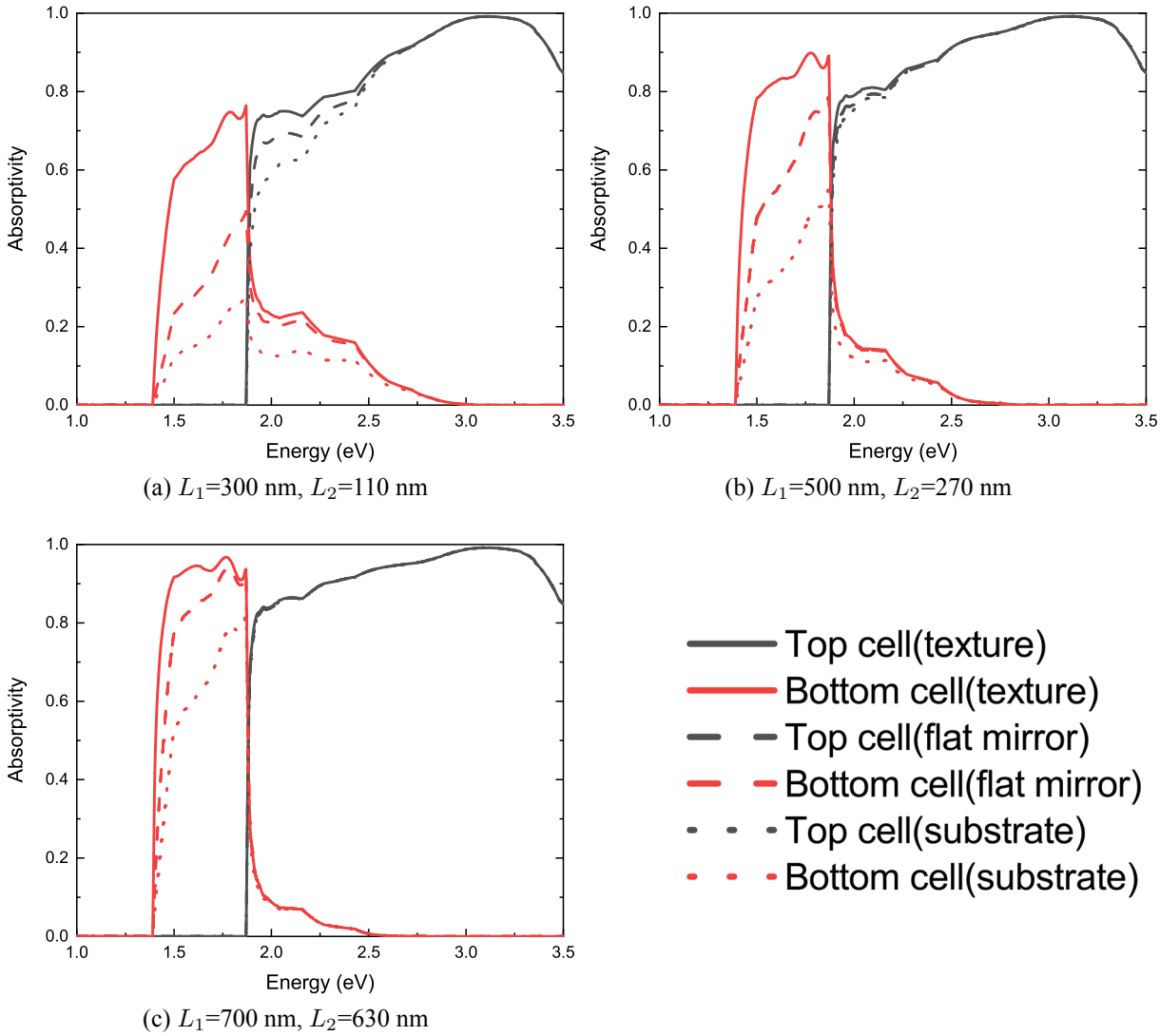

(a) L_1=300 nm, L_2=110 nm

(b) L_1=500 nm, L_2=270 nm

(c) L_1=700 nm, L_2=630 nm

Figure 2.2: Simulated subcell absorptivity for InGaP/GaAs solar cells with rear texture (solid), mirror (dashed) and substrate (dots). The absorptivity of InGaP top cell is denoted in red lines and that of GaAs bottom cell is denoted in black lines.

requisite total thickness of textured InGaP/GaAs two-junction solar cell would be decreased by 29.56% and 53.39% respectively, comparing with mirror flat and substrate rear structure cells.

For J_{sc1} the green surface, under a fixed L_2, J_{sc1} increase with L_1 for thicker top cell has enough optical path length to absorb incident photon with larger energy, so as to the increasing of J_{sc2} the red surface under fixed L_1. But J_{sc1} decrease with the increase of L_2 under a fixed L_1. And J_{sc2} decreases with the increasing of L_1 under a fixed L_2. This is because of the competitive relationship between subcells, which will be analyzed in Figure 2.4. This can also be construed as setting a series of surfaces that are perpendicular to L_1 axis. These surfaces intersect the surface of J_{sc1} (green) with several intersection curve. Projected on the surface parallel with L_2 and J_{sc} axis, the serial of curves reveal the relationship between J_{sc1} and L_2. As for the relationship between J_{sc2} and L_1, it can also be extracted from Figure 2.5 by setting series of surfaces which are perpendicular to L_2 axis, and project the intersection curve on the plane parallel with both L_1 and J_{sc} axis.

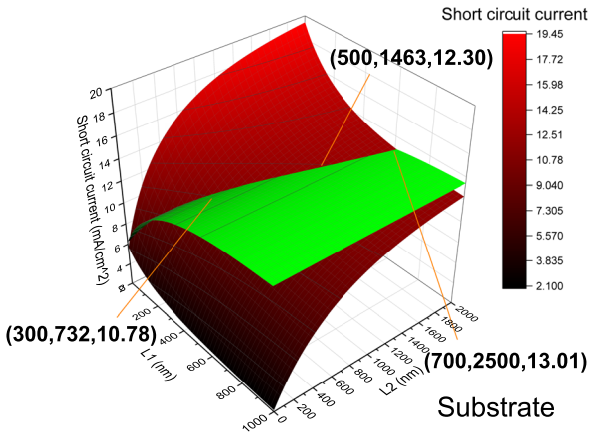

(a) J_{sc} at substrate rear surface

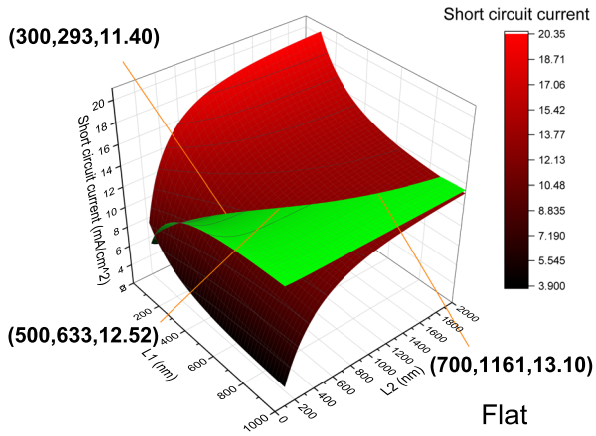

(b) J_{sc} at flat mirror rear surface

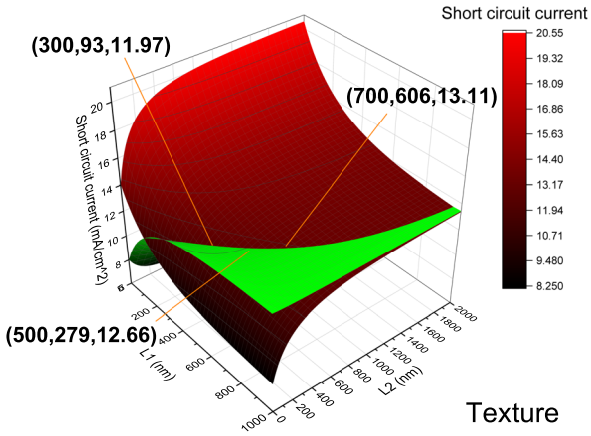

(c) J_{sc} at rear textured surface

Figure 2.3: J_{sc} for (a) substrate, (b) flat and (c) textured rear surface at current matching. Green surface denotes for light generated short circuit current of InGaP top cell and red surface stands for that of GaAs bottom cell. Points of L_1=300, 500 and 700 nm on the intersection curve which is at current matching are extracted in the form of coordinates (L_1, L_2, J_{sc}).

The relationship between light generated short circuit current J_{sc} and the thickness of the other subcell in an InGaP/GaAs dual-junction solar cell, that is the influence of increasing L_2 from 100 to 2000 nm on J_{sc1} and the change of J_{sc2} with the increase of L_1 from 100 to 1000 nm are demonstrated in Figures 2.4(a) and 2.4(b) respectively.

In Figure 2.4(a), the value of J_{sc1} are obviously different among three kinds of rear side surface. Under the same thickness of L_2 within 900 nm, the highest light generated short circuit current is always offered by textured rear surface, followed by that of flat and substrate successively. J_{sc1} of rear substrate surface cells, no matter with L_1=300 500 or 700 nm, are all horizontal line, influenced little by L_2. This is because of the high absorption efficient of absorptive substrate. And that is also one of the reasons why a gold or silver layer would be plated on the rear surface of a solar cell between active layer and substrate. In the range of L_2 larger than 900 nm, J_{sc1} changes little since 900 nm L_2 is enough for absorption of almost all incident photons. The increase of L_1 brings higher and higher J_{sc1} because it is exactly the source of J_{sc1}. Figure 2.4(b) illustrate the deceasing of J_{sc2} with increasing L_1 from 100 to 1000 nm. Note that in Figure 2.4(b), the red dash line for L_2=1000 nm flat cell is covered by the black solid line of L_2=500 nm texture. All photons with relative high energy larger that the band gap of InGaP could be absorbed by both top InGaP and bottom GaAs subcells, for which J_{sc2} deceases with increasing L_1 under all circumstances of L_2.

In both figures of Figure 2.4, J_{sc} decreases with the increase of the other subcell in an InGaP/GaAs dual-junction solar cell. And these curves distribute more in the upper area and less

in the lower area of Figures 2.4(a) and 2.4(b), which means that the enhancement effect of each layer deceases with the increase of this layer's thicknesses. There are two conclusions from Figure 2.3:

1. The J_{sc} increment of each subcell becomes weakly with the increasing of its own thickness;
2. The increase of each subcell's thickness in actual confines performance of the other subcells.

This introduces the cost-effectiveness problem of how to optimize the thickness of each subcell in a multijunction solar cell to realize both satisfied output performance and acceptable cost.

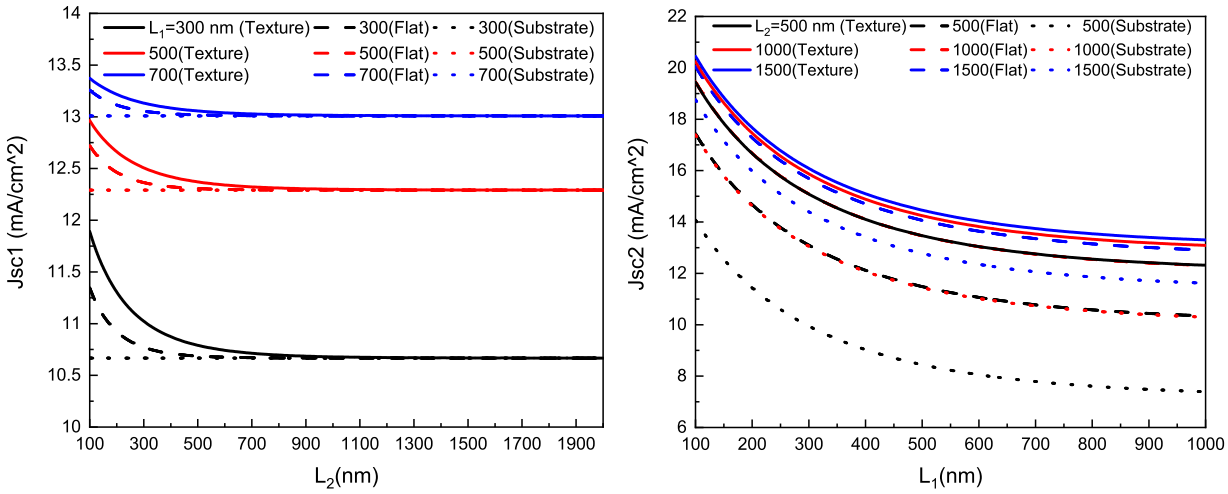

(a) J_{sc1} vs. L_2 (b) J_{sc2} vs. L_1

Figure 2.4: (a) short circuit current of top InGaP subcell (J_{sc1}) vs. length of bottom GaAs subcell (L_2) from 100 to 2000 nm and (b) short circuit current of bottom GaAs subcell (J_{sc2}) vs. length of top InGaP subcell (L_1) from 100 to 1000 nm in an InGaP/GaAs dual-junction solar cell. In (a), black, red and blue line denotes for the length of L_1 in 300, 500 and 700 nm, respectively. In (b), these three kinds of lines represent length of L_2 in 500, 1000 and 1500 nm. Different rear side structures – texture, flat and substrate – are marked in solid, dash and dot lines, respectively.

The data on intersection curve of J_{sc1} and J_{sc1} in Figure 2.3 have been extracted and the projection method has been again used to explore J_{sc1} with L_1 and L_2 respectively at current matching. The results are shown in Figure 2.5. The vertical range of each kind of rear surface is the same between those tow figures. For instance, in the case of texture rear surface (black line), J_{sc1} ranges from 11.11542 to 13.41677 mA/cm^2. Under all circumstances, J_{sc} increases with both L_1 and L_2, but their slopes decease, which has been analyzed above. Note that in the case of textured rear surface (black line), it always gives the best J_{sc} performance; while in the other two cases – flat (red) and substrate (blue) – their distribution has been replaced by each other. In Figure 2.5(a), the performance of cell with substrate rear structure is higher than that of flat rear surface. And in Figure 2.5(b), J_{sc} of cell with flat rear surface is larger than that of substrate structure. As for the reason of this, in the case of solar cell with flat rear surface, photons with

energy larger than InGaP band gap would go though the space of bottom GaAs subcell first then comes the turn of top InGaP subcell, giving opportunity of the photon to be first absorbed by the bottom GaAs subcell, which is definitely an energy loss. For a 400 nm InGaP/ 500 nm GaAs dual junction solar cell, the short circuit current density of that with texture and flat rear structure are 12.35624 and $11.67801 mA/cm^2$ respectively, increasing by approximately 5.81%.

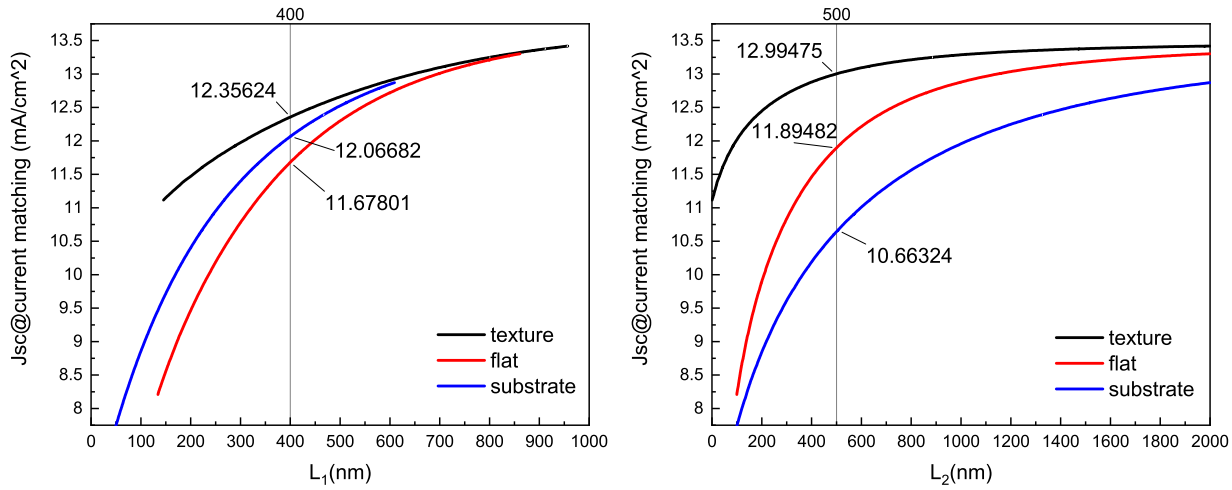

(a) J_{sc} at current matching vs. L_1

(b) J_{sc} at current matching vs. L_2

Figure 2.5: Short circuit current J_{sc} at current matching vs. length of (a) top InGaP (L_1 ranges from 100 to 1000 nm.) and (b) bottom GaAs (L_2 ranges from 100 to 2000 nm.) subcells in an InGaP/GaAs dual-junction solar cell. The black, red and blue lines represents for texture, flat and substrate rear surface, respectively. Reference line in (a) and (b) are L_1=400 nm and L_2=500 nm. The corresponding value of J_{sc} in (a) and (b) are marked in situ. Because the value of J_{sc} at current matching is limited by L_2 in (b), the lines in (a) end before L_1 reaches 1000 nm.

Figure 2.5(a) has been fitted by the following equation to calculate corresponding J_{sc} at current matching.

$$J_{sc}(L_1) = \begin{cases} 10.03072 + 1.88278\left(1 - e^{-\frac{L_1}{416.25815}}\right) + 1.88278\left(1 - e^{-\frac{L_1}{416.25814}}\right), texture \\ 4.6523 + 4.48988\left(1 - e^{-\frac{L_1}{262.06103}}\right) + 4.48988\left(1 - e^{-\frac{L_1}{262.06103}}\right), flat \\ 6.37505 + 3.48286\left(1 - e^{-\frac{L_1}{233.04479}}\right) + 3.48286\left(1 - e^{-\frac{L_1}{233.04479}}\right), substrate \end{cases} \tag{2.8}$$

Projecting points on intersection curve in Figure 2.3 to the plane of L_1 and L_2, Figure 2.6 demonstrates the requisite L_1 and L_2 under current matching. For a selected L_1, textured rear surface always offers the thinnest L_2 for current matching, followed by flat and substrate rear structure. With increasing of L_1, L_2 increases sharply, that is reflected by the increasing slopes of all three lines. The performance of bottom subcell confines the over all output of such an InGaP/GaAs solar cell. For convenience, three curves in Figure 2.6 have been fitted in Equation (2.9).

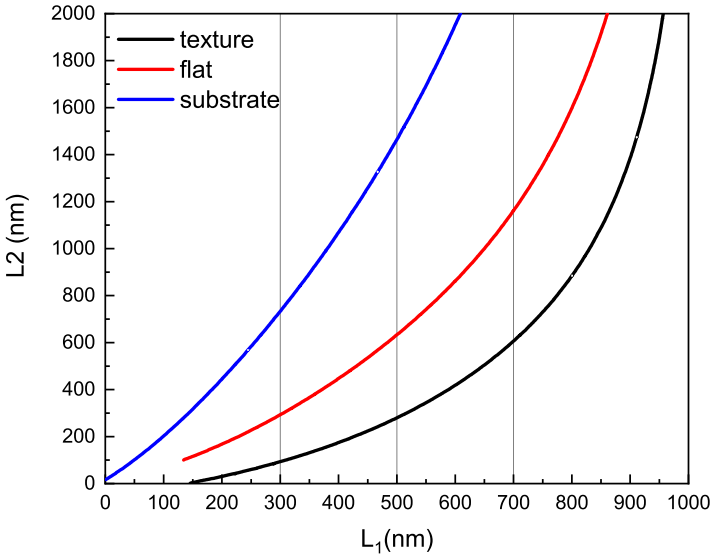

Figure 2.6: Requisite L_1 (maximum 1000 nm) and L_2 (maximum 2000 nm) under current matching. Black, red and blue lines represents for texture, flat and substrate rear surface, respectively. The perpendicular reference lines are at the point of L_1=300, 500 and 700 nm, respectively.

$$L_2\left(L_1\right)=\begin{cases}53.6003+15.91919\times e^{0.00496L1}, texture\\ -114.88895+170.30789\times e^{0.00290L1}, flat\\ -1060.87434+1066.03293\times e^{0.00173L1}, substrate\end{cases} \tag{2.9}$$

With Equations (2.8) and (2.9), thickness of L_2 at a selected L_1 could be directly calculated, together with their light generated short circuit current J_{sc}.

Table 2.1 are some data extracted out from Figures 2.5 and 2.6. L_1 is set to be 300, 500 and 700 nm for thin, medium and thick cells, respectively. Their corresponding L_2 are calculated via above method, together with current matched J_{sc} in $mA/cm2$. Their total thicknesses are calculated and standardized to compare the benefit of textured rear surface among all three kinds, so as to J_{sc}.

Table 2.1: Requisite L_2 and total thickness at current matching of fixed L_1

	L_1 (nm)	L_2 (nm)	Standar -dized L_2	Total thickness(nm)	Standardized total thickness	J_{sc} $(mA/cm2)$	Standar -dized J_{sc}
Texture		92.89675	0.1269	392.89675	0.3806	11.97222	1
Flat	300	292.82956	0.3999	592.82956	0.5743	11.39539	0.9518
Substrate		732.28573	1	1032.28573	1	10.77709	0.9002
Texture		279.23442	0.1908	779.23442	0.3969	12.65838	1
Flat	500	632.59228	0.4323	1132.59228	0.5769	12.5234	0.9893
Substrate		1463.38789	1	1963.38789	1	12.29616	0.9714
Texture		605.71818	0.2423	1305.71818	0.4080	13.11019	1
Flat	700	1161.25098	0.4645	1861.25098	0.5816	13.09593	0.9989
Substrate		2500.1054[1]	1	3200.1054	1	13.0087	0.9923

For a settled L_1, the requisite L_2 reaches its minimum value in the case of textured rear surface, followed by that of flat and substrate rear surface. At the same top-cell thickness L_1, the required bottom-cell thickness L_2 for a texture rear is less than 60% of that for rear mirror and less than 20% for absorptive substrate. On average, the total thickness of cells with texture

[1]This value does not exist in Figures 2.5 and 2.6, but estimated by their trend.

and flat rear structure are only 40% and 60% of that with absorptive substrate rear surface. But current matched J_{sc} of flat and substrate rear structure are 98% and 95% of that with textured rear surface. The difference of standardized J_{sc} among three kinds of rear structure is getting smaller and smaller. This indicates that textured rear structure is most effective in thin solar cells. In a word, textured rear structure enables a cell to perform best with thinnest thickness. This is the optimized thicknesses characterizing cost-effectiveness.

Absorptivity is recalculated after applying above optimizing method in Figure 2.7, which exhibits cells with $L_1 = 300, 500$ and 700 nm reveal the obvious absorption enhancement at the region close to each subcell bandgap in thin and medium solar cells due to the light-trapping rear texture, and that the simulated absorptivity's with or without rear-textured designs obtained by the proposed models are consistent very well, especially in thick cells, just as analyzed in Table 2.1. Matlab source code of the model employed in this chapter is listed in Appendix II – Source code.

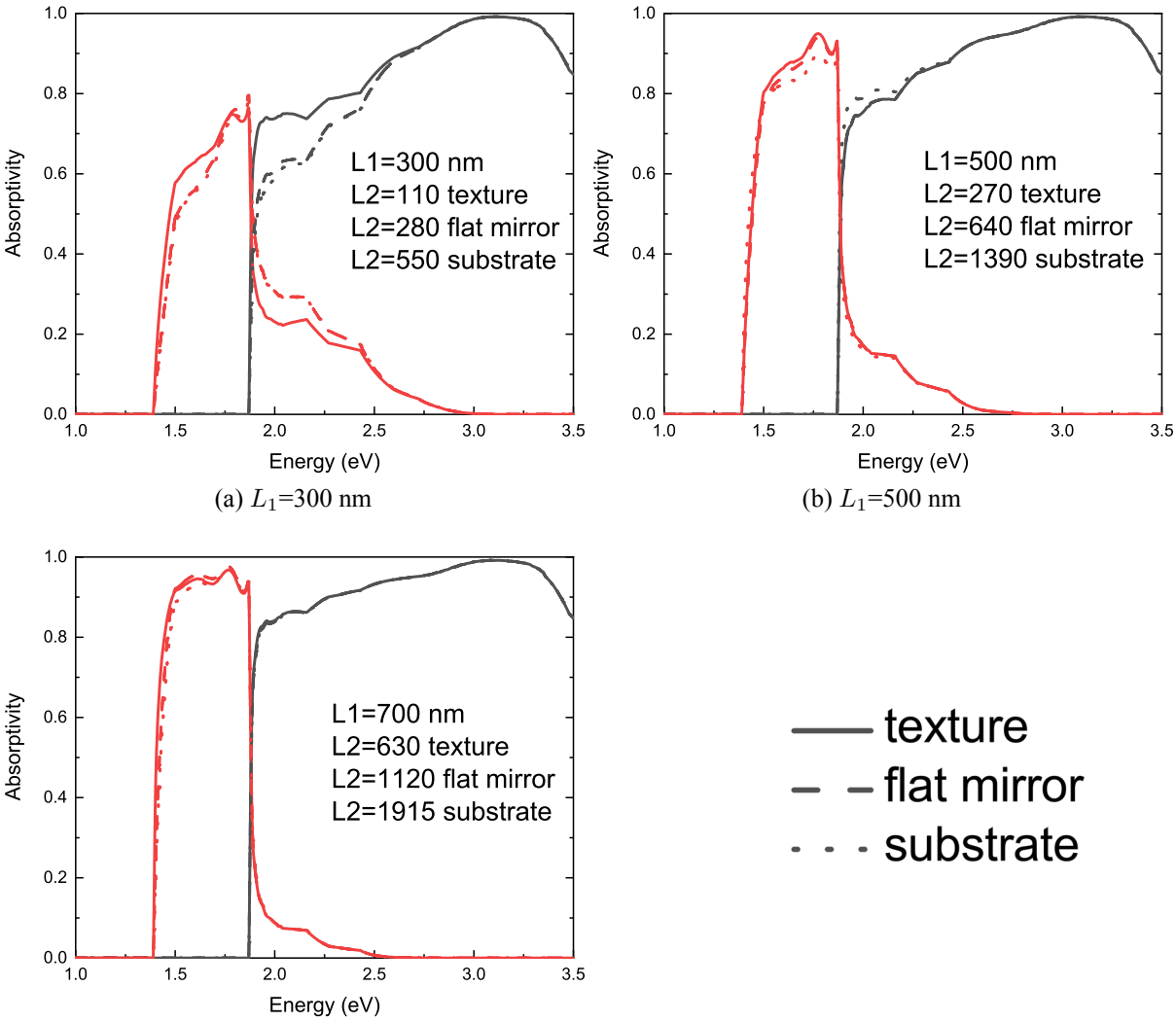

(a) L_1=300 nm (b) L_1=500 nm

(c) L_1=700 nm

Figure 2.7: Absorptivity simulation result of InGaP/GaAs dual-junction solar cells with rear texture (solid), mirror (dots) and substrate (dashed) at current-matching subcell thickness combination. The absorptivity of InGaP top cell is denoted in red lines and that of GaAs bottom cell is denoted in black lines.

Chapter 3

Texture fabrication by colloidal lithography

In this chapter, fabrication processes from distributing colloidal mask (Section 1) to ICP-RIE etching (Section 3) are introduced. In, detail, the importance of surface oxidization treatment addressed and the effect by several oxidant is shown in Section 2.

1 Colloidal mask

Mask, functioning as a method of interdiction and protection, is a layer structure between two spaces. In epidemiology, medical masks could intercept and trap virus or other harmful particles in their fibers so that these harmful particle or virus cannot get into human body system though respiratory tract and oral mucosa. In photolithography, a photo mask is used to cover some area on a sample from being exposed under ultraviolet ray to print pattern as designed. Here in this project, a monolayer colloidal nano particle mask is used to cover the rear side surface of GaAs contact layer. The area not being covered or between two nano particles has larger probability to react with high-energy plasma ions, being etched down to form 3D structure. That is, the texture on the rear side of a solar cell.

Figure 3.1 illustrates (a) the reaction probability between plasma ions in ICP-RIE with GaAs rear contact layer with four sphere particles on it as colloidal mask, and (b) the imagined morphology of texture after reactive-ion etching. For those area not covered by sphere particle mask on the left and right side in Figure 3.1(a), the probability of reaction between plasma ion and GaAs is considered unity and the highest. When going from the area not being covered to that being covered, the probability of reaction reduces, reaching the lowest reaction probability right at the bottom of a sphere particle mask. For the area between two adjacent sphere masks, the reaction probability reaches the second maximum point at where those two sphere are tangent with each other. Geometrically, the point right under the contact point of two adjacent sphere particles on GaAs surface is considered to be not being covered. But in practice, the contact of two adjacent sphere particles do have some effect on the area below.

In Figure 3.1(b), the morphology of GaAs layer after reactive-ion etching is demonstrated.

The area not being covered is directly etched down. While at the area covered by sphere particles, almost no etching reaction occurs at near around of contact point between sphere particle and GaAs surface and the etching depth increase with the distance between the contact point and another arbitrary point under a sphere particle. The difference is, at the boundary of covered and not-covered area, the slope is larger than that between two tangent sphere particles. The etching depth in Figure 3.1(b) is proportional with the reaction probability in Figure 3.1(a).

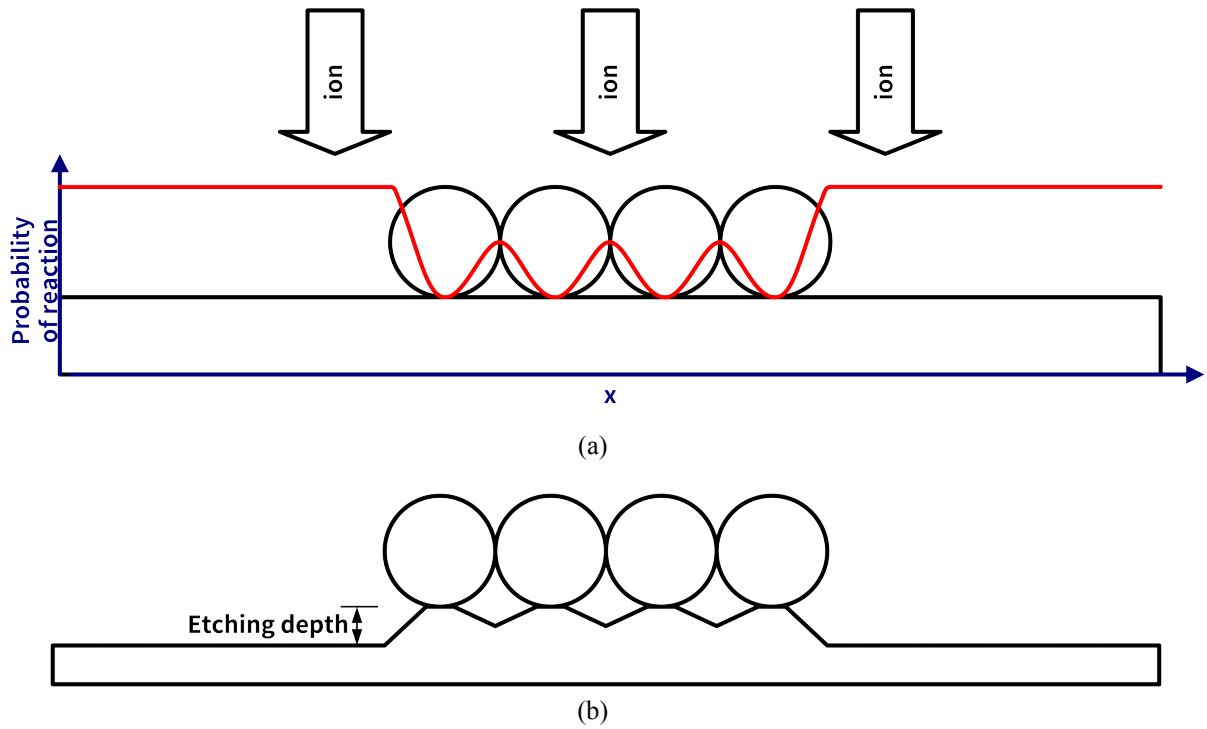

Figure 3.1: (a) reaction probability distribution with colloidal mask covered on GaAs rear contact layer. There are four sphere particles right at the center, functioning as colloidal mask during reactive-ion etching. Plasma ions driven by electromagnetic field moves downward perpendicularly, reacting with GaAs at those area not being covered by colloidal mask or between two neighbouring sphere particles. The red curve denotes for probability of reaction distribution on x axis. It is not accurate probability but just shows the probability difference between the areas covered or not by colloidal mask. (b) The morphology of GaAs contact layer after etched by plasma ions. The height of a trapezoid structure which is a single unit of light trapping texture pattern demonstrate the etching depth.

In this project, GaAs is etched in Cl_2/Ar, for which $\varnothing 500\ nm$ SiO_2 colloid is selected as mask during colloidal lithography. The key of this fabrication method lies in the high density of monolayer colloidal mask. In the following content in this section since each colloidal mask matches with one single unit of texture, the basic of colloidal particle distribution – sedimentation – is first introduced, followed by its problem – vertical aggregation and the solution – spin coating.

1.1 Sedimentation

A colloid, in chemistry, is a mixture of dispersed phase in dispersion medium. In this case, $\varnothing 500nm$ SiO_2 particles are the solid dispersed phase and dispersion medium is H_2O. Sedimentation process intrinsically goes on in SiO_2 colloid under the effect of gravity, which could be described by Stock's law.

$$F_d = 6\pi\mu R v, \tag{3.1}$$

where F_d is the frictional force –known as Stokes' drag –acting on the interface between the fluid and the particle, μ is the dynamic viscosity, R is the radius of the spherical object which is, here, 500 nm, and v is the flow velocity relative to the object.

In dispersion medium H_2O, on perpendicular direction, a single SiO_2 particle is controlled by gravity F_g and buoyancy F_b. The difference of those two forces decide kinestate of every single particle. If gravity is larger than buoyancy ($F_g > F_b$), particles sediment down to to bottom; if buoyancy is larger than gravity ($F_b > F_g$), particles are buoyant up to the surface. The difference is actually decided by the density difference between dispersion medium and dispersed phase and given by

$$F_v = (\rho_p - \rho_m)\, g \times \frac{4}{3}\pi R^3, \tag{3.2}$$

where ρ_p and ρ_m are, respectively, the mass density of SiO_2 and H_2O, g is gravitational acceleration. And further more, the terminal velocity of SiO_2 failing in H_2O is described by

$$v = \frac{2\,(\rho_p - \rho_m)}{9\mu} g R^2. \tag{3.3}$$

Substitute the parameter of SiO_2 and H_2O, the terminal velocity of SiO_2 in H_2O is supposed to be $895\ nm/s$. For an area of 3 mm thick colloid, it takes almost an hour to sediment down to the bottom. And this result is even base on static velocity field. In practice, an operator uses a tool, for instance a dropper, to drop colloid on a surface, which offers kinetic energy to both SiO_2 and H_2O molecules. This molecular movement extend period of sedimentation to hundreds of hours [34–36]. But there is another problem arises from sedimentation – vertical aggregation.

1.2 Vertical aggregation

The intrinsic sedimentation process results in particles aggregating layer by layer, forming a 3D vertical aggregation. Figure 3.2 comes from the work of Jason D. Forster, Jin-Gyu Park and etc [37], demonstrating a SiO_2 particle layer overlay on several layers of that. Figure 3.2(a) demonstrates a dense layer of dumbbells, where each single one is stuck at inter-particular between two dumbbells underneath. In this way, the pattern of each layer is supposed to be the

translation of that underneath. Figure 3.2(b) illustrates the vertical structure of multi-layer dumbbells.

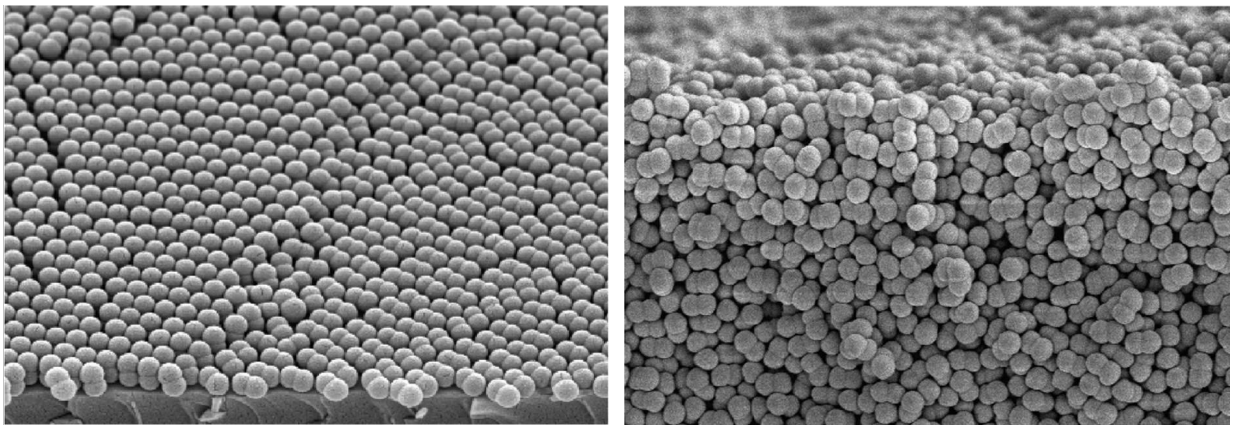

(a) (b)

Figure 3.2: Dumbbells crystallize in confinement, but not in the bulk. (a) SEM image of dry dumbbells cast into thin films by vertical deposition. Dumbbells form ordered mono- and bi-layers. (b) SEM image of dumbbells cast into an amorphous thick film. The fields of view in (a) and (b) are 7.6 µm across. [37]

Such kind of aggregation is an expected good result in [37], but definitely a disaster in this project which requires a monolayer colloidal mask. Based on the analysis in Section 1, such a multi-layer 3D stack colloidal mask prevent plasma ions from reactant, let alone reactive-ion etching. Figure 3.3 are two cross sectional diagram which illustrate the Figure 3.3(a) probability of reaction and Figure 3.3(b) the surface morphology after reactive-ion etching.

In Figure 3.3(a), a layer of GaAs is located on the bottom, the lower left corner of which is set to be the origin of probability vs x coordinate. There are in total seven spherical colloidal mask particles in two layers, four of which are located in the first floor and the left ones are on the second floor. Each sphere particle is stuck in the inter-spherical space. Each particle is contact and, in Figure 3.3, tangent with others around it. Driven by electric field in reaction chamber, the plasma ions move downward, reacting with GaAs from its top surface. The reaction probability in area not being covered is supposed to be maximum, but it reaches its minimum in the area covered by multi-layer spherical masks. Between those two areas is the boundary, where the probability reaction decreases from the area not being covered to that being covered. The difference between Figure 3.3 and Figure 3.1 is that with such multi-layer colloidal mask particle aggregation, the reaction in area not being covered is completely blocked. As shown in Figure 3.3(b), the area not being covered is etched down with etching depth controlled by bias power and reaction time during ICP-RIE, making the area covered by the multi-layer colloidal masks as a ridge. In this way, the expected texture structure for light trapping cannot be fabricated.

The solution to this problem is quite direct in theory – split the multi-layer colloidal particles to monolayer distribution.

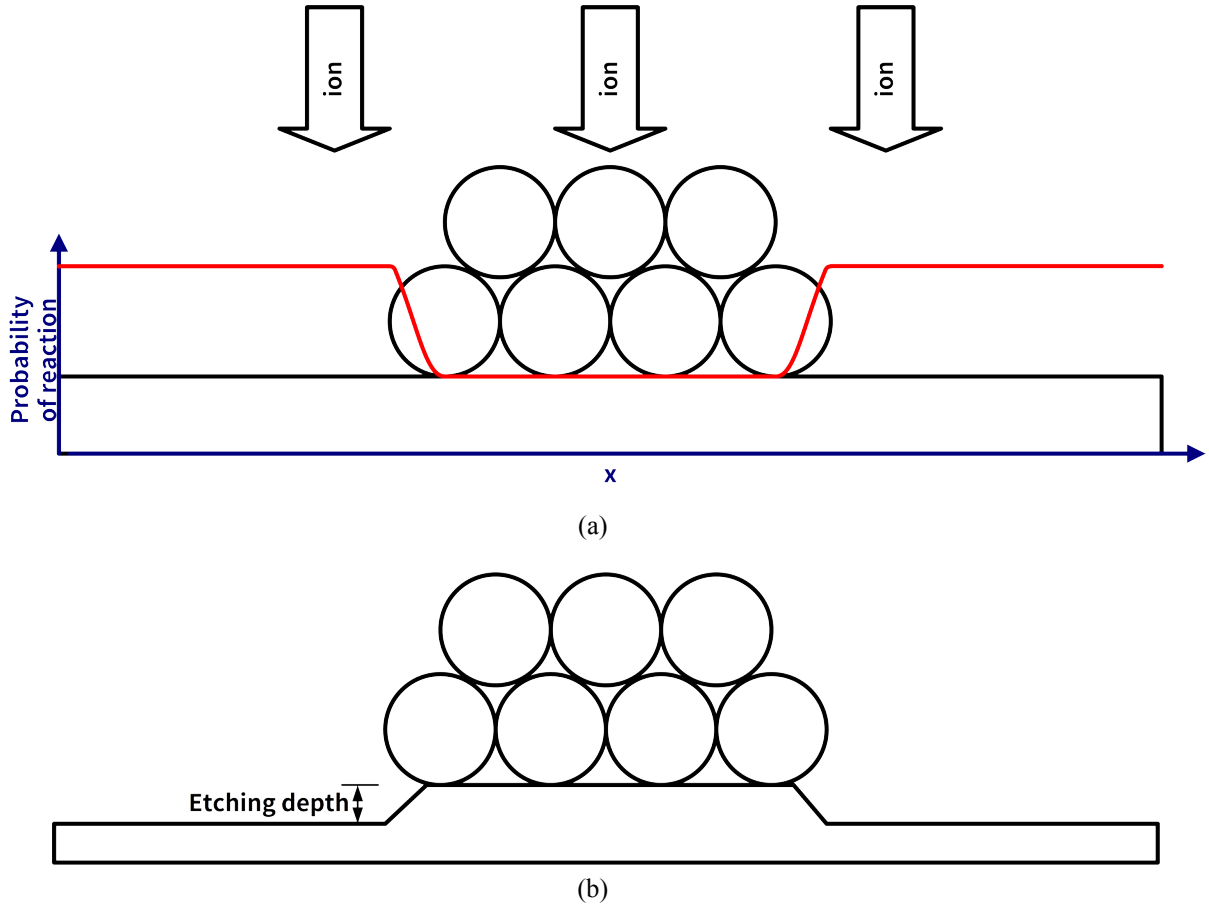

Figure 3.3: (a) reaction probability distribution with multi-layer colloidal mask covered on GaAs rear contact layer. There are in total seven sphere particles right at the center, functioning as colloidal mask during reactive-ion etching. They distribute in two layers – one with four particles with another three particles it. The second layer particles just cover the tangent point of the particles in the first layer. Plasma ions driven by electromagnetic field moves downward perpendicularly, but cannot react with GaAs at those area being covered by the multi-layer colloidal mask . The red curve denotes for probability of reaction distribution on x axis. It is not accurate probability but just shows the probability difference between the areas covered or not by colloidal mask. (b) The morphology of GaAs contact layer after etched by plasma ions. The height of a trapezoid structure which is a single unit of light trapping texture pattern demonstrate the etching depth.

1.3 Spin coating

Spin coating was the first technique for growth of 2D colloidal crystal masks for colloidal lithography due to the fact that it allows easy and quick formation of 2D crystals over large area [38]. Refer to Newton's laws of motion, there is a centripetal force

$$F_c = ma_c = m\omega^2 r, \tag{3.4}$$

where m is the mass of this body, $\omega = \frac{2\pi}{T}$ denotes for angular velocity, r represents radius of

curvature and a_c is the centripetal acceleration, on a body who follows a curved path, pointing from the barycenter of the body to the spin center. Its corresponding force is called centrifugal force, which is a pseudo force acting on all objects when viewed in a rotating reference frame. In a rotating system, centripetal force is offered by, for instance, universal gravitation in astrophysics and in this on plane rotating system the hydrogen bond between hydrogen atom on surface and oxygen atom on silica Figure 3.5. And for a sphere particle contacting with others, centripetal force comes from the contact force among all other particles around it.

If the centripetal force is enough to maintain a steady rotating system, a sphere particle remains where it is. Otherwise it moves towards the direction far from rotating center, acting like the centrifugal force is applied on it.

Figure 3.4 introduces a three-step spin coating method for SiO_2 particles [39]. This schematic demonstrates a plane semiconductor material on a spin coater with multi-layer SiO_2 particles on it. During high-speed spin coating, those sphere particles on upper layer would first move towards the direction far away from rotating center for its relatively weaker contact force between others around it. When those particles reaches the boarder between covered and not covered area in its own layer, they fall down to the lower layer. Or, if there is enough space in a lower layer due to the dispersion of this layer, particles in upper layer can directly fill in this blank space. The capillary force between two adjacent particles further compresses particles' distribution. The three-step spin coating is set to be $0 \xrightarrow{2\ s} 200$ rpm for 60 s $\xrightarrow{8\ s} 1000$ rpm for 120 s $\xrightarrow{10\ s} 2000$ rpm for 10 s $\xrightarrow{20\ s} 0$ in this project.

The effect of monolayer fabrication based on spin coating is decided by the hydrogen bond between hydrogen atom on surface and oxygen atom on silica, for which the hydrophilic treatment of semiconductor substrate is of vital importance.

2 Surface hydrophilic treatment

The surface of silica particles is covered by siloxane bonds ($\equiv Si-O-Si\equiv$) and silanol groups ($\equiv Si-OH$), which enables SiO_2 particles intrinsically own characteristic of hydrophilia. The schematic is shown in Figure 3.5.

Based on the analysis above, if hydroxide ion (OH^-) could be attached on semiconductor surface, it would be easier to trap SiO_2 particles on semiconductor surface. A general method is to attach hydroxide ion (OH^-) on the semiconductor surface.

$$O^{2-} + H_2O \rightarrow 2OH^- \tag{3.5}$$

In this project, aiming at developing a simple and fast fabrication process, some common chemicals, for instance deionized water, 99.5% ethanol and 30% hydrogen peroxide, are selected for semiconductor surface treatment. The treatment method is just immersing samples in those chemicals for a certain period of time under room temperature and pressure. The following contents in this section demonstrate SEM pictures of SiO_2 particles distribution after applying above three-step spin coating.

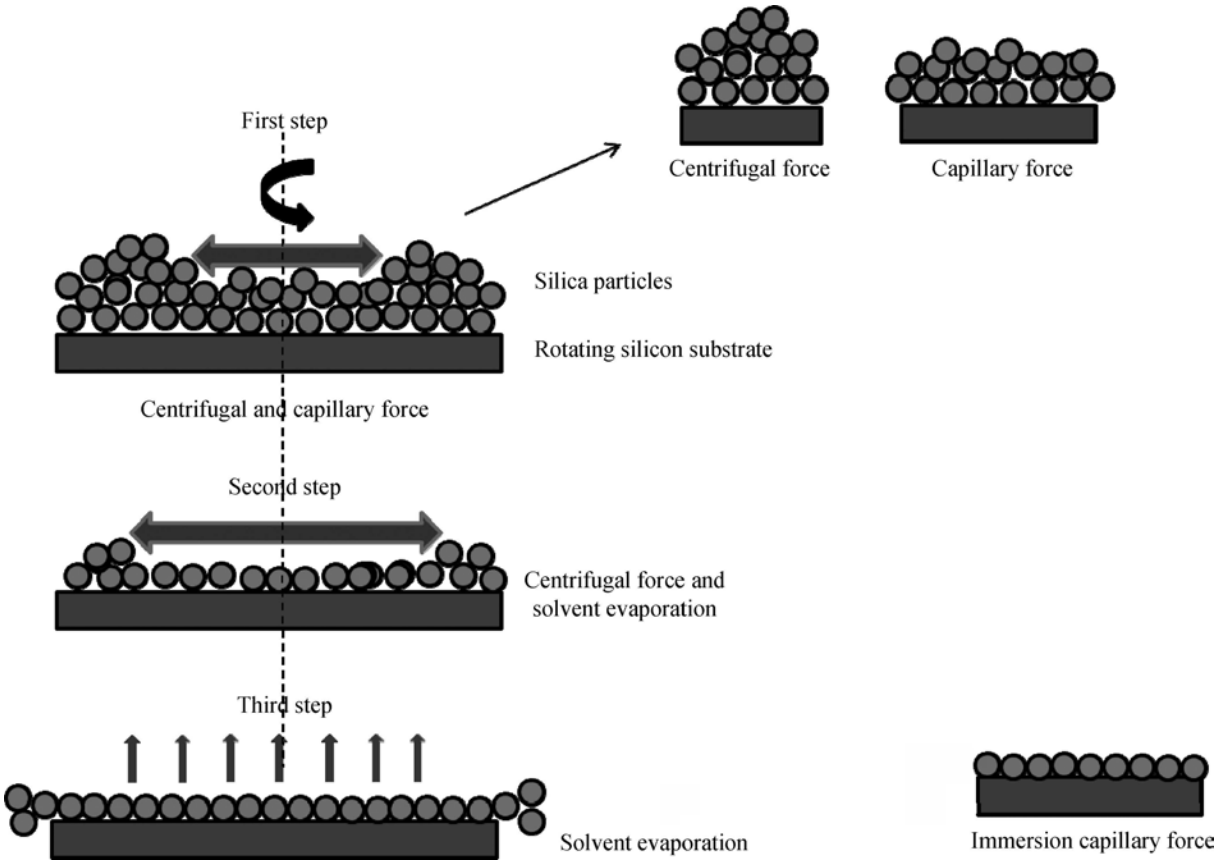

Figure 3.4: Schematic illustration of possible phenomena that occurred during three-step spin-coating method of SiO_2 particles [39]. On the plane semiconductor material, silica particles aggregate in multi-layers. Spin coating pushes particles towards side and immersion capillary force holds adjacent particles tightly.

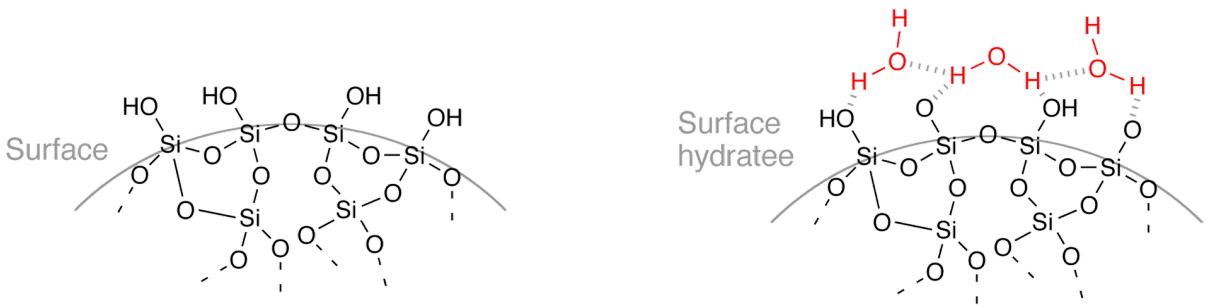

Figure 3.5: Schematic representation of the silica gel surface [40]. In contact with water, the colloidal silica surface is covered by siloxane bonds and silanol groups. The oxygen atoms connect with hydrogen atom in H_2O molecule through hydrogen bond.

2.1 Surface treatment by water

Figure 3.6 shows the SiO_2 particle distribution on a water treated GaAs surface after three-step spin coating. The results of surface treatment in water for 3, 6 and 12 hours are not as effective as 24 hours, for which only SEM pictures of 24 hours treatment is illustrated. From (a) to (c) in Figure 3.6, in an arbitrary area on this sample, SiO_2 particles aggregate in groups consisted of dozens to hundreds of particles in monolayer. In some area as shown in Figure 3.6 (d), SiO_2

particles aggregate in quite high density, which is exactly the expected distribution density.

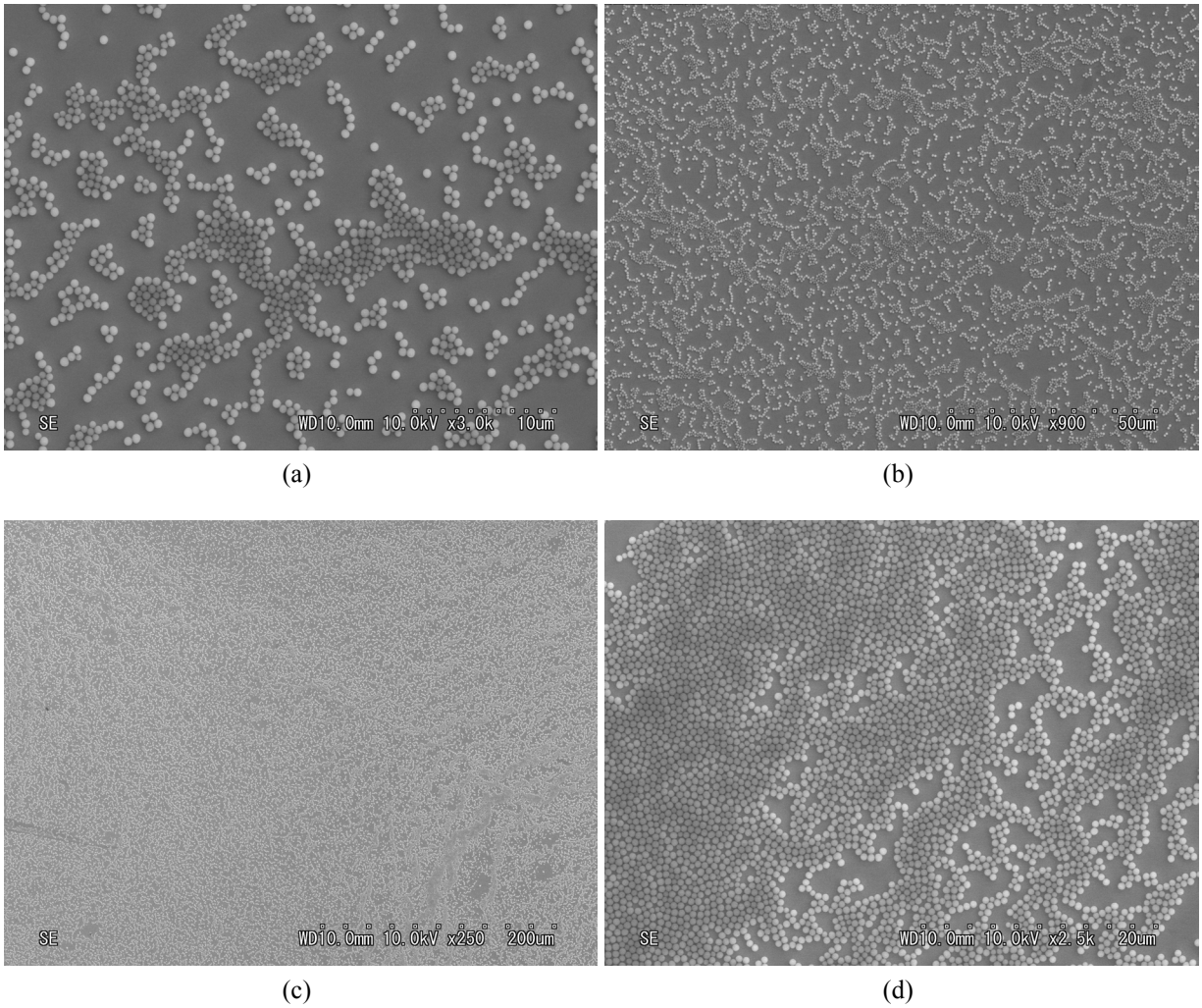

Figure 3.6: Surface treatment in water for 24 hours. From (a) to (c) are in the scale of 10, 50 and 200 μm respectively. An area of high density aggregation in the scale of 20 μm is shown in (d).

But there is a problem in this method. After the 24 hours treatment in water, all of the sample surface turns to dark color from GaAs's original mirror-like surface. It seems that the GaAs surface has been somehow corroded. One possible reason is that the hydrogen ion from self-ionization of water corroded GaAs surface. The following reaction inherently goes on in water.

$$H_2O + H_2O \rightleftharpoons H_3O^+ + OH^-, \tag{3.6}$$

which is usually written as

$$H_2O \rightleftharpoons H^+ + OH^- \tag{3.7}$$

for convenience. The ion product constant of water is measured to be $K_w = 1 \times 10^{-14}$ [41] under 25°C, 0.1 MPa.

$$K_w = [H^+][OH^-] \tag{3.8}$$

When more and more OH^- attached on GaAs surface, the balance of water self-ionization in Equation (3.7) turns to forward direction, which increase the amount and concentration of H^+ in water. The acid environment corrodes surfaces of GaAs samples.

2.2 Surface treatment by ethanol

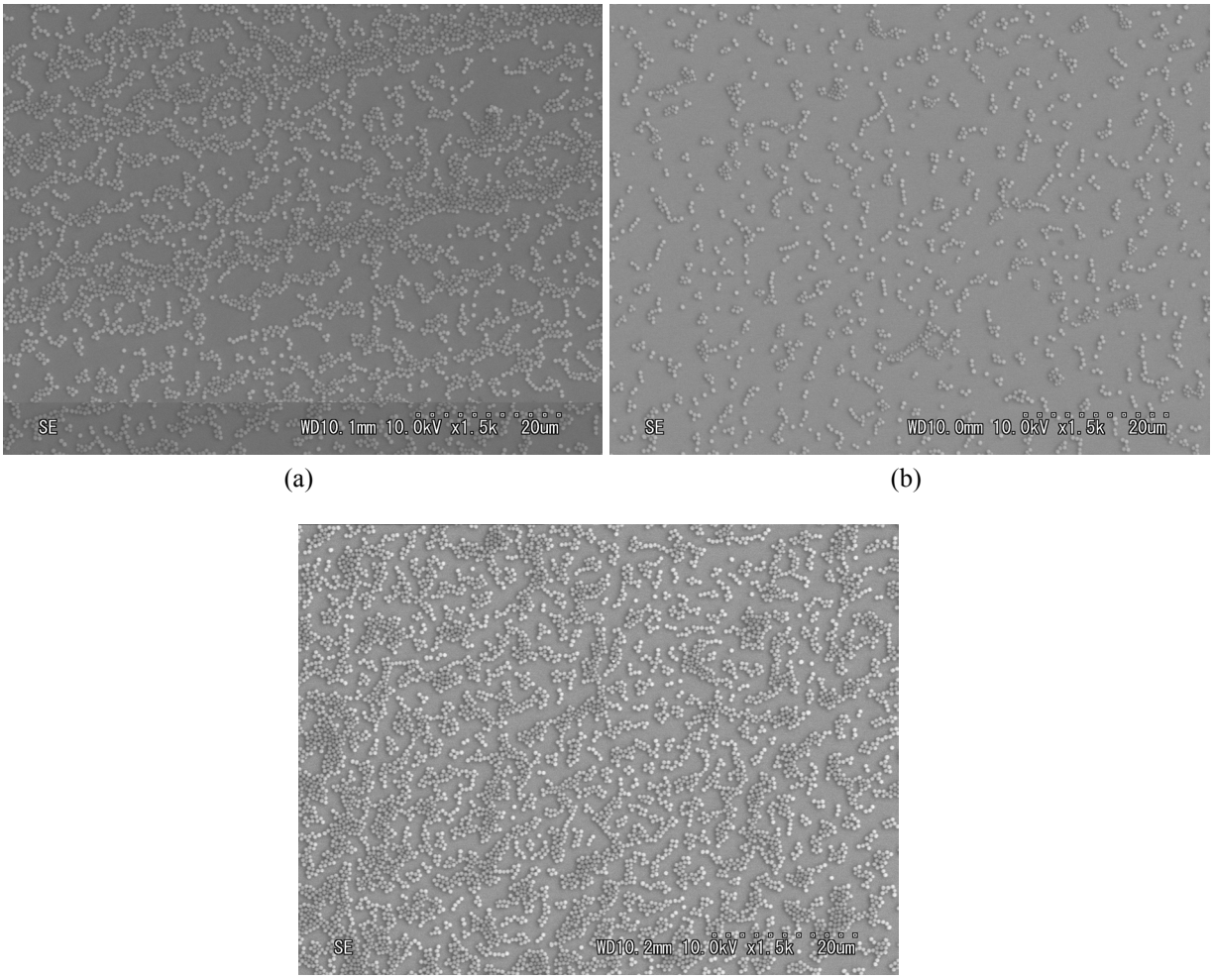

(a) (b)

(c)

Figure 3.7: Surface treatment in 99.5% ethanol for 3, 6 and 24 hours under the scale of 20 μm.

Figure 3.7 shows the SiO_2 particle distribution on a water treated GaAs surface after three-step spin coating. It is obvious that each group in Figure 3.7 is smaller than that of Figure 3.6. In each group, dozens of SiO_2 particles aggregate, whose amount is relatively stable than that treated by water. The distribution density on sample treated by 99.5% ethanol for 6 hours is apparently lower than that of 3 hours and 24 hours.

2.3 Surface treatment by hydrogen peroxide

Figure 3.8 shows the SiO_2 particle distribution on a water treated GaAs surface after three-step spin coating. With the treatment time increasing from 3 to 24 hours, the SiO_2 particle distribution density increases obviously. In Figure 3.8(a), the amount of SiO_2 particles in each cluster is generally lower than 30. In Figure 3.8(b), dispersive particles start to gather, forming clusters consisting of dozens of SiO_2 particles. As for the samples treated for 12 hours, large scale high density particle clusters show up for the first time, as shown in Figure 3.8(c). The 24 hours treatment offers the highest particle distribution density in Figure 3.8(d). Hundreds to thousands of SiO_2 particles aggregate to form an area of continuous colloidal mask distribution.

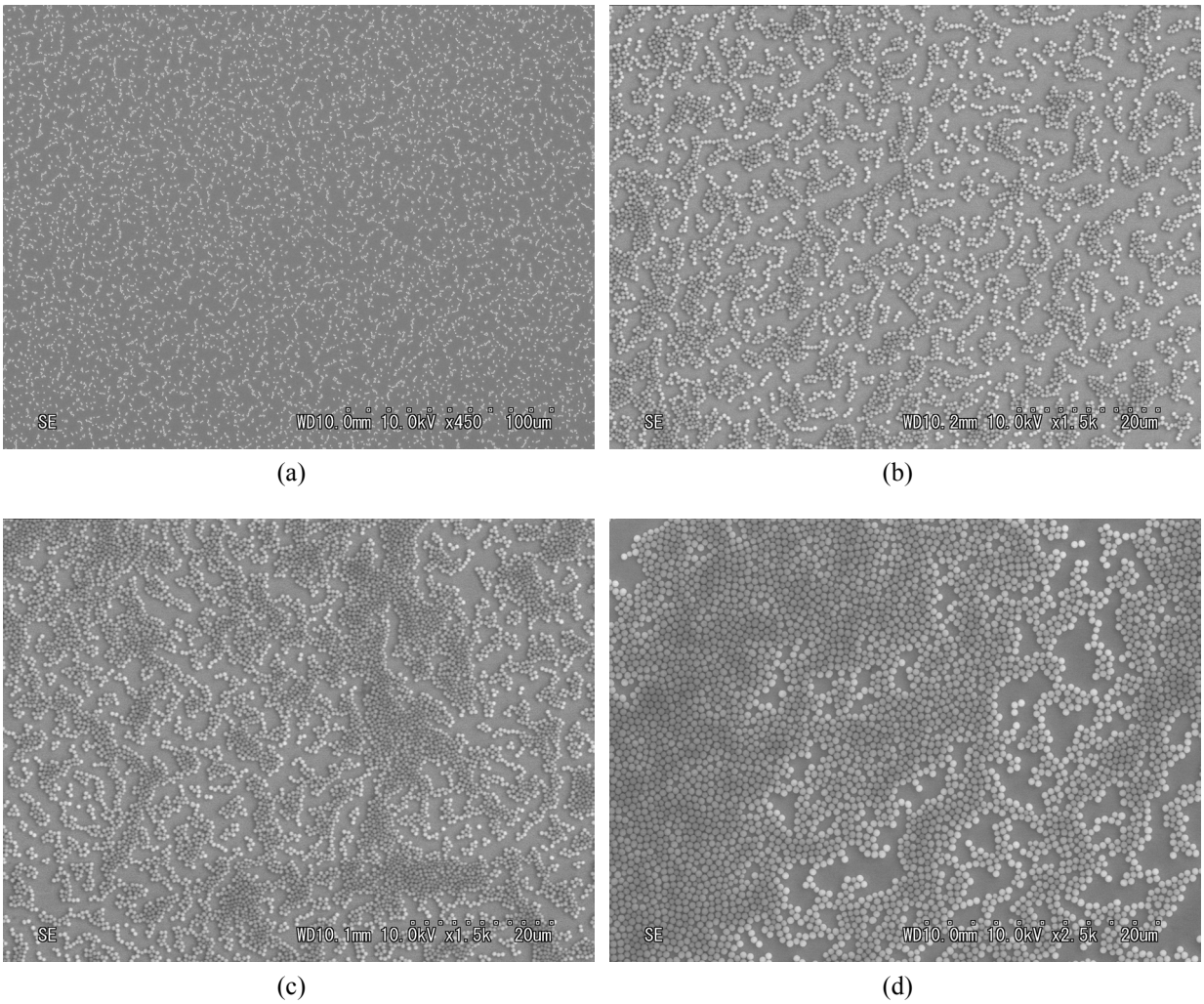

Figure 3.8: Surface treatment in 30% hydrogen peroxide for (a) 3, (b) 6, (c) 12 and (d) 24 hours.

3 ICP-RIE

As mentioned above in Section 1, the texture structure for light trapping on rear side GaAs surface is fabricated by Inductively Coupled Plasma Reactive-Ion Etching after distributing SiO_2 colloidal mask on the sample surface to be etched.

Figure 3.9 shows the GaAs surface with SiO_2 colloidal mask on it after Reactive-Ion Etching. Comparing with the area not being covered by SiO_2 colloidal mask, the area consisting of numerous texture units uplift. In the area not being covered by SiO_2 colloidal mask, the surface are randomly etched down during the RIE reaction, forming conterminous pits in this area. The size of these pits are generally smaller than 100 nm, which is considered to contribute almost nothing to light trapping effect. So this kind of area will be treated as plain surface in the following chapters.

In total, there are two kinds of distribution in Figure 3.9 – face and line distribution. As its name suggests, face distribution means, in a cluster of SiO_2 colloidal particles, only a surface can be drawn to pass through all the SiO_2 particles'center. Similarly, if a line can be drawn to pass through all the SiO_2 particles'center, this distribution is called line distribution. These two kinds of distribution correspond to divergent texture structure.

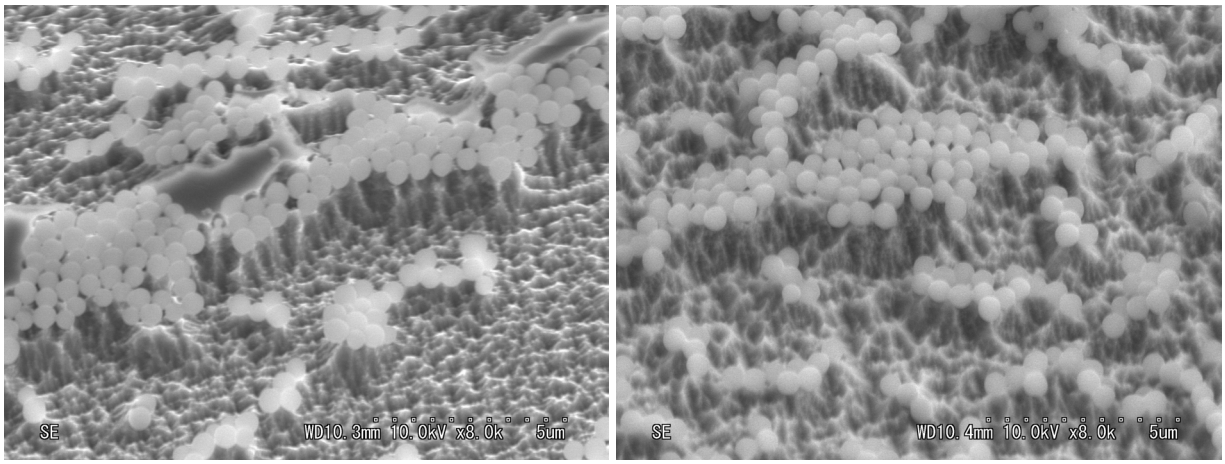

(a) (b)

Figure 3.9: SEM picture of texture structure with SiO_2 particles. The tint while spheres are SiO_2 particles as colloidal mask, underneath which is the texture units. The area not being covered by SiO_2 mask has been randomly etched down, with non-unity etching depth. Surrounded by the area not being covered by SiO_2 colloidal mask, the texture units look like mountains on a plain.

After removing SiO_2 colloidal mask by buffered HF solution, the SEM image of texture is illustrated in Figure 3.10. An area of high density texture units is shown in Figure 3.10(a), in which the texture parts can be divided into two categories – face and line distribution, as stated above. In the area of face distribution, each single texture unit is approximately conical frustum, whose top surface is a plane. Between adjacent conical frustum is the part being etched down to etching depth. As for the texture of line distribution as shown in the top of Figure 3.10(a), this kind of texture is like mountain range, with a ridge at its center and going down to piedmont of mountain. As shown in the picture, face distribution dominates on the GaAs rear surface, for

which the texture of line distribution will be ignored in Chapter 4's simulation.

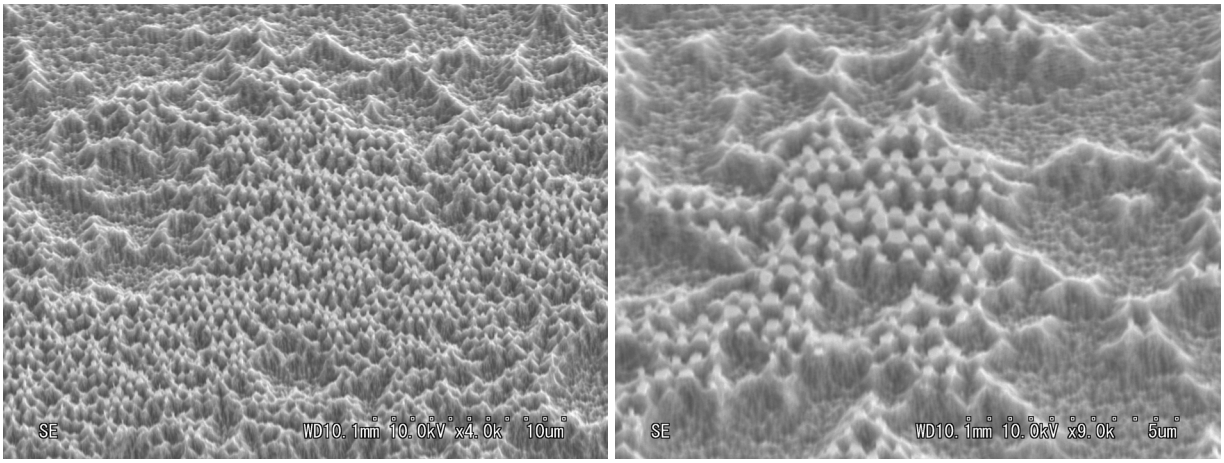

(a) (b)

Figure 3.10: An aerial view of texture structure after removing SiO_2 colloidal mask in (a) 4.0 k and (b) 9.0 k ratio.

Figure 3.11 demonstrates the cross-sectional view of the boundary between the textured area (left) and randomly etched area (right) because of the lacking of SiO_2 colloidal mask. The morphology of texture unit is like a inverted funnel – first etched straight down, then the etched area decrease, occluding at one point. This proves the conjecture of reaction probability in Figure 3.1. On the right side of this picture, its random morphology is influenced by the distribution of plasma ions during reactive-ion etching.

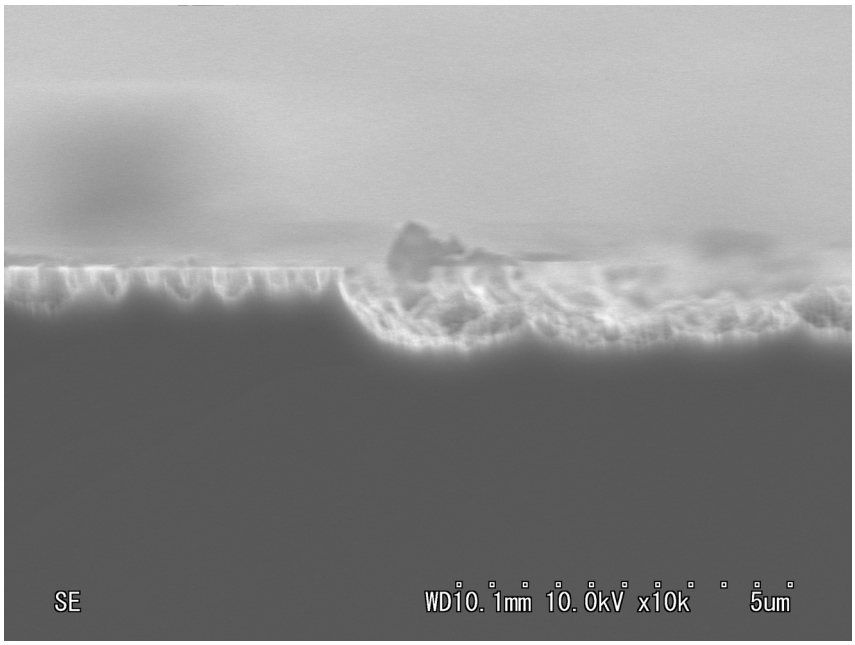

Figure 3.11: A cross section view of the boundary between the area covered (left) and not covered (right) by SiO_2 colloidal mask. The etching depth is larger than 500 nm in this picture.

The bias power and etching time are set to be 30w and 10s to get 400 to 500 nm etching depth.

Chapter 4

Optical performance simulation

In this chapter, two models – ray optics model and electromagnetic field model – extracted from SEM images in Section 3, Chapter 2 are demonstrated in Sections 1 and 2, testing its optical and electromagnetic performance. Notice that in the following simulation, reflection is assumed to be perfect and ideal, no energy dissipation.

1 Ray optics simulation

Based on the SEM images in Section 3, as one SiO_2 particle matches with one texture unit, the combination constitutes a basic element of texture structure as shown in Figure 4.1, whose side view is shown in Figure App.1, Appendix I – Figures.

In practice, thousands of the conical frustum units and the left part of GaAs rear contact layer are a whole. The incident light is expected to be reflected back by inner surface of the conical frustum unit, as shown in Figure 4.2. Two parallel incident lights start from the dark blue point and end at the dark red arrow. Their optical path are marked from dark blue to dark red. One incident light reaches the bottom of conical frustum and reflected by it into the inner space of solar cell, directly. While the other one first reaches the side surface of the conical frustum, reflected by it and immediately hit on the other side, reflecting for a second time back into solar cell's inner space.

3D model of four-layer InGaP/GaAs dual-junction flat and texture solar cells are established in Figure 4.3. From top to bottom are GaAs top contact, InGaP top subcell, GaAs bottom subcell and GaAs rear contact. Other layers like window layer, BSF layer and tunnel junction has been eliminated from the model for the aim of simplification, since there have little influence on ray optical performance of the solar cell.

In this simulation, two kinds of light sources – grating light source and natural light source are applied. Figure 4.4 shows the initial status of a flat and a texture cells under grating light source which is conical distribution and whose origin is $\mathbf{O}(2E4, 2E4, 3.6E3)$. Its cone axis points from $\mathbf{O}$ to $(-1E3, -1E3, -2E3)$ with cone angle $\frac{\pi}{4}$. Within the cone, ray direction is defined by the number of polar (N_θ) and azimuthal (N_ϕ) angles; plus the cone axis, there are

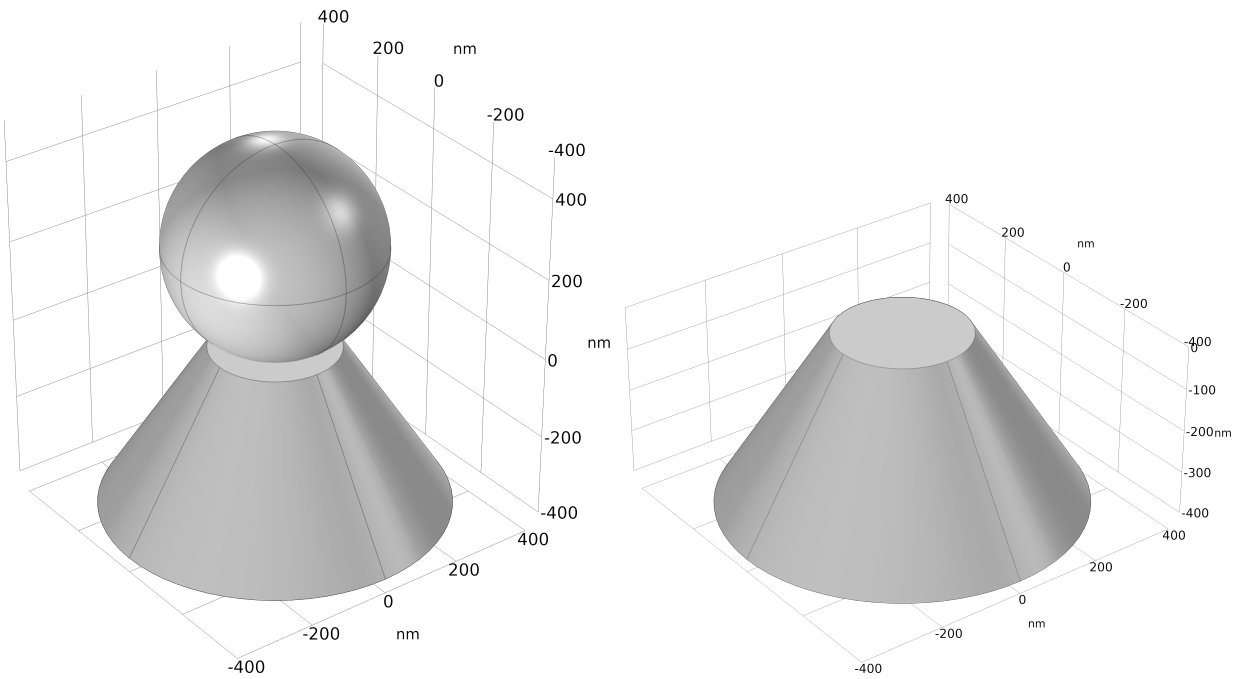

(a) (b)

Figure 4.1: 3D model extracted from SEM image. The texture units is a conical frustum (a) with and (b) without SiO_2 particles on it. The SiO_2 particle is denoted by the $\varnothing 500\ nm$ sphere in (a), right underneath which is the conical frustum texture unit, whose top and bottom radius are set to be 150 nm and 400 nm, respectively. Its 400 nm height is equal to the etching depth during ICP-RIE.

in total $N_\theta \times N_\phi + 1$ rays in each conical grating. Bottom surfaces of these two cells are set to be ideal mirror. Amount of polar angle changes from 3 to 83, while the amount of azimuth is fixed to 3. Optical path length is $6 \times 10^3\ nm$, which is several times to the cell thickness, giving maximized opportunity to each ray to escape our of the cell. Refraction in between layers of each cell is ignored. Whether a ray escape out of the cell or not is judged by z component of ray vector at its end point. Two images of this simulation at end point is demonstrated in Figure App.3, Appendix I – Figures.

Table 4.1: Table of light escape under grating light source in flat and texture solar cells.

amount of polar angle N_θ	amount of azimuth N_ϕ	Ray amount of grating light source	flat		texture		reduced by
			escaped	proportion	escaped	proportion	
3	3	10	8	80%	4	40%	50%
13	3	40	36	90%	20	50%	44%
23	3	70	62	89%	33	47%	47%
33	3	100	90	90%	48	48%	47%
53	3	160	145	91%	76	48%	48%
83	3	250	226	90%	123	49%	46%

Result of this simulation in Table 4.1 illustrates how the rear texture function with incident lights that own divergent incident angle. Generally, over 50% lights can be trapped inside the solar cell, reducing on average 47% lights from escaping out of the cell.

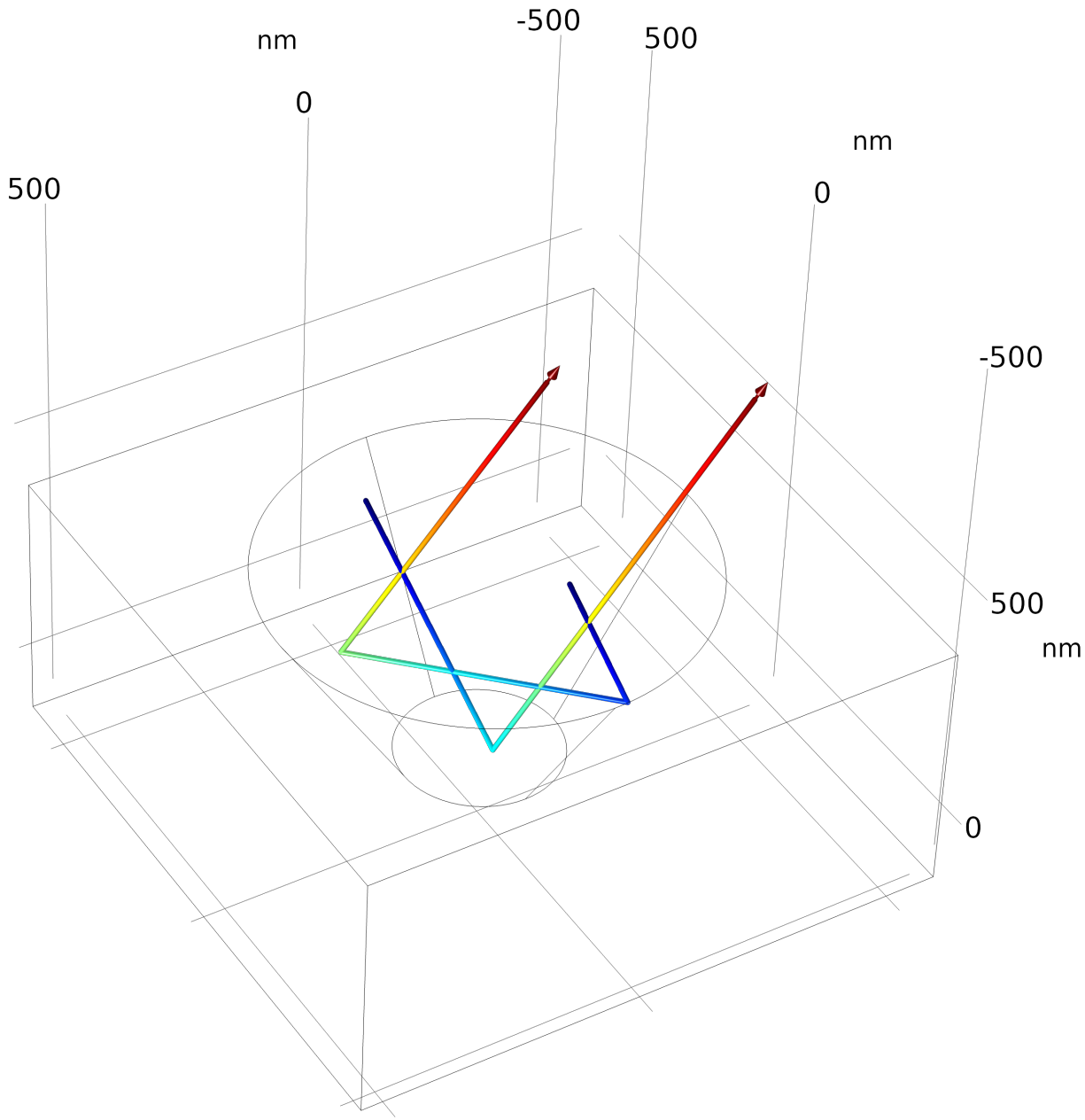

Figure 4.2: Two parallel incident lights are reflected by the inner surface of texture unit. In a $500\ nm \times 500\ nm \times 400\ nm$ cuboid, a conical frustum whose size is exactly the same with that of Figure 4.1(b) is eliminated from it. Two parallel incident lights which are reflected for multiple times start from the dark blue point and end at the red arrow.

Figure 4.5 is the ray optical simulation under natural light source. The incident lights are a $N_x \times N_y$ array whose direction is base on global meteorological data of Tokyo, Japan at 9:00:00 of July 1st, 2020. Disturbance within conical angle of $\frac{\pi}{6}$ is added to each incident light to simulate the relatively random incident angle.

Table 4.2 is the result of cells under natural light source. Flat rear surface would reflect back all incident lights and they will directly escape out of the cell Figure App.4(a), Appendix I – Figures. As for the textured cell, the texture units can change the direction of light propagation, trapping some of the incident lights within solar cell's inner space. Comparing with that of flat cell, on average, 60% incident lights can escape out of the texture solar cell, reducing by 40%

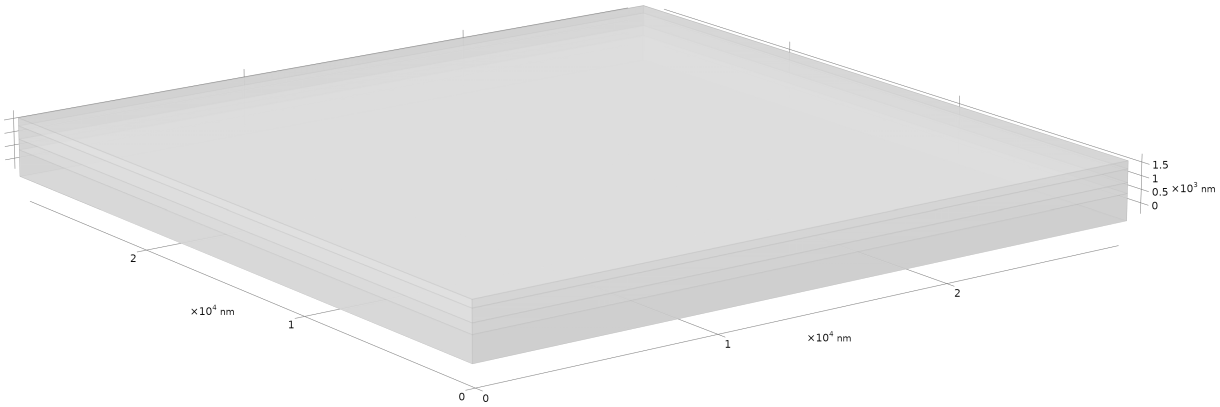

(a)

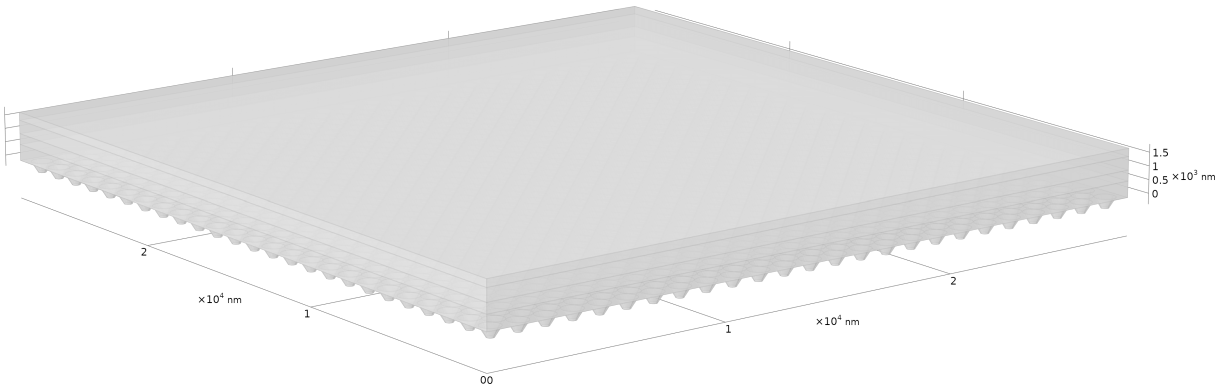

(b)

Figure 4.3: 3D model of (a) flat cell and (b) texture cell. These two cells are in $2\sqrt{2} \times 10^4 nm^2$ size. Thickness of their four layers are, from top to bottom, 300, 1000, 600 and 1000 nm, respectively. In (b) the texture cell, its bottom layer has been etched down for 400 nm, which is equal to the height of texture unit. On the bottom of the texture cell, there are in total $(25 \times 25 + 24 \times 24 =)\, 1201$ texture units. The side and bottom view of texture solar cell in Figure 4.3(b) is demonstrated in Figure App.2, Appendix I – Figures.

as shown in Figure App.4(b), Appendix I – Figures.

Table 4.2: Table of light escape under natural light source in flat and texture solar cells.

N_x	N_y	Ray amount of Natural light source	flat escaped	flat proportion	texture escaped	texture proportion	reduced by
2	5	10	10	100%	7	70%	30%
5	8	40	40	100%	24	60%	40%
7	10	70	70	100%	43	61%	39%
10	10	100	100	100%	60	60%	40%
10	16	160	160	100%	95	59%	41%
10	25	250	250	100%	144	58%	42%

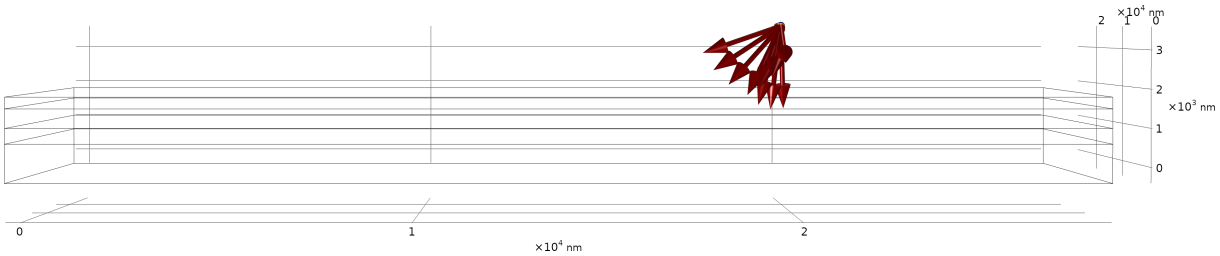

(a)

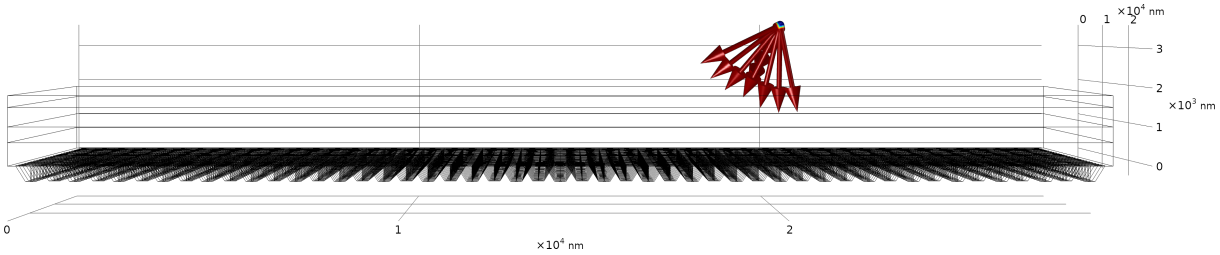

(b)

Figure 4.4: Initial status of (a) flat and (b) texture cells under grating light source. The nearest surface is x-z surface in which the horizontal and vertical axis are, respectively, x and z axis. The y axis is perpendicular with the paper surface, pointing from inside to outside.

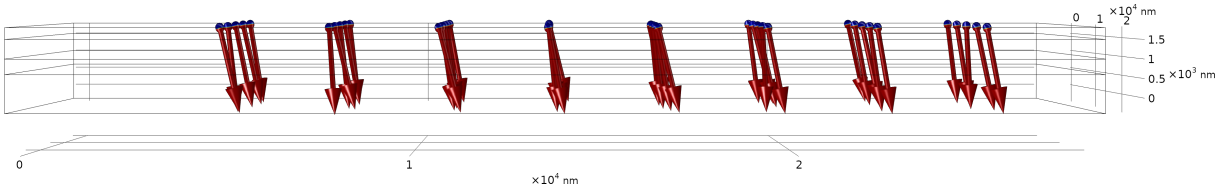

(a)

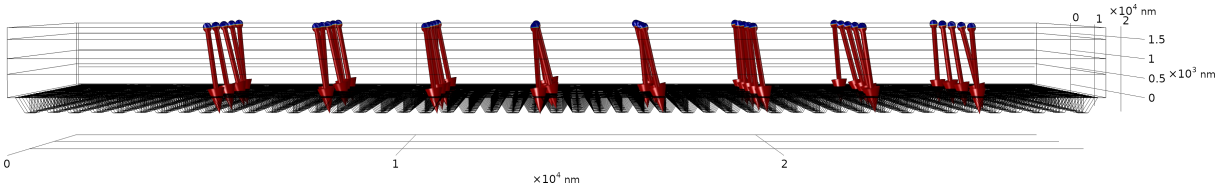

(b)

Figure 4.5: Initial status of (a) flat and (b) texture cells under natural light source. The nearest surface is x-z surface in which the horizontal and vertical axis are, respectively, x and z axis. The y axis is perpendicular with the paper surface, pointing from inside to outside.

2 Electromagnetic wave simulation

In the previous section, the function of rear texture consisting of conical frustum units has been tested by how they change optical propagation direction. In this section, the performance of texture solar cells comparing with that of flat cells is tested in electromagnetic field to take absorption coefficient into consideration.

2.1 Methodology

Figure 4.6 demonstrates two solar cells with equal but not enough thicknesses, and the same input I_0 is applied on both of these two solar cells. Assume that no reflection occurs on the front outer surface of these two cells but their rear surfaces are perfect mirror. For the flat cell in Figure 4.6(a), some portion of the incident light reaches its rear surface and is directly reflected back by its rear surface for the perfect reflection, escaping right out of the solar cell with intensity I_1. As for the texture cell in Figure 4.6(b), the first-time reflection on textured rear surface would change propagation direction of the incident light. Also, scattering occurs on the textured rear surface, dividing the incident light into several components, some of which reaching the front surface would be reflected back for a second time due to its relatively larger angle of incidence, for which a second chance is given to the textured cell to absorb more incident light. As a result, only some portion of incident light with intensity I_2 is able to escape out of the cell.

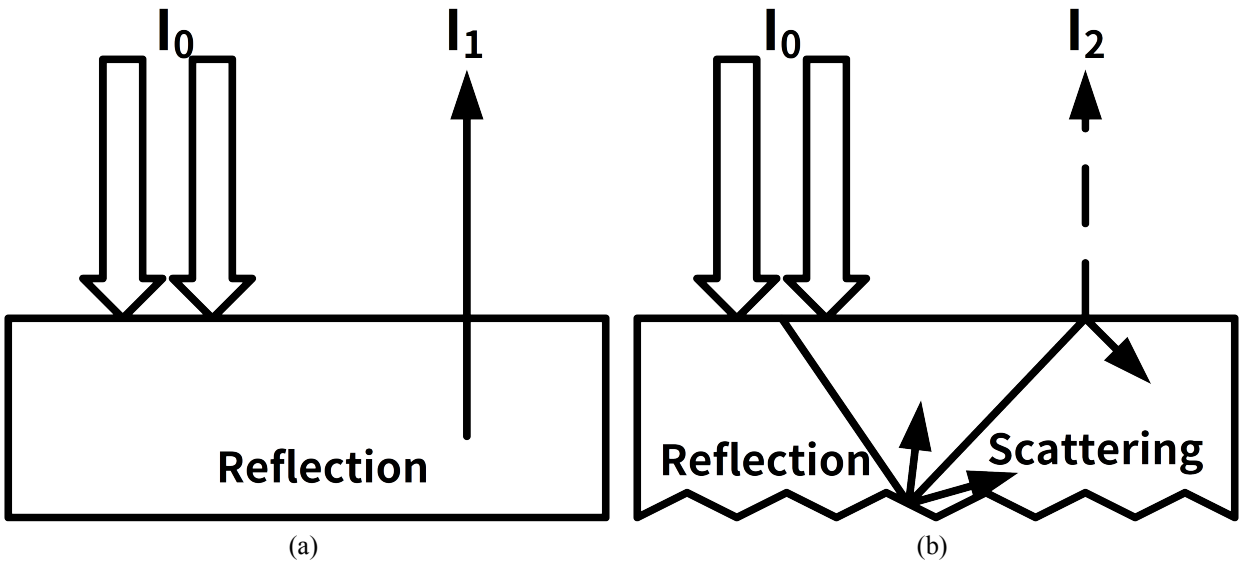

Figure 4.6: Measurement of escaped lights. There are one (a) flat and one (b) texture cells with the same thickness. Incident light with intensity I_0 is applied on them. Portion of the incident light would be reflected back by the front and rear surface of these two solar cells, with intensity I_1 and I_2 respectively.

If the following relationship

$$I_2 < I_1 < I_0 \tag{4.1}$$

can be measured in not only this simulation but also the subsequent experiment, the function of texture rear surface can be proved, together with the enhancement of absorption.

2.2 Gaussian distribution

A Gaussian or normal distribution in probability theory is a type of continuous probability distribution for a real-valued random variable. Its general probability density function is

$$f(x) = \frac{1}{\sigma\sqrt{2\pi}} e^{-\frac{1}{2}\left(\frac{x-\mu}{\sigma}\right)^2}, \tag{4.2}$$

where μ is the expectation of the distribution which also decide the position of axis of symmetry, and σ is its standard deviation which describes the width of this distribution.

In this simulation, an electromagnetic field input satisfying Gaussian distribution as shown in Figure 4.7(a), whose function is

$$E_0 = 360e^{-\left(\frac{x}{3500}\right)^2} V/m \quad x \in \left[-10000\sqrt{2}, 10000\sqrt{2}\right] nm, \tag{4.3}$$

is applied on the top boundary of the simulation model in Figure 4.7(b). The distribution width is equal with that of testee solar cells – from $-10000\sqrt{2}$ nm to $10000\sqrt{2}$ nm. The maximum electric field module is set to be $360\ V/m$ which is converted from $340\ W/m^2$ [42] – the total amount of energy received per second at the top of Earth's atmosphere. As shown in Figure 4.7(b), the input source would be reflected back by both the front and bottom surface (blue) of the solar cell. These two portion of light would interfere with each other in the upper space of Figure 4.7(b) which is air and will be introduced in detail in the next section.

2.3 Simulation model

Figure 4.8 demonstrates the model in this electromagnetic field simulation. The source field is only allowed to be applied on the top boundary of this model as shown in Figure App.5(a), Chapter. The component layers are illustrated in detail in Figure App.5, Chapter. As mentioned in the last section in Figure 4.7(b), the input electromagnetic field would be reflected back by both the front and rear surface of solar cell, interfering with each other in the space of air located at the upper half area in each model. The intensity of interference can directly shows how much electromagnetic wave has escaped out of the cell in each case.

2.4 Simulation result

Refer to Fresnel equations, in S polarization, which is exactly the source used in this simulation, the reflectance on the interface for lights incident from GaAs front contact layer to InGaP top cell is

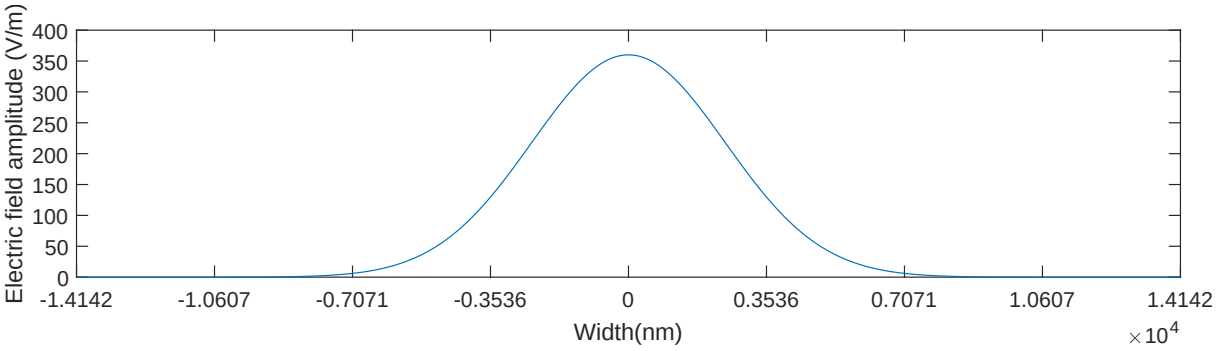

(a)

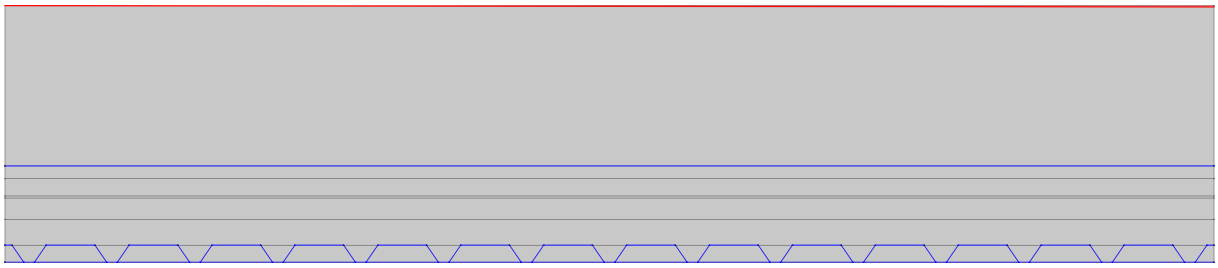

(b)

Figure 4.7: An electromagnetic field satisfying Gaussian distribution with amplitude of 360 V/m as input is applied on the top boundary (red) in (b) which is a texture cell with 12 units whose width is $20000\sqrt{2}$ (from $-10000\sqrt{2}$ nm to $10000\sqrt{2}$ nm). The front and rear surface of cells are marked in blue.

$$R_s = \left| \frac{n_1 \cos\theta_i - n_2\sqrt{1-\left(\frac{n_1}{n_2}\sin\theta_i\right)^2}}{n_1 \cos\theta_i + n_2\sqrt{1-\left(\frac{n_1}{n_2}\sin\theta_i\right)^2}} \right|^2 , \tag{4.4}$$

where n_1 and n_2 are the refractive indexes of the two mediums and here are GaAs and InGaP respectively. θ_i denotes for the incident angle and is supposed to be 0.

The interference effect concentrates in the area between input and front surface of solar cells. Notice that the source of this electromagnetic field has not been hided in following images from Figure 4.9 to Figure 4.11. Without anti-reflection coating, a portion of electromagnetic wave would be directly reflected back by the front surface of solar cells. The reflectance R_s is calculated through Equation (4.4) and demonstrate in Table 4.3.

Table 4.3: Reflectance R_s on the interface between air and GaAs contact layer under wavelength of 400, 700 and 1000 nm.

Wavelength (nm)	n_1 (Air) [43]	n_2 (GaAs) [44, 45]	R_s
400	1.00029382	4.4590	0.4014
700	1.00028685	3.7700	0.3371
1000	1.00028520	3.5039	0.3090

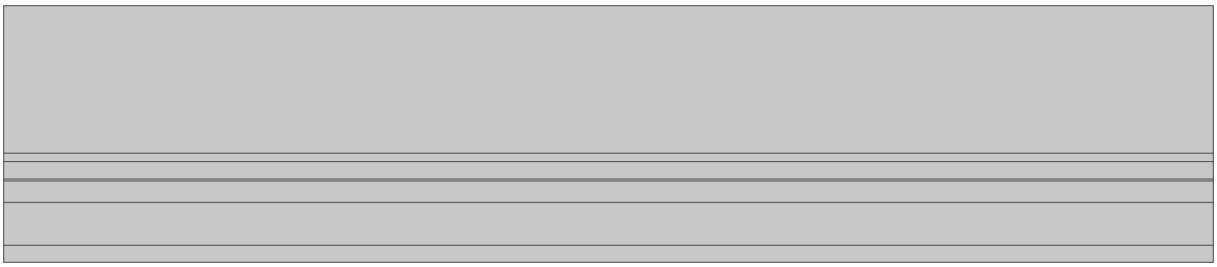

(a)

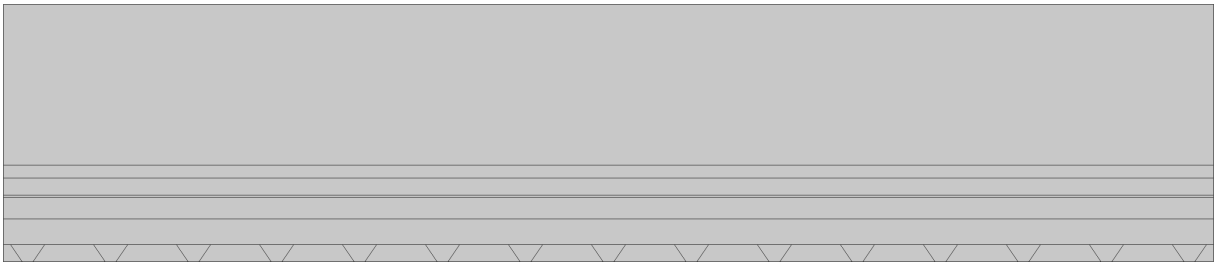

(b)

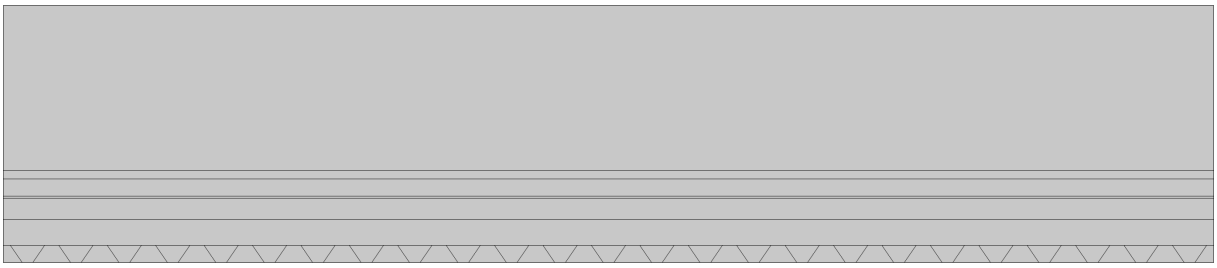

(c)

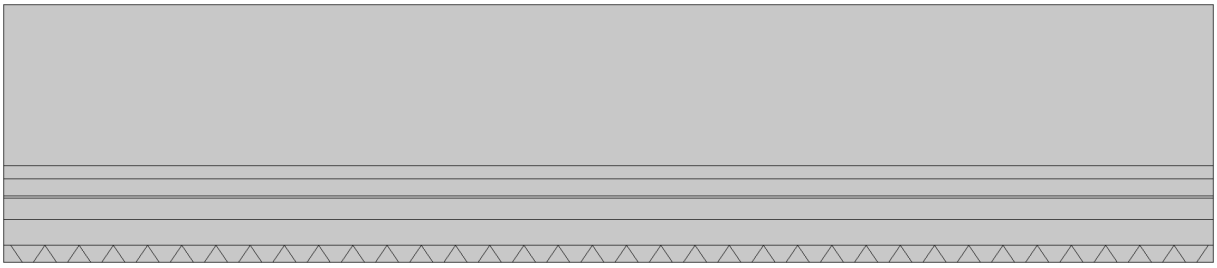

(d)

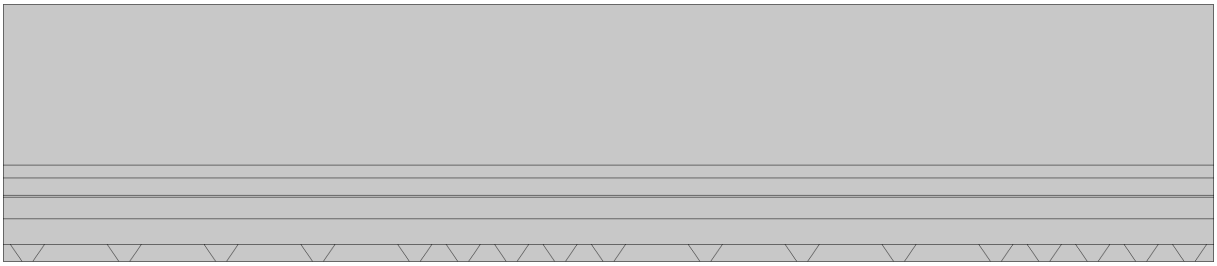

(e)

Figure 4.8: (a) A flat and four texture cells with (b) 15, (c) 25, (d) 35 and (d) 17 random texture units. The upper entire area is air (6000 nm), and the lower area is solar cell, from whose top to bottom are GaAs top contact (300 nm), InGaP top cell (400 nm), tunnel junction (50 nm), GaAs bottom cell (500 nm) and GaAs rear contact (1000 nm). Width of these cells is $2000\sqrt{2}$ nm. The position of each layer is demonstrated in Figure App.5, Appendix I – Figures. The size of texture units in (b) (d) is defined by the model in Figure 4.1 extracted from SEM image.

Based on the data from [44–46], the value of n_1 and n_2 under divergent wavelength are used to calculate R_s and the result is in Table 4.4.

Table 4.4: Reflectance R_s on the interface between GaAs contact layer and InGaP top cell under wavelength of 400, 700 and 1000 nm.

Wavelength (nm)	n_1 (GaAs) [44, 45]	n_2 (InGaP) [46]	R_s
400	4.4590	4.5537	0.0001
700	3.7700	3.4943	0.0014
1000	3.5039	3.2193	0.0018

Due to the too small R_s, the reflectance on the interface between GaAs contact layer and InGaP top cell is ignored in this paper.

Figure 4.9 demonstrates the 400 nm wavelength electromagnetic field distribution in flat cell and texture cells with 15, 25, 35 and 17 random texture units. In the outer space of solar cells, electromagnetic wave from source interferes with that reflected back by front surface of solar cells. Its maximum electric field module is supposed to be

$$360 \times (1 + R_s\,(Air\ to\ GaAs,\ 400\ nm)) = 504.504\ V/m. \tag{4.5}$$

Due to the field with high photon energy, almost all incident electromagnetic waves are absorbed by both InGaP and GaAs subcells, for which the electric field module inside solar cells tends to be zero.

Figure 4.10 shows the electric field module of proposed solar cells under 700 nm wavelength electromagnetic field source. The interference effect concentrates not only in the area between input and front surface of solar cells but also the area between the front and rear surfaces of solar cells. For the flat cell, the high electric field module concentrates in both air and rear contact area. The PV active layer shows its relatively lower electric field module for absorptive effect but the absorptivity of 700 nm photons is apparently lower than that of 400 nm as analyzed in Chapter 2. For texture cells with 15 and 17 random texture units, maximum value shows up not only in the air but also inside the solar cell, especially at the area near the interval between two adjacent texture units. This is because the electromagnetic wave reflected back by the interval interferes with that by side surface of conical frustum texture units near by. Also, in these two kinds of cells, electromagnetic field is detected on their both sides, which proves that scattering occurs inside texture solar cells. As for the texture cells with 25 and 35 units, these is no maximum value inside solar cells and that outside the solar cells are obviously weaker and disperse, which indicates that the absorptivity is enhanced.

The result under 1000 nm source is demonstrated in Figure 4.11, where the maximum value concentrates in, mostly, the air. There is no absorption in this case for the 1.24 eV (1000 nm) too low photon energy. In the flat cell, all incident electromagnetic wave would be reflected back, interfering with the source in the area of air. The intensity is supposed to be $(360 \times 2 =)\ 720\ V/m$. For these texture cells, the maximum value is lower than that of the flat cell due to scattering, as the field detected on the side of each cells in Figure 4.11.

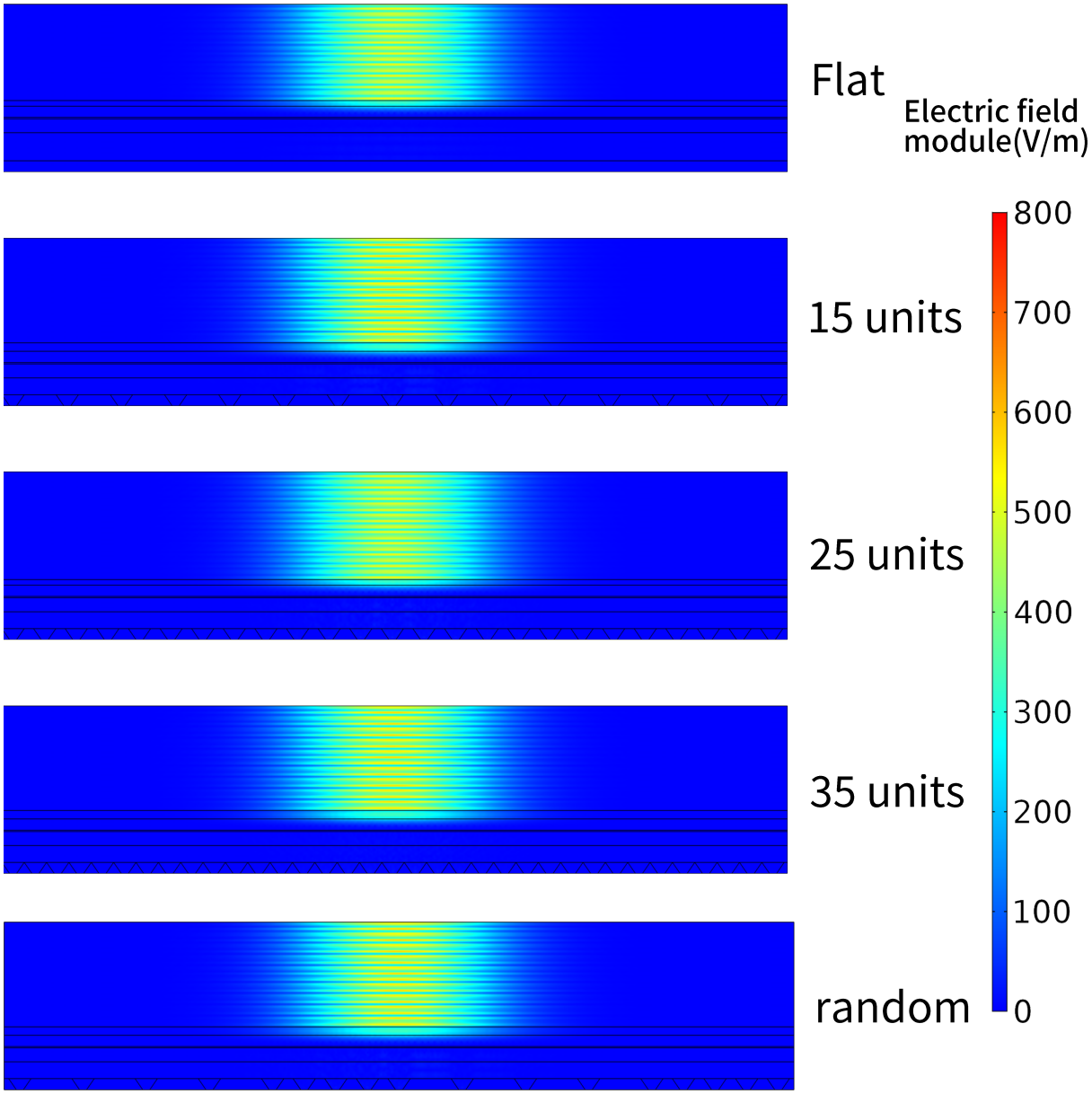

Figure 4.9: Distribution of Electromagnetic field module with wavelength 400nm. From the first to the last one are flat cell and texture ones with 15, 25, 35, and 17 random texture units.

A line segment, as shown in Figure 4.12, is set above these cells in the area of air to calculate the flux of electromagnetic wave reflected back by the front and rear surfaces of each cell. The integral of electromagnetic field vector on the upward normal direction is given by

$$\mathbf{\Phi} = \int_{-7E-6}^{7E-6} \mathbf{E} \cos\theta dx, \tag{4.6}$$

where Φ is the flux, E is the module of the applied electromagnetic field on an arbitrary point and θ is the included angle between $\mathbf{E}$ and the defined normal direction. The flux of input electromagnetic field is

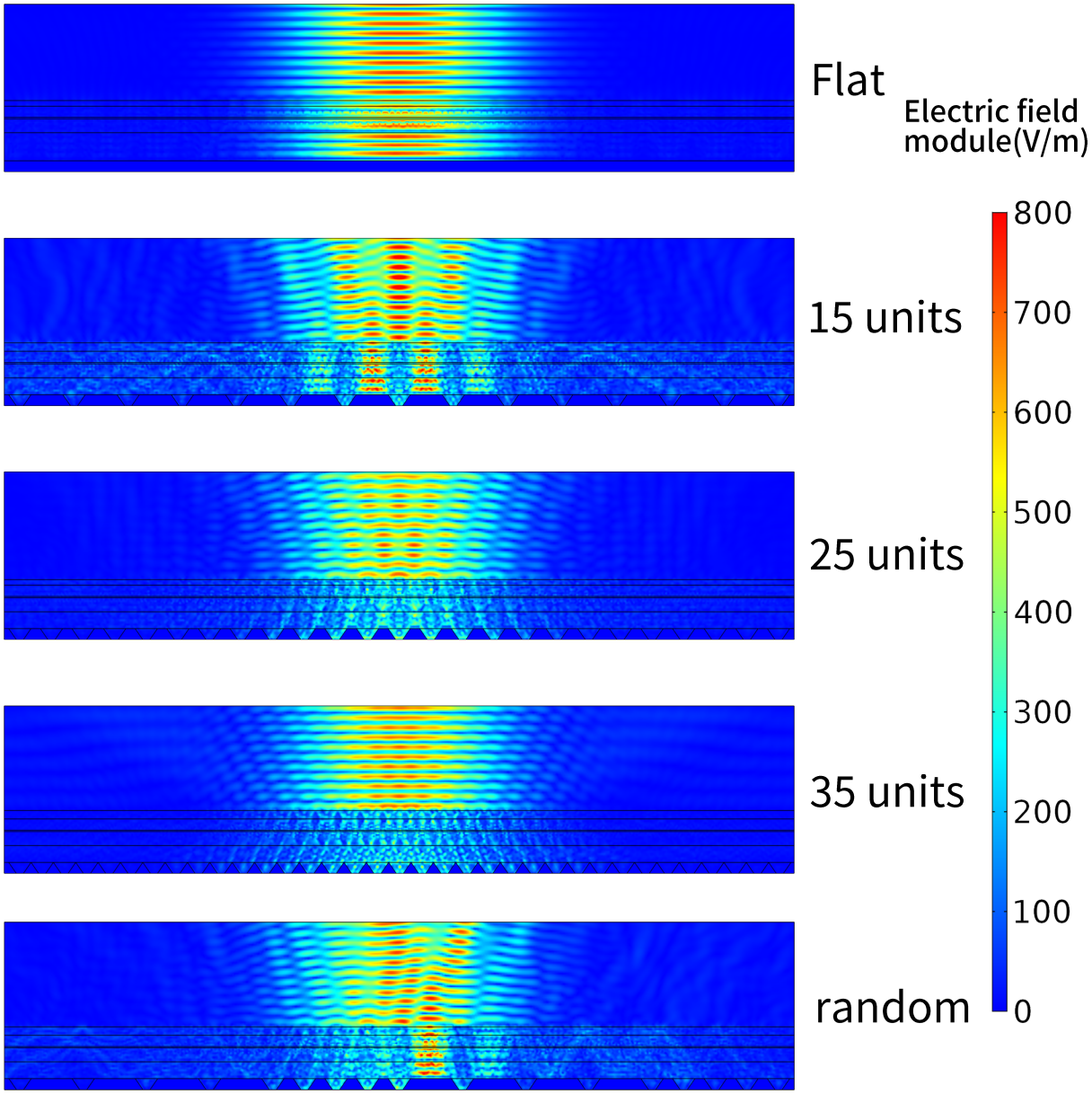

Figure 4.10: Distribution of Electromagnetic field module with wavelength 700nm. From the first to the last one are flat cell and texture ones with 15, 25, 35, and 17 random texture units.

$$\Phi_0 = \int_{-7E-6}^{7E-6} E_0 \cos\theta dx = 5 \times 10^{-3}\ V, \tag{4.7}$$

where $\cos\theta = 1$.

The result is illustrated in Figure 4.13 where source wavelength from 100 to 1000 nm is applied. The maxima on each line denote for constructive interference. On the other hand, the minima represent destructive interference. In the range of wavelength less than 660 nm, the flux remains in a relatively low level because of the large band gap of InGaP which is the top subcell. While in the wavelength range from 660 to 860 nm, the flux gradually increases due to the narrow band gap of GaAs and its decreasing as introduced in Section 3.1. And in the wavelength range larger than 860 nm locate the maximum points of each line for not absorption

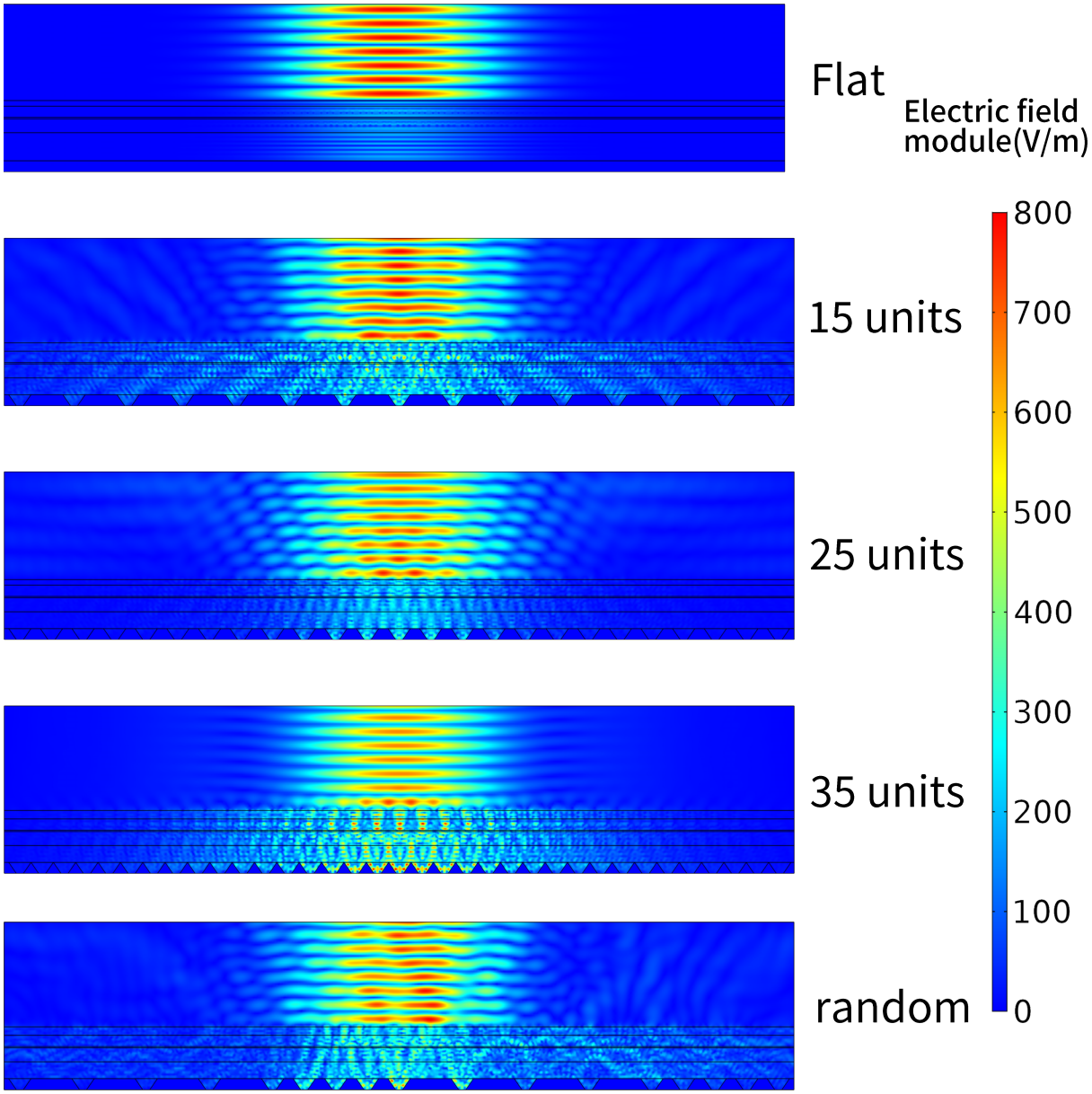

Figure 4.11: Distribution of Electromagnetic field module with wavelength 1000 nm. From the first to the last one are flat cell and texture ones with 15, 25, 35, and 17 random texture units.

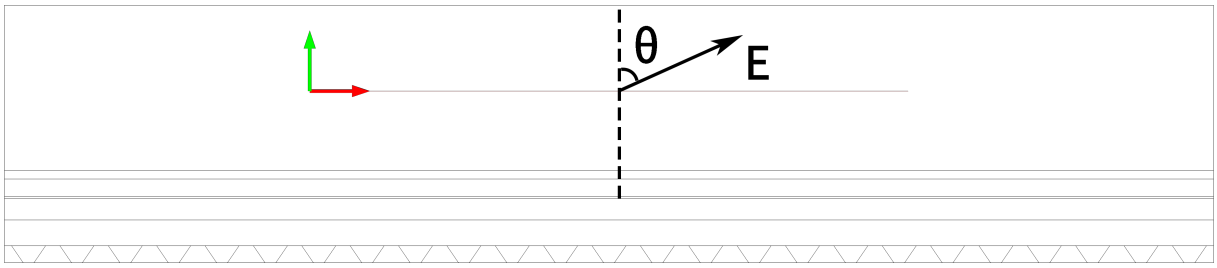

Figure 4.12: A line segment is drawn to calculate the flux of upward component of electromagnetic field. Green arrow is defined as the normal direction of flux to be calculated.

occurred on photons with such low energy.

In these texture cells especially the one with 15 units, there are in total three components of

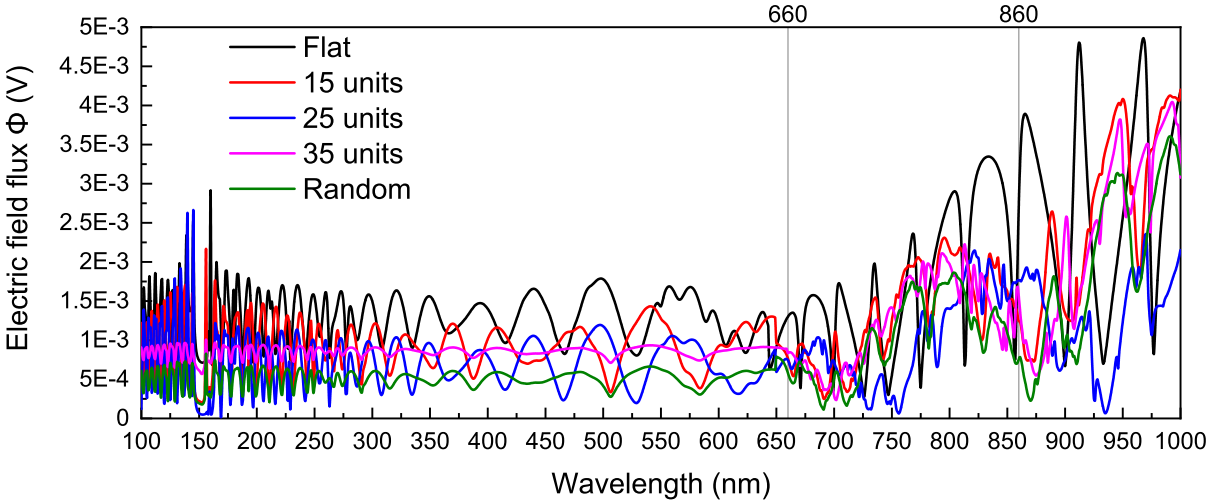

Figure 4.13: Electric field module (V/m) of the electromagnetic wave that has been reflected back by the top and rear surface of solar cells which are flat (black) and texture cells with 15 (red), 25 (blue), 35 (purple) and 17 random (green) texture units, from 100 nm to 1000 nm wavelength. Vertical reference line at wavelength 660 and 860 nm are, respectively, denoted for the band gap of InGaP and GaAs.

electromagnetic wave participating in the interference, as shown in Figure 4.14. The interference in Figure 4.13 is consist of three combinations – P_2&P_0, P_1&P_0 and P_2&P_1.

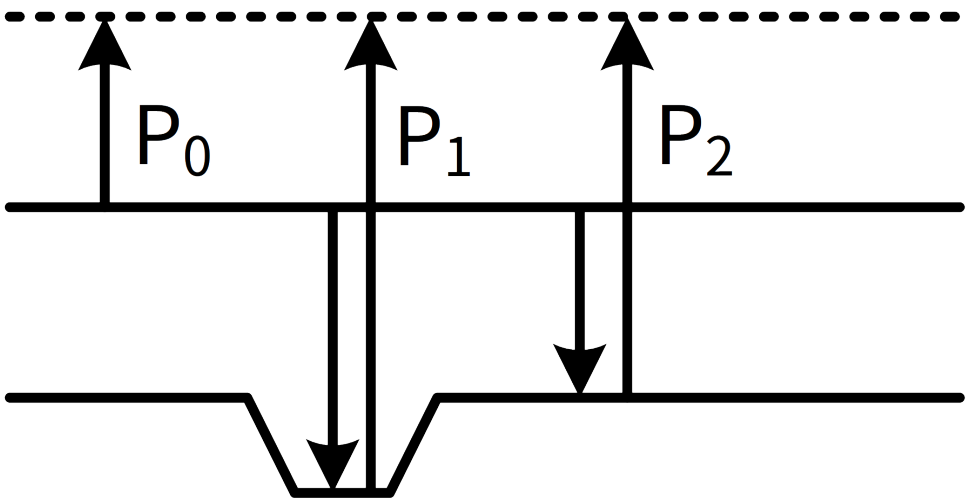

Figure 4.14: Three components contribute to the interference. P_0 is the component reflected directly by the front surface of solar cell; P_1 is the component reflected by the bottom of conical frustum texture and P_0 is that reflected by the intervals between two adjacent texture units. The incident electromagnetic wave that is reflected by the side surface of conical frustum texture is ignored in this discussion due to its low proportion.

Their optical path difference is the key to calculate the wavelength of constructive interference. That is

$$\begin{bmatrix} P_2 - P_0 \\ P_1 - P_0 \\ P_1 - P_2 \end{bmatrix} = \begin{bmatrix} 3700 \\ 4500 \\ 800 \end{bmatrix} = \begin{bmatrix} l\lambda_l \\ m\lambda_m \\ n\lambda_n \end{bmatrix}, \tag{4.8}$$

where $l, m, n \in Z_+$ and $\lambda_l, \lambda_m, \lambda_n \in [100, 1000]$ represent for wavelength. The valid wavelength points are marked in circle as illustrated in Figure 4.15. Each circle denotes for a peak and Figure 4.15 explains well why the peak-to-peak distance increases from 100 to 1000 nm wavelength on each curve. In the short wavelength part especially lower than 500 nm, the peaks density is quite high and some peaks are near with or even overlap others near by, generating a new peak. While in the long wavelength part larger than 500 nm, the peaks density is relatively very low.

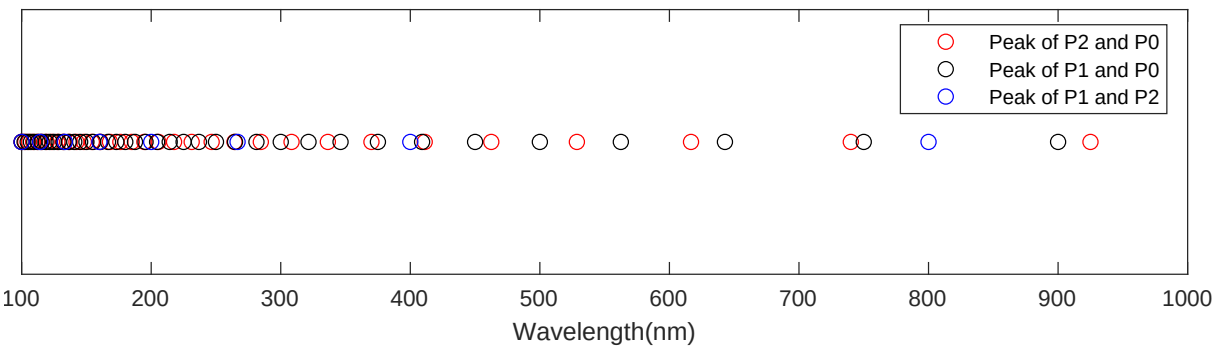

Figure 4.15: Peaks distribution from 100 to 1000 nm.

The peak-to-peak distance of flat cell and texture cells with 35 texture units is apparently larger than that of texture cells with 15 units. It is obvious in Figures 4.10 and 4.11 that a portion of electromagnetic wave reaching rear side of the texture cells with 15 units is directly reflected back by intervals between texture units instead of the bottom of conical frustum texture units, resulting in the portion of P_1 and P_2 are different in these two kinds of cells. In flat and 35-units-texture cells, interference consists of P_1&P_0 (black circle in Figure 4.15), no P_2. But in the 15-units-texture cell, P_2 does take a portion in the interference phenomenon (red and blue circle in Figure 4.15).

Chapter 5

Fabrication of the InGaP/GaAs multi-junction solar cell

Since the texture structure fabrication has been introduced in Chapter 3, this chapter will skip that part, introducing from layer transfer after the inverted lattice match sample structure. Figure 5.1 is the cross-sectional sample structure of the InGaP/GaAs two junction solar cell.

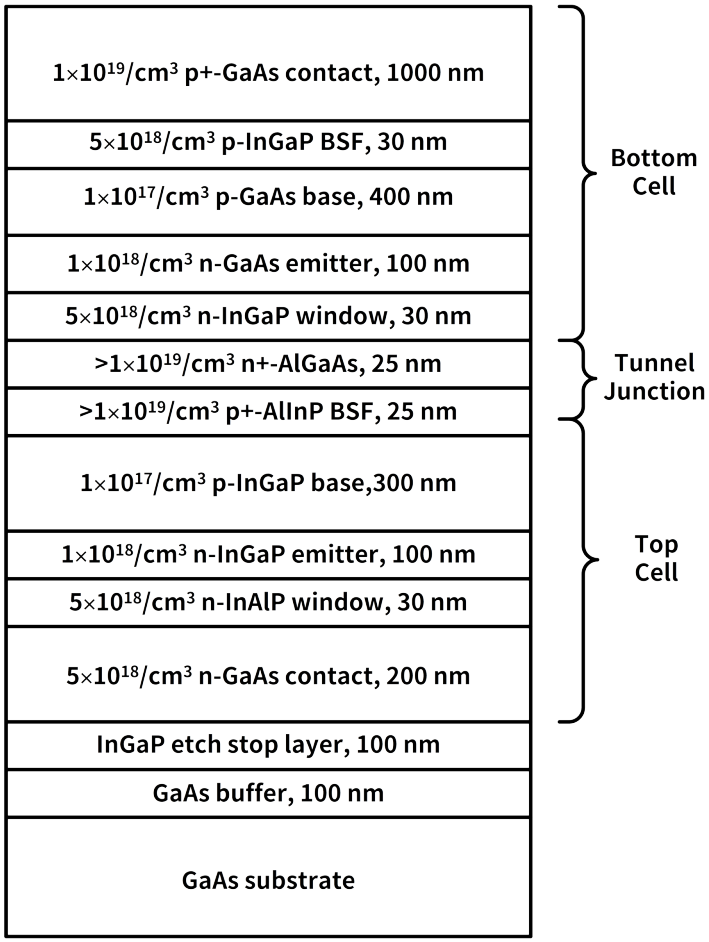

Figure 5.1: Layer structure of the inverted lattice match InGaP/GaAs two junction solar cell sample grown by MOVPE.

This sample is grown on a GaAs substrate by inverted lattice match MOVPE. Besides the GaAs substrate, from bottom to top are 100 nm non-doping GaAs buffer and InGaP etch stop layer, top InGaP cell, tunnel junction and GaAs bottom cell. The tunnel junction is heavily doped for a lower impedance.

1 Layer transfer

For an inverted lattice match growth solar cell, it is necessary to flip the sample and bond it on a support layer, which is called layer transfer, then remove the substrate.

On the left side are three main parts of the InGaP/GaAs two junction cell grown on GaAs substrate just as shown in Figure 5.1. The texture is first fabricated on front surface of the inverted sample. And a layer of Ag/Au electrode is coated on the textured surface for ohmic contact. Then the texture surface is bonded on a silicon support layer through polymer adhesive bonding by using "PHOTONEECE PW1200" polyimide on GaAs texture surface and "CYCROTENE 3022-46" resin on silicon surface. The GaAs substrate, buffer layer and InGaP etch stop layer are then removed through wet etching – 29% NH_4OH:30% H_2O_2:H_2O=1:1:2 for GaAs substrate and 35% HCL:H_2O=2:1 for InGaP etch stop layer. The finished device is shown in Figure 5.2.

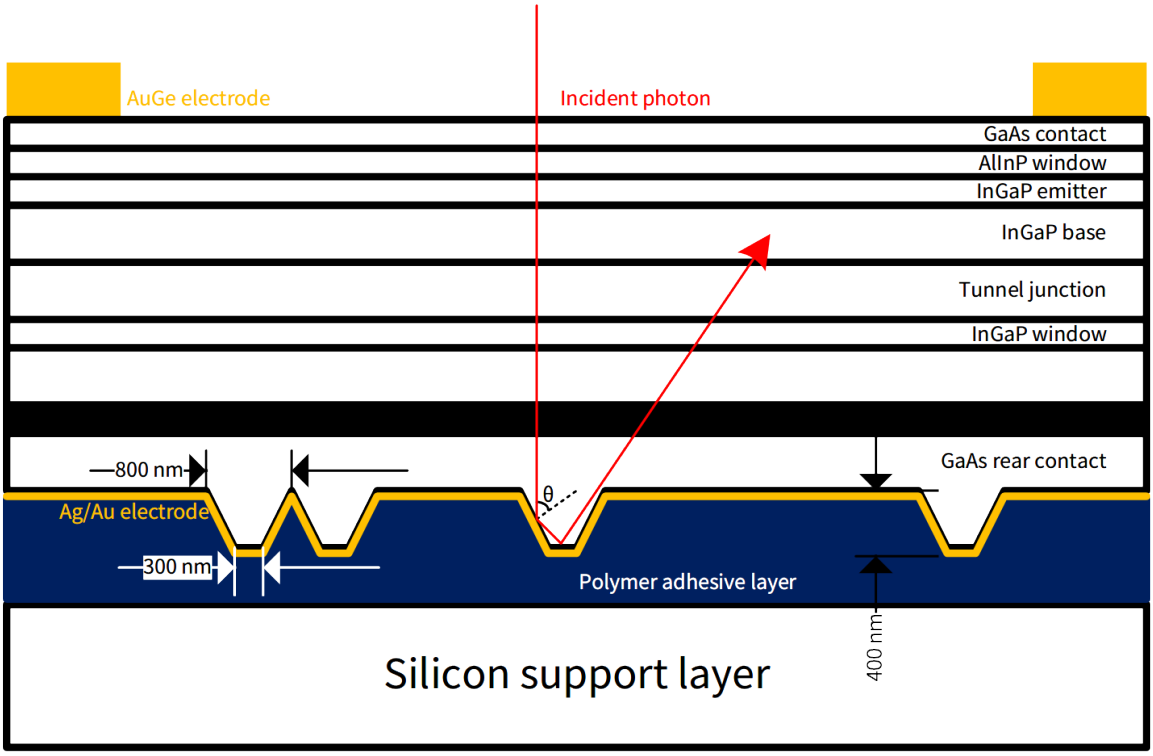

Figure 5.2: Cross-sectional structure of the InGaP/GaAs two junction cell.

On the front surface, AuGe electrode is fabricated by photolithography. As the red line shows, a photon enters perpendicularly into the cell, hitting the side of a texture units with incident angle θ, reflected towards its bottom surface where occurs the second time reflection. The propagation direction of this photon is eventually changed and trapped inside solar cell space.

2 Reflectance measurement

Reflectance of the testee solar cells are measured after removing GaAs substrate and InGaP etch stop layer. Source lights perpendicularly enter cells and are reflected back by front and rear surface of these samples simultaneously, after which the reflected lights interfere with each other at the space above the cells. The result is illustrated in Figure 5.3, in which the simulation results of flat, 17 random and 25 periodic texture cells are normalized as dot line. Three kinds of texture cells after treatment in hydrogen peroxide for 6, 12 and 24 hours are fabricated in the experiment, together with flat cell. Then tendency of measured curves is almost the same with simulation result, including the peak-to-peak distance as analyzed before. Within the absorption wavelength (< 860 nm), the overall reflectance from low to high are 12h, 6h, 24h and flat cells. While in the range of wavelength larger that 860 nm, the sequence is 6h, 12h, 24h and flat ones. The absorption does have been enhanced by texture structure. And the most suitable treatment duration in hydrogen peroxide ranges from 6 to 12 hours. The simulated result of flat and random texture cells offer the highest and lowest reflectance, respectively. Different from the measured results which own high reflectance even if at the destructive interference wavelength. But in the normalized simulation result, the reflectance at destructive interference wavelength is quite low, matching with the clear boundary between two constructive interference area in Figure 4.11. The ideal geometry of simulation model makes the interference rules strictly obeyed, which is apparently difference from the real situation.

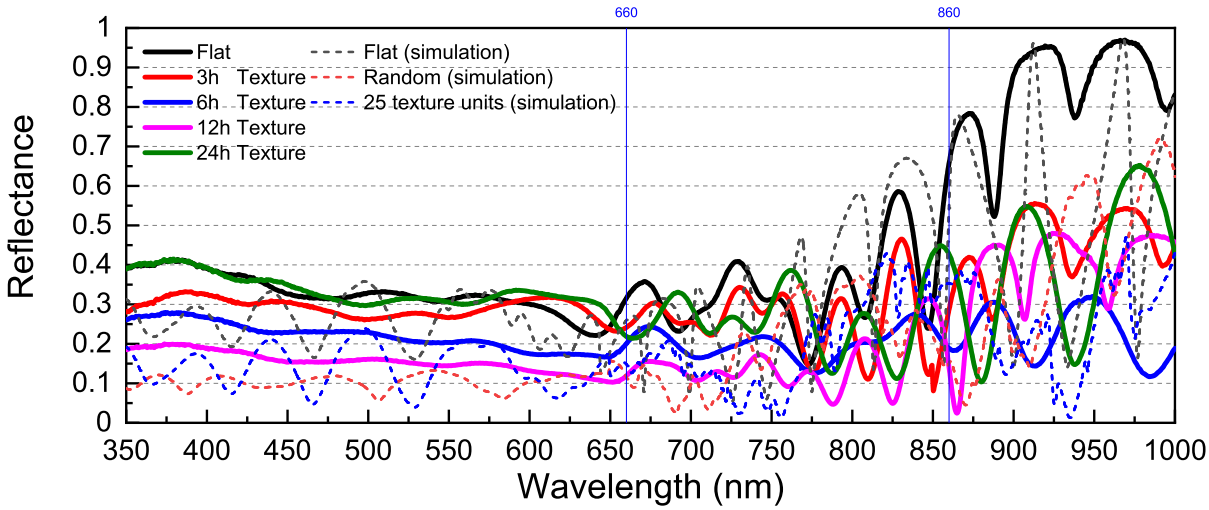

Figure 5.3: The reflectance of cells which is flat (black) and are treated in hydrogen peroxide for 3 (red), 6 (blue), 12 (purple) and 24 (green) hours, respectively . The simulation result of a flat cell (black), the cell with 17 random texture units (red) and the one with periodic 25 texture units are normalized by Equation (4.7) and denoted in dash lines. Vertical reference line at wavelength 660 and 860 nm are denoted for the band gap of InGaP and GaAs, respectively.

Notice that peaks of two flat cells – fabricated and simulated – matched well especially in the range of wavelength larger than 800 nm, so as to the 17 random texture cell in simulation with 6-hours-treated fabricated cell. This indicates that the simulation model in Chapter 4 is quite accurate.

3 Output characteristic

Figure 5.4 demonstrates the I-V characteristic of flat and texture cells treated in hydrogen peroxide for 3, 6, 12 and 24 hours. Texture cells treated in hydrogen peroxide for 6 and 12 hours give the almost equal and maximum short circuit current density $8.72mA/cm^2$, following by that for 3 and 24 hours for their too-low and too-high texture density. The lowest short circuit current density $6.25mA/cm^2$ is given by the flat cell. Texture rear structure improves the short circuit current by approximately 40%, more than the 5.81% calculation result in Section 2, Chapter 2. The difference of open circuit current among each sample may be caused by sample damage during long experiment process, especially the wet etching.

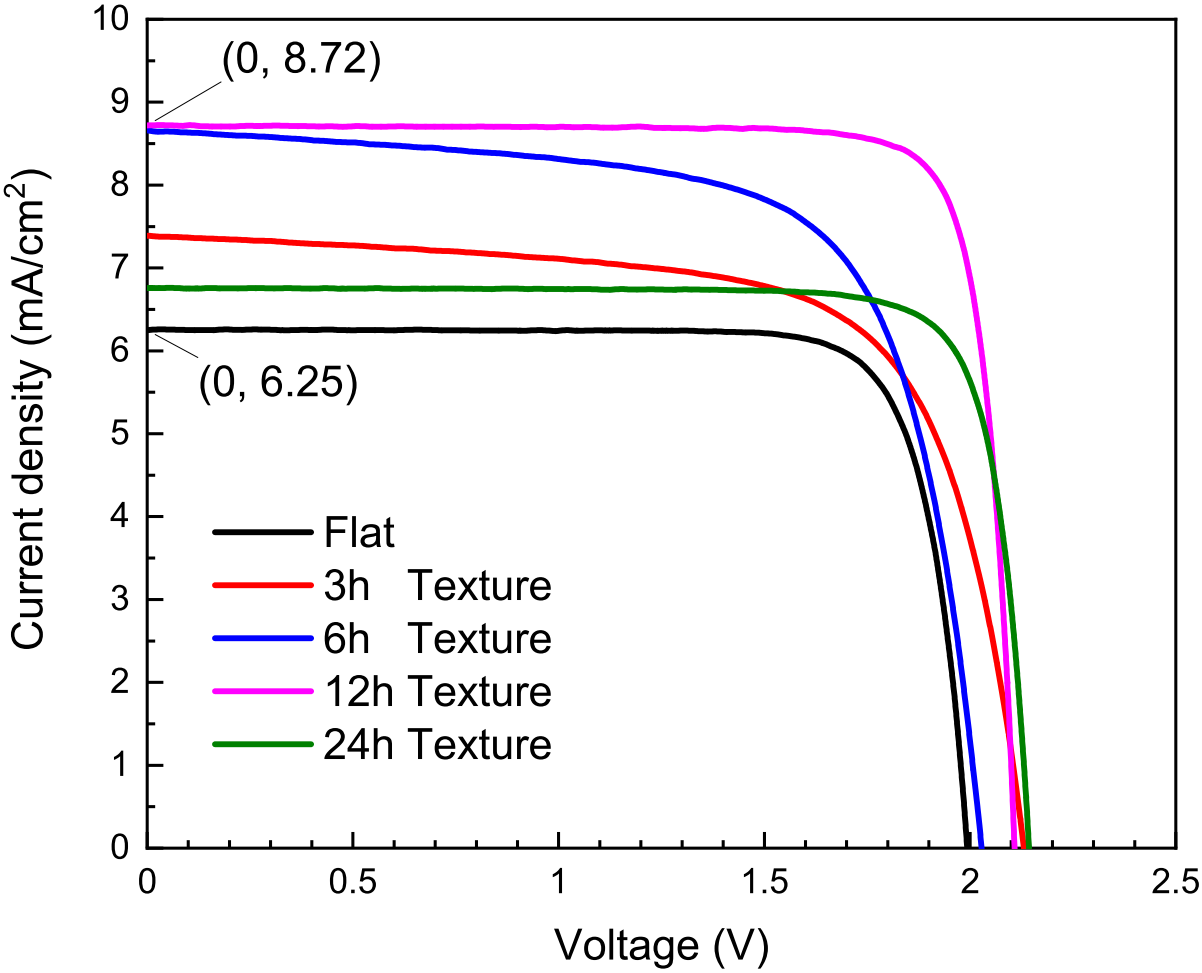

Figure 5.4: I–V characteristics under AM 1.5G illumination for a flat cell (black) and several texture cells treated by hydrogen peroxide for 3 (red) , 6 (blue) , 12 (purple) and 24 (green) hours.

Chapter 6

Summary

This project proposed a an InGaP/GaAs thin-film multi-junction solar cell whose photocurrent is enhanced by colloidal lithography.

In Chapter 2, a mathematical model for PV active layer thickness calculation is first introduced. The absorptivity of cells whose rear side are texture, flat and substrate in certain thickness is calculated and compared. Then a vital factor for multijunction solar cells – current matching – is taken into consideration. The influence of each subcell's thickness on the short circuit current of all subcells has been analyzed – the increasing thickness of one subcell enhances the absorptive effect of this subcell but cut the output performance of the other for those two subcells are in competitive relation for photons with energy in their common absorption range. For the increasing top InGaP subcell thickness, much more increment of GaAs subcell thickness is required.

Fabrication process of colloidal lithography based texture structure is demonstrated in Chapter 3. How to cover a single-layer $\varnothing 500\ nm$ SiO_2 colloidal mask is the key for high density texture structure. Hydrophilic treatment of GaAs surface by hydrogen peroxide is the selected solution in this project. A two-step spin coating is applied to prevent vertical aggregation of SiO_2 particles.

The obtained texture morphology is extracted to establish models in Chapter 4's ray optics simulation and electromagnetic field simulation. Results of both simulations indicate that the conical frustum texture morphology can effectively change propagation direction of incident light. In other words, it can effectively trap incident photons inside solar cell space.

Chapter 5 illustrates the experiment process except for texture fabrication. Reflectance of cells is measured and compared with that from electromagnetic field simulation, which suggests that the simulation model is accurate and hydrogen peroxide treatment between 6 and 12 hours is the most appropriate.

In conclusion, light trapping is necessary and effective for III–V multijunction solar cells. Refer to the optics simulation and experiment result, neither too-high nor too-low texture density can produce obvious photocurrent enhancement for the InGaP/GaAs dual junction solar cell. In this case, hydrophilic treatment in hydrogen peroxide for from 6 to 12 hours is appropriate to give an approximately 40% photocurrent enhancement.

Reference

[1] Greg Kopp and Judith L Lean. A new, lower value of total solar irradiance: Evidence and climate significance. *Geophysical Research Letters*, 38(1), 2011.

[2] REN21. Renewables 2019: Global status report. *REN21 Secretariat*, 2019.

[3] Wikimedia Commons. File:solar spectrum en.svg — wikimedia commons, the free media repository, 2019. [Online; accessed 27-May-2020].

[4] IEA-PVPS – IEA Photovoltaic Power Systems Programme TCP, May 2020. [Online; accessed 27. May 2020].

[5] Solar Power Europe. Global market outlook for solar power 2018–2022. *Solar Power Europe: Brussels, Belgium*, 2018.

[6] Wikimedia Commons. File:solargif1.gif — wikimedia commons, the free media repository, 2019. [Online; accessed 27-May-2020].

[7] Pierre Auger. Sur les rayons β secondaires produits dans un gaz par des rayons x. *CR Acad. Sci.(F)*, 177:169, 1923.

[8] WTRW Shockley and WT Read Jr. Statistics of the recombinations of holes and electrons. *Physical review*, 87(5):835, 1952.

[9] Re N Hall. Electron-hole recombination in germanium. *Physical review*, 87(2):387, 1952.

[10] Bart Van Zeghbroeck. Principles of semiconductor devices. *Colarado University*, 34, 2004.

[11] Wikipedia contributors. Direct and indirect band gaps — Wikipedia, the free encyclopedia. https://en.wikipedia.org/w/index.php?title=Direct_and_indirect_band_gaps&oldid=953458470, 2020. [Online; accessed 28-May-2020].

[12] JE Parrott. Radiative recombination and photon recycling in photovoltaic solar cells. *Solar energy materials and solar cells*, 30(3):221–231, 1993.

[13] Tom Markvart and Luis Castañer. *Chapter IA-2. Semiconductor Materials and Modelling*, pages 95–121. 12 2003.

[14] Cun-Zheng Ning, Letian Dou, and Peidong Yang. Bandgap engineering in semiconductor alloy nanomaterials with widely tunable compositions. *Nature Reviews Materials*, 2(12):1–14, 2017.

[15] William Shockley and Hans J Queisser. Detailed balance limit of efficiency of p-n junction solar cells. *Journal of applied physics*, 32(3):510–519, 1961.

[16] Jeffrey F Wheeldon, Christopher E Valdivia, Alexandre W Walker, Gitanjali Kolhatkar, Abdelatif Jaouad, Artur Turala, Bruno Riel, Denis Masson, Norbert Puetz, Simon Fafard, et al. Performance comparison of algaas, gaas and ingap tunnel junctions for concentrated multijunction solar cells. *Progress in Photovoltaics: Research and Applications*, 19(4):442–452, 2011.

[17] Jose Maria Roman. State-of-the-art of iii-v solar cell fabrication technologies, device designs and applications. *Advanced Photovoltaic Cell Design*, 4, 2004.

[18] Natalya V Yastrebova et al. High-efficiency multi-junction solar cells: Current status and future potential. *Centre for Research in Photonics, University of Ottawa*, 2007.

[19] Vijay Kris Narasimhan and Yi Cui. Nanostructures for photon management in solar cells. *Nanophotonics*, 2(3):187–210, 2013.

[20] Roberto Murri. *Silicon Based Thin Film Solar Cells*. Bentham Science Publishers, 2013.

[21] Inductively Coupled Plasma - Reactive Ion Etching (ICP-RIE) | Corial, Jun 2020. [Online; accessed 15. Jun. 2020].

[22] Martin A Green, Ewan D Dunlop, Jochen Hohl-Ebinger, Masahiro Yoshita, Nikos Kopidakis, and Anita WY Ho-Baillie. Solar cell efficiency tables (version 55). *Progress in Photovoltaics: Research and Applications*, 28(NREL/JA-5900-75827), 2019.

[23] PT Chiu, DC Law, RL Woo, SB Singer, D Bhusari, WD Hong, A Zakaria, J Boisvert, S Mesropian, RR King, et al. 35.8% space and 38.8% terrestrial 5j direct bonded cells. In *2014 IEEE 40th Photovoltaic Specialist Conference (PVSC)*, pages 0011–0013. IEEE, 2014.

[24] Maxime Giteau, Kentaroh Watanabe, Hassanet Sodabanlu, Naoya Miyashita, Masakazu Sugiyama, Andrea Cattoni, Stéphane Collin, Jean-François Guillemoles, and Yoshitaka Okada. Epitaxial lift-off of ultrathin heterostructures for hot-carrier solar cell applications. In *2019 Compound Semiconductor Week (CSW)*, pages 1–1. IEEE, 2019.

[25] Maxime Giteau, Kentaroh Watanabe, Naoya Miyashita, Hassanet Sodabanlu, Julie Goffard, Amaury Delamarre, Daniel Suchet, Ryo Tamaki, Zacharie Jehl, Laurent Lombez, et al. Light absorption enhancement in ultra-thin layers for hot-carrier solar cells: first developments towards the experimental demonstration of an enhanced hot-carrier effect with light trapping. In *Physics, Simulation, and Photonic Engineering of Photovoltaic Devices VIII*, volume 10913, page 109130D. International Society for Optics and Photonics, 2019.

[26] Hitoshi Sai, Haijun Jia, and Michio Kondo. Impact of front and rear texture of thin-film microcrystalline silicon solar cells on their light trapping properties. *Journal of Applied Physics*, 108(4):044505, 2010.

[27] Alexandre Gaucher, Andrea Cattoni, Christophe Dupuis, Wanghua Chen, Romain Cariou, Martin Foldyna, Lo1□c Lalouat, Emmanuel Drouard, Christian Seassal, Pere Roca i Cabarrocas, et al. Ultrathin epitaxial silicon solar cells with inverted nanopyramid arrays for efficient light trapping. *Nano letters*, 16(9):5358–5364, 2016.

[28] Nikhil Deep Gupta and Vijay Janyani. Design and analysis of light trapping in thin film gaas solar cells using 2-d photonic crystal structures at front surface. *IEEE Journal of Quantum electronics*, 53(2):1–9, 2017.

[29] Yi-An Chang, Zhen-Yu Li, Hao-Chung Kuo, Tien-Chang Lu, Su-Fan Yang, Li-Wen Lai, Li-Hong Lai, and Shing-Chung Wang. Efficiency improvement of single-junction ingap solar cells fabricated by a novel micro-hole array surface texture process. *Semiconductor science and technology*, 24(8):085007, 2009.

[30] Lin ZhU, Anurag Reddy, Kentaroh Watanabe, Masakazu Sugiyama, Yoshiaki Nakano, and Hidefumi Akiyama. Design of ingap/gaas/lngaas multi-junction cells with reduced layer thicknesses using light-trapping rear texture. In *2017 IEEE 44th Photovoltaic Specialist Conference (PVSC)*, pages 3528–3533. IEEE, 2017.

[31] Sanjeev J Koppal. Lambertian reflectance. *Computer Vision: A Reference Guide*, pages 441–443, 2014.

[32] Frank L Pedrotti, Leno M Pedrotti, and Leno S Pedrotti. *Introduction to optics*. Cambridge University Press, 2017.

[33] Jeffery L Gray. The physics of the solar cell. *Handbook of photovoltaic science and engineering*, 2:82–128, 2011.

[34] Raul Mayoral, Joaquin Requena, José S Moya, Cefe López, Adelaida Cintas, Hernán Miguez, Francisco Meseguer, Luis Vázquez, Miguel Holgado, and Álvaro Blanco. 3d long-range ordering in ein sio2 submicrometer-sphere sintered superstructure. *Advanced Materials*, 9(3):257–260, 1997.

[35] H Miguez, F Meseguer, C Lopez, A Mifsud, JS Moya, and L Vazquez. Evidence of fcc crystallization of sio2 nanospheres. *Langmuir*, 13(23):6009–6011, 1997.

[36] H Mıguez, Cefe López, Francisco Meseguer, A Blanco, Luis Vázquez, R Mayoral, Manuel Ocaña, Vicente Fornés, and A Mifsud. Photonic crystal properties of packed submicrometric sio 2 spheres. *Applied Physics Letters*, 71(9):1148–1150, 1997.

[37] Jason D Forster, Jin-Gyu Park, Manish Mittal, Heeso Noh, Carl F Schreck, Corey S O' Hern, Hui Cao, Eric M Furst, and Eric R Dufresne. Assembly of optical-scale dumbbells into dense photonic crystals. *ACS nano*, 5(8):6695–6700, 2011.

[38] U Ch Fischer and Hans P Zingsheim. Submicroscopic pattern replication with visible light. *Journal of Vacuum Science and Technology*, 19(4):881–885, 1981.

[39] SS Shinde, S Park, and J Shin. Spin synthesis of monolayer of sio 2 thin films. *Journal of Semiconductors*, 36(4):043002–10, 2015.

[40] Wikimedia Commons. File:schematic silica gel surface.png — wikimedia commons, the free media repository, 2020. [Online; accessed 19-June-2020].

[41] Andrei V Bandura and Serguei N Lvov. The ionization constant of water over wide ranges of temperature and density. *Journal of physical and chemical reference data*, 35(1):15–30, 2006.

[42] Martin Wild, Doris Folini, Christoph Schär, Norman Loeb, Ellsworth G Dutton, and Gert König-Langlo. The global energy balance from a surface perspective. *Climate dynamics*, 40(11-12):3107–3134, 2013.

[43] A Börzsönyi, Zs Heiner, MP Kalashnikov, AP Kovács, and K Osvay. Dispersion measurement of inert gases and gas mixtures at 800 nm. *Applied optics*, 47(27):4856–4863, 2008.

[44] GE Jellison Jr. Optical functions of gaas, gap, and ge determined by two-channel polarization modulation ellipsometry. *Optical Materials*, 1(3):151–160, 1992.

[45] T Skauli, PS Kuo, KL Vodopyanov, TJ Pinguet, O Levi, LA Eyres, JS Harris, MM Fejer, B Gerard, L Becouarn, et al. Improved dispersion relations for gaas and applications to nonlinear optics. *Journal of Applied Physics*, 94(10):6447–6455, 2003.

[46] Mathias Schubert, V Gottschalch, Craig M Herzinger, Huade Yao, Paul G Snyder, and John A Woollam. Optical constants of ga x in1- x p lattice matched to gaas. *Journal of Applied Physics*, 77(7):3416–3419, 1995.

Appendix I – Figures

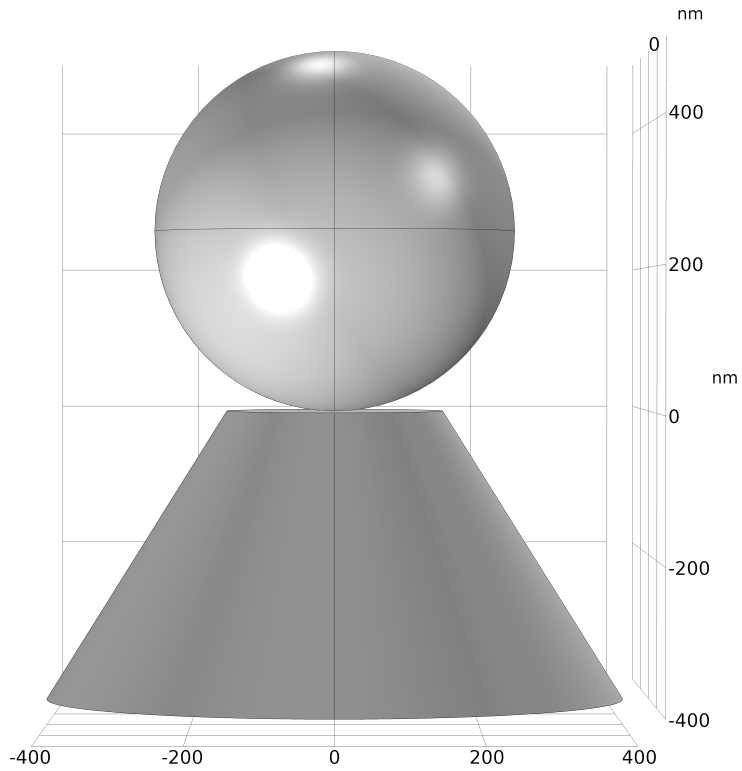

(a)

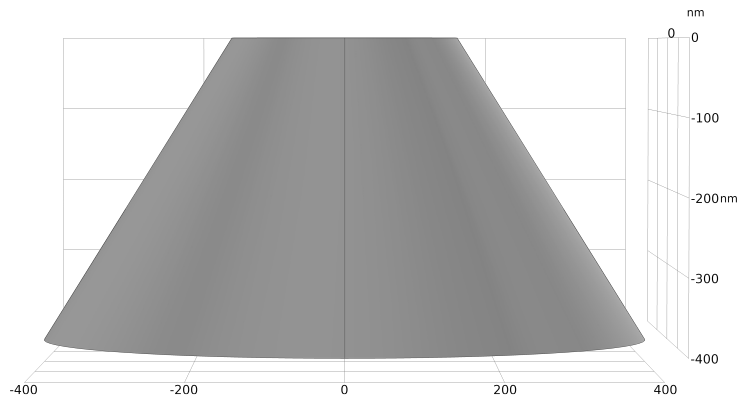

(b)

Figure App.1: The side view of a single texture units extracted from SEM image (a) with and (b) without SiO_2 particle on it.

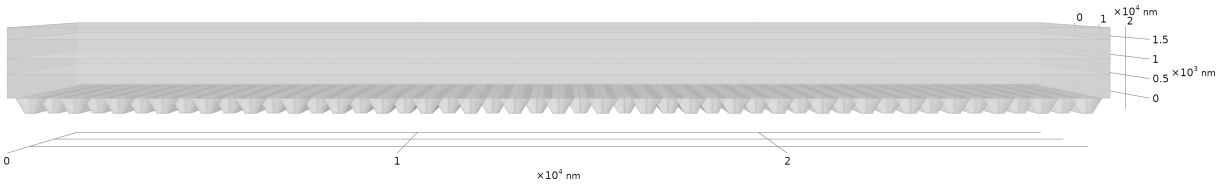

(a)

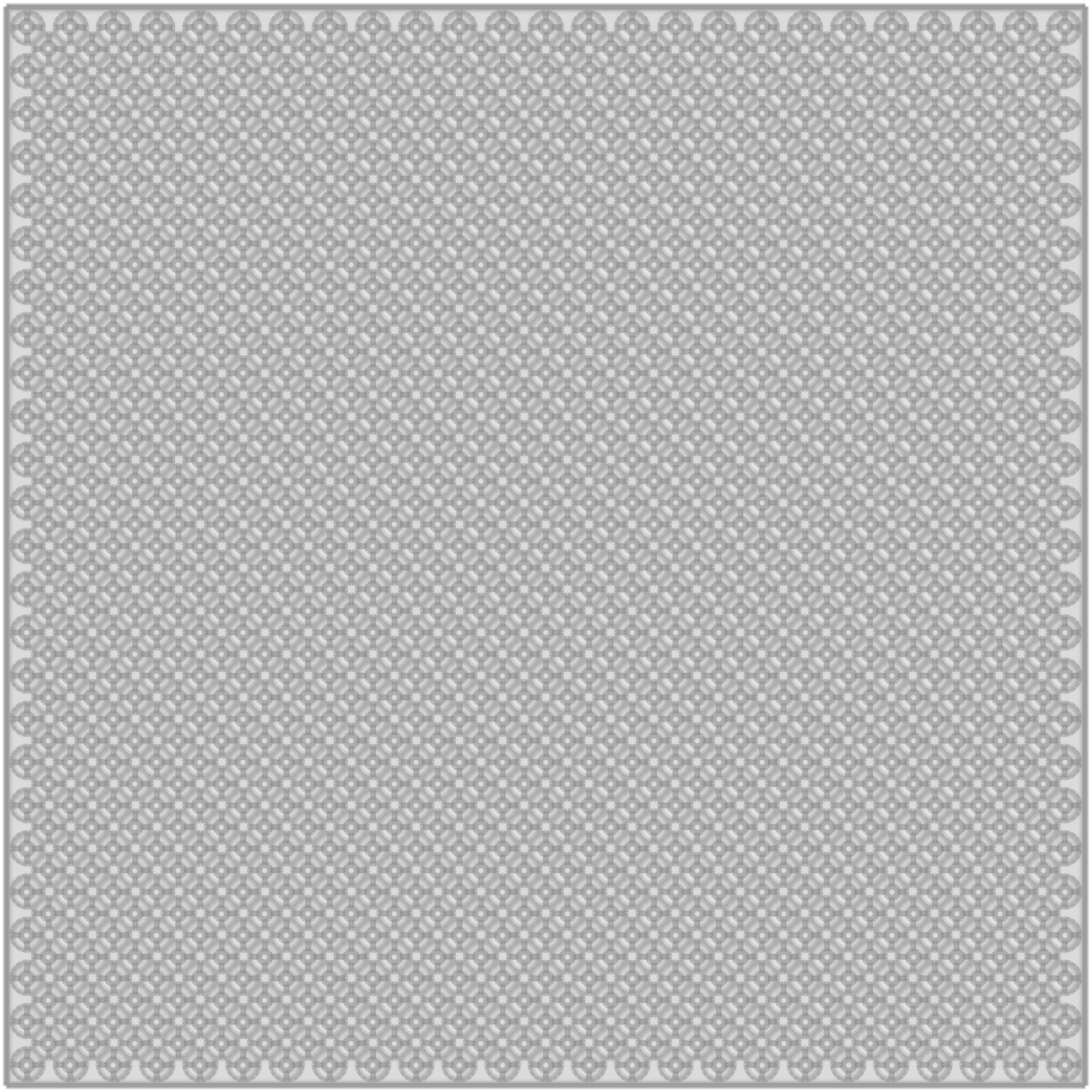

(b)

Figure App.2: The (a) side and (b) bottom view of texture cell.

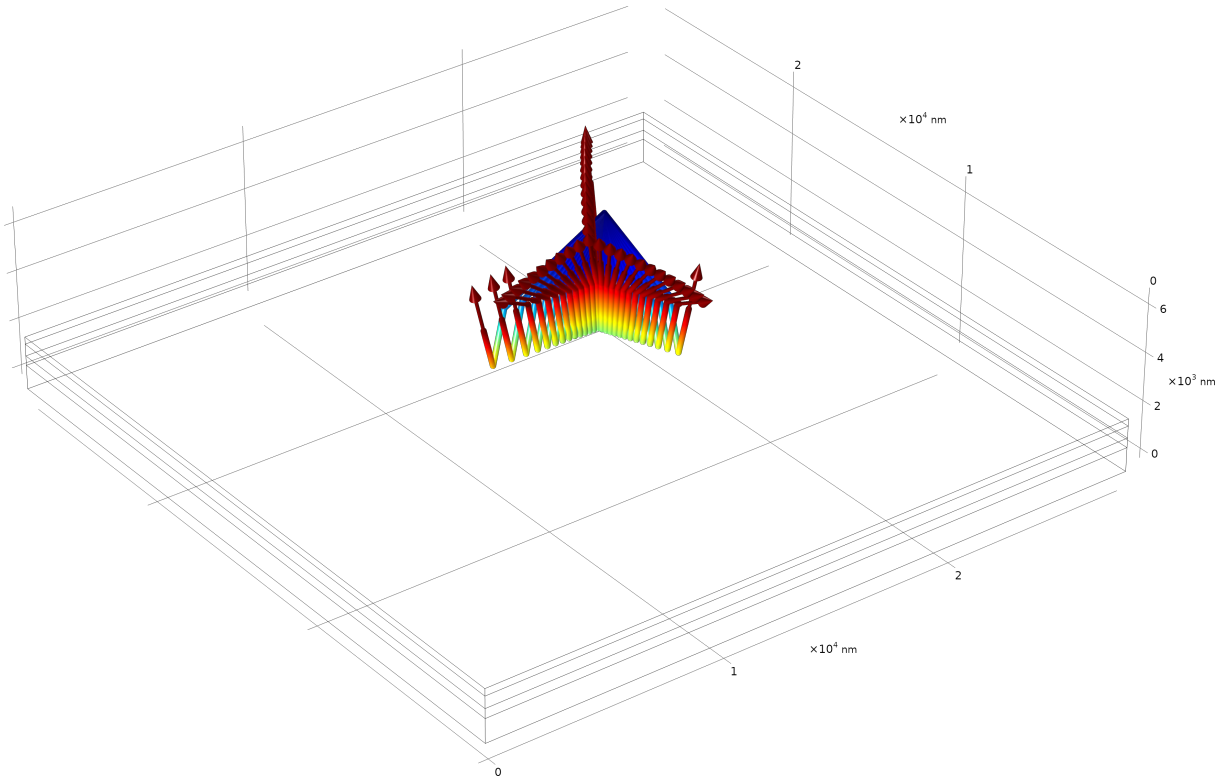

(a)

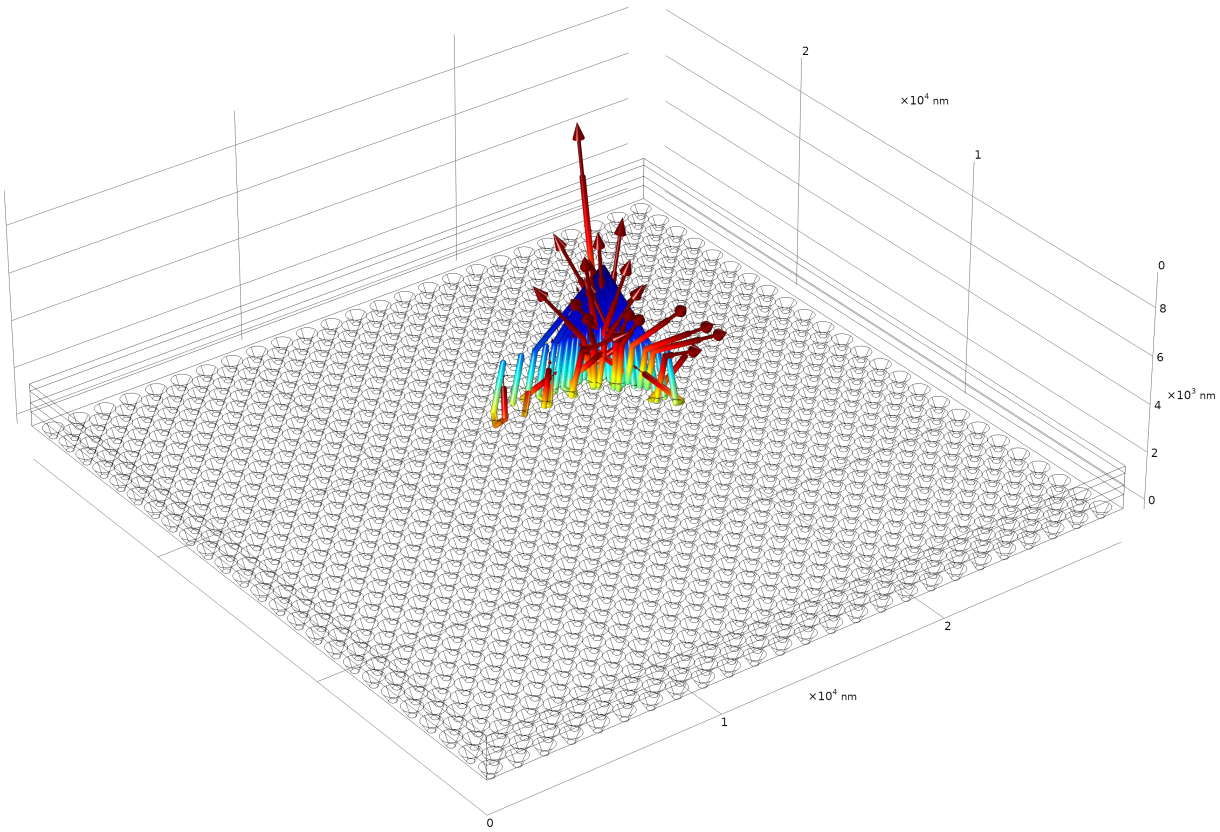

(b)

Figure App.3: 3D plot of (a) flat and (b) texture cells under grating light source.

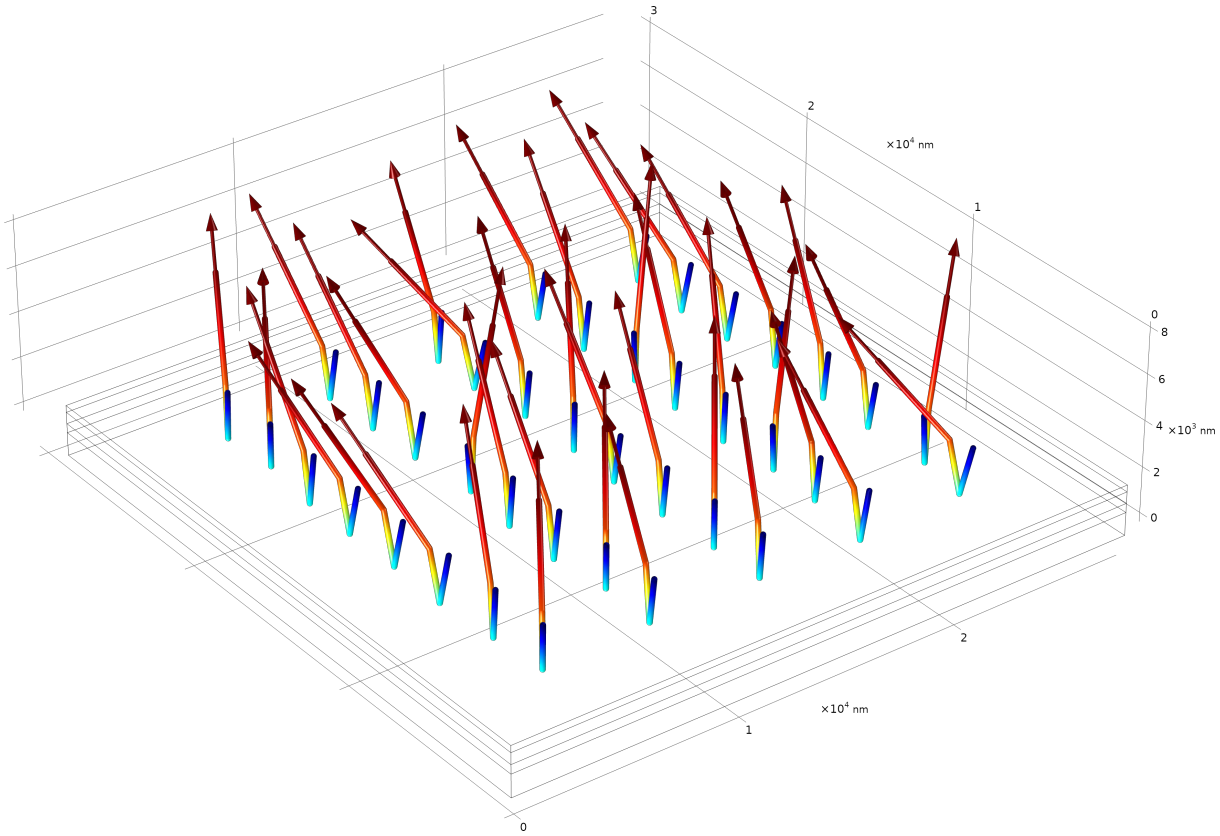

(a)

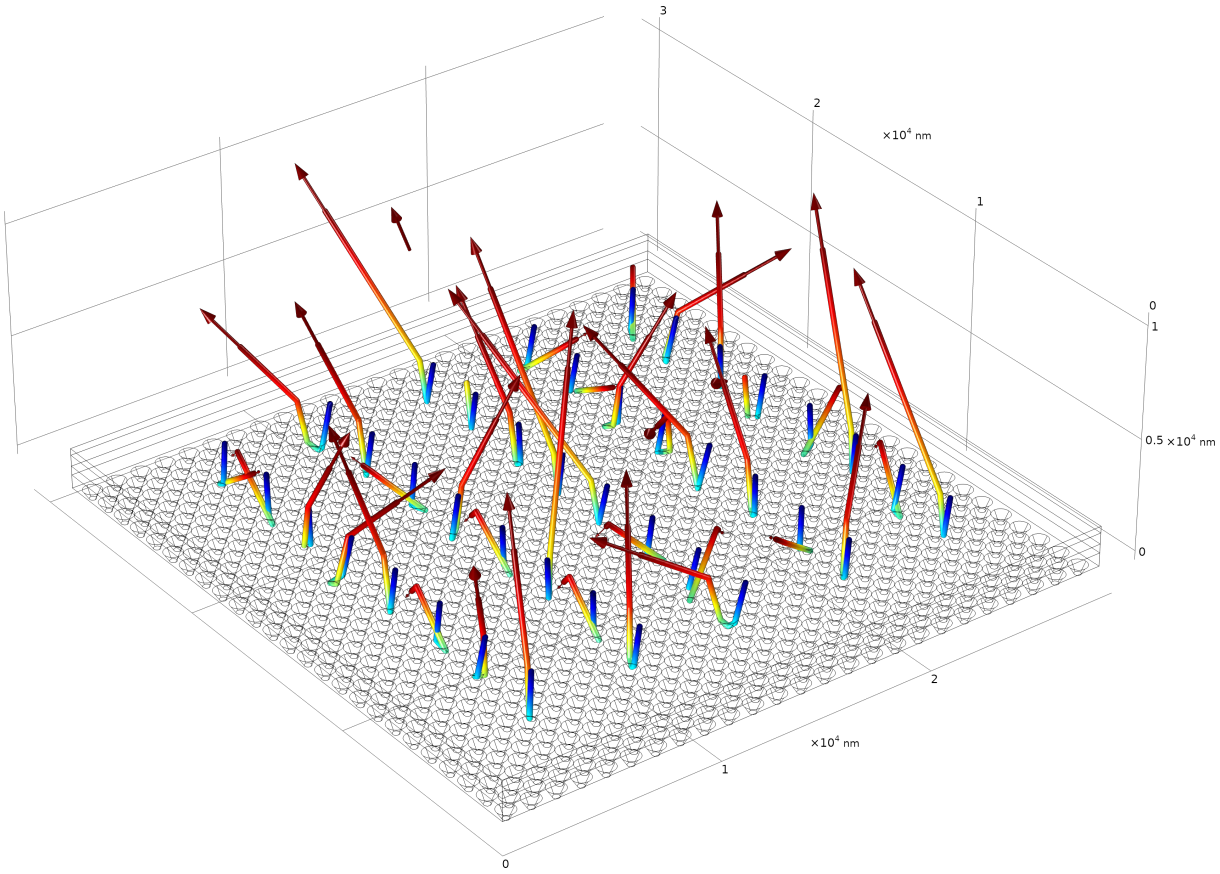

(b)

Figure App.4: 3D plot of (a) flat and (b) texture cells under natural light source.

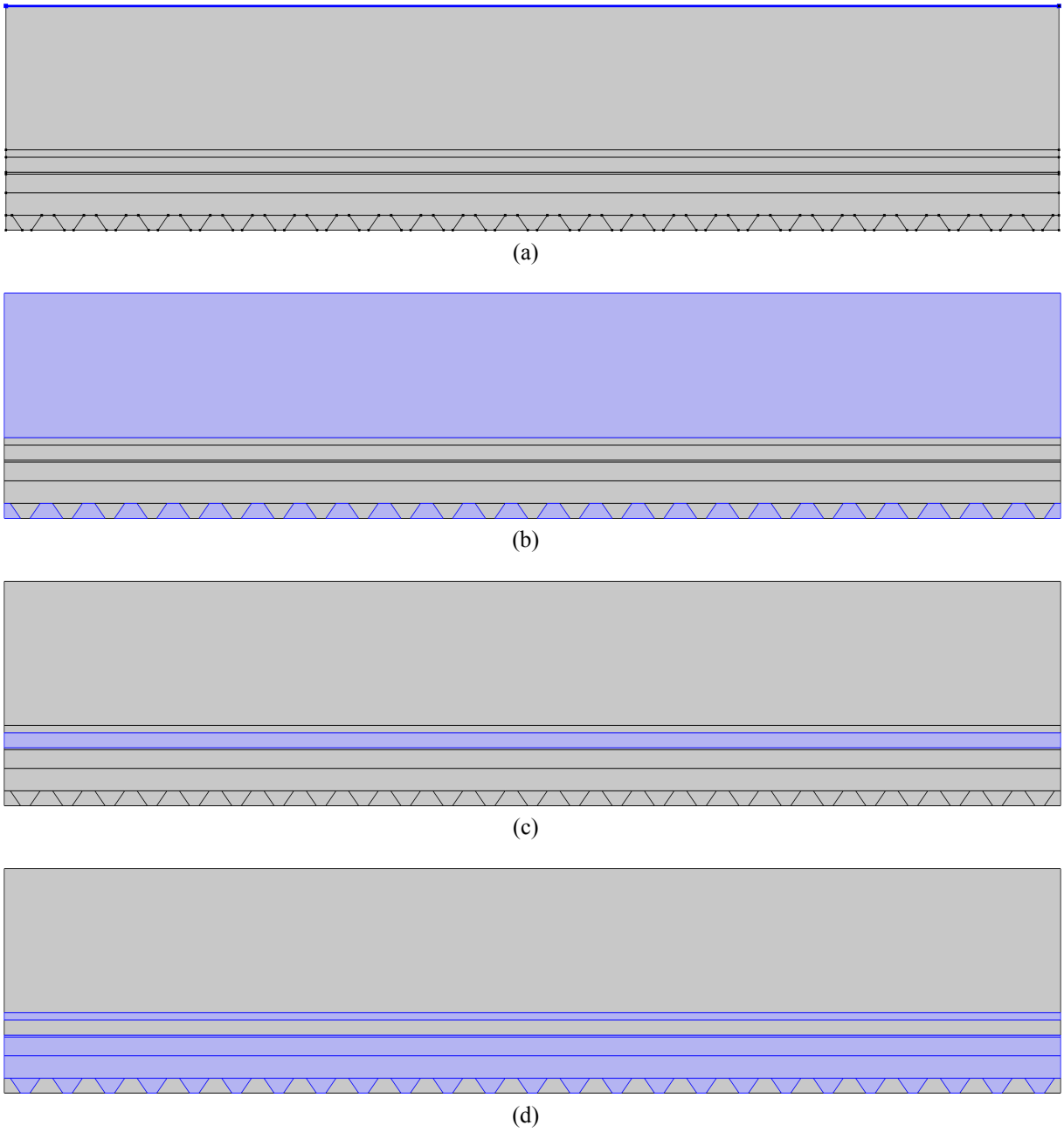

Figure App.5: Layers of solar cell in interference simulation. The light purple area from top to bottom are (a) input, (b) air, (c) InGaP top cell and (d) GaAs bottom cell and rear contact.

Appendix II – Source code

The Matlab source code of the model employed in Chapter 2 is listed below.

```
% Resolution is o.01 eV
% Interpolation for Reflectivity were Linear

% Defining cahrge units in coloumb
q = 1.6*(10^-19);

% Sourcefile Definition
AMsourcefile = 'ASTMG173.xls';
AlphaInGaPsourcefile = 'absorption_coefficient_InGaP.xlsx';
%AlphaInGaPsourcefile = 'absorption_coefficient_GaAs.xlsx';%replace the
    InGaP sourcefile with GaAs's
AlphaGaAssourcefile = 'absorption_coefficient_GaAs.xlsx';
Reflectivitysourcefile = 'Reflectivity.xlsx';

AM = xlsread(AMsourcefile);
AlphaInGaPread = xlsread(AlphaInGaPsourcefile);
AlphaGaAsread = xlsread(AlphaGaAssourcefile);
Reflect = xlsread(Reflectivitysourcefile);

% General Value assignment units in eV
BandgapInGaP = 1.89;
BandgapGaAs = 1.41;

RefractiveIndexInGaP = 3.4;
RefractiveIndexGaAs = 3.62;
RefractiveIndexSubstrate = 3.63;
% assuming no AR coating
Criticalangle = round(asin(1/RefractiveIndexInGaP),2); % units in radians,
    round

% Angle array generation units in radians
Thetamin = 0;
Thetamax = round(pi/2,2);
Thetaresol = .01;
Theta = Thetamin : Thetaresol : Thetamax;
[~,sizetheta] = size(Theta);
Criticalanglecount = (Criticalangle - Thetamin)/Thetaresol +1;

% Energy array generation units in eV
Energymin = .73;
Energymax = 3.5;
Energyresol = .01;
Energy = Energymin:Energyresol:Energymax;
[~,sizeenergy] = size(Energy);
```

```
% Getting values of corresponding wavelengths from Energy array units in,
% engergy of photon equation
Wavelength = (1240 ./ Energy) * 10^-9  ;

% Thickness of each layer definition units in m
LengthInGaP = (100:10:1000)*(10^-9);%thicknesses range from 100 nm to 1000
    nm
[~,sizelenInGaP] = size(LengthInGaP);
LengthGaAs = (100:10:2000)*(10^-9);%thicknesses range from 100 nm to 2000
    nm
[~,sizelenGaAs] = size(LengthGaAs);

% Setting values of possibble variables and matrices to zero for speedy
% execution

Rbacksub = zeros(1,sizeenergy); Rbackmir = zeros(1,sizeenergy);
Rbacktex = zeros(1,sizeenergy); spectralradiance = zeros(1,sizeenergy);

AlphaInGaP = zeros(1,sizeenergy); AlphaGaAs = zeros(1,sizeenergy);

Rfront = zeros(1,sizeenergy); RfrontAR = zeros(1,sizeenergy);
Transmission_InGaP = zeros(1,sizeenergy);
Transmission_GaAs = zeros(1,sizeenergy);
T1 = zeros(1,sizeenergy);
T2 = zeros(1,sizeenergy); T3 = zeros(1,sizeenergy);
Transmission_InGaPtemp = zeros(sizeenergy,sizetheta);
Transmission_GaAstemp = zeros(sizeenergy,sizetheta);
T1temp = zeros(sizeenergy,sizetheta);
T2temp = zeros(sizeenergy,sizetheta); T3temp = zeros(sizeenergy,sizetheta);

a11 = zeros(1,sizeenergy); a11AR = zeros(1,sizeenergy);
a11tex = zeros(1,sizeenergy); a11ARtex = zeros(1,sizeenergy);
a11sub = zeros(1,sizeenergy); a11ARsub = zeros(1,sizeenergy);
a21 = zeros(1,sizeenergy); a21AR = zeros(1,sizeenergy);
a21tex = zeros(1,sizeenergy); a21ARtex = zeros(1,sizeenergy);
a21sub = zeros(1,sizeenergy); a21ARsub = zeros(1,sizeenergy);
a22 = zeros(1,sizeenergy); a22AR = zeros(1,sizeenergy);
a22tex = zeros(1,sizeenergy); a22ARtex = zeros(1,sizeenergy);
a22sub = zeros(1,sizeenergy); a22ARsub = zeros(1,sizeenergy);

Jsc1elem = zeros(1,sizeenergy); Jsc1ARelem = zeros(1,sizeenergy);
Jsc1elemtex = zeros(1,sizeenergy); Jsc1ARelemtex = zeros(1,sizeenergy);
Jsc1elemsub = zeros(1,sizeenergy); Jsc1ARelemsub = zeros(1,sizeenergy);
Jsc2elem = zeros(1,sizeenergy); Jsc2ARelem = zeros(1,sizeenergy);
Jsc2elemtex = zeros(1,sizeenergy); Jsc2ARelemtex = zeros(1,sizeenergy);
Jsc2elemsub = zeros(1,sizeenergy); Jsc2ARelemsub = zeros(1,sizeenergy);
Jsc1fin = zeros(sizelenInGaP,sizelenGaAs);
Jsc1ARfin = zeros(sizelenInGaP,sizelenGaAs);
Jsc2fin = zeros(sizelenInGaP,sizelenGaAs);
Jsc2ARfin = zeros(sizelenInGaP,sizelenGaAs);
Jsc1fintex = zeros(sizelenInGaP,sizelenGaAs);
Jsc1ARfintex = zeros(sizelenInGaP,sizelenGaAs);
Jsc2fintex = zeros(sizelenInGaP,sizelenGaAs);
Jsc2ARfintex = zeros(sizelenInGaP,sizelenGaAs);
Jsc1finsub = zeros(sizelenInGaP,sizelenGaAs);
Jsc1ARfinsub = zeros(sizelenInGaP,sizelenGaAs);
Jsc2finsub = zeros(sizelenInGaP,sizelenGaAs);
```

```
Jsc2ARfinsub = zeros(sizelenInGaP,sizelenGaAs);
Integrala11num1elem = zeros(sizeenergy,sizetheta);
Integrala11num1 = zeros(1,sizeenergy);
Integrala11num2elem = zeros(sizeenergy,sizetheta);
Integrala11num2 = zeros(1,sizeenergy);
Integrala11denomelem = zeros(sizeenergy,sizetheta);
Integrala11denom = zeros(1,sizeenergy);
Integrala21num1elem = zeros(sizeenergy,sizetheta);
Integrala21num1 = zeros(1,sizeenergy);
Integrala21num2elem = zeros(sizeenergy,sizetheta);
Integrala21num2 = zeros(1,sizeenergy);
Integrala21denomelem = zeros(sizeenergy,sizetheta);
Integrala21denom = zeros(1,sizeenergy);
Integrala22num1 = zeros(1,sizeenergy);
Integrala22num2elem = zeros(sizeenergy,sizetheta);
Integrala22num2 = zeros(1,sizeenergy);
Integrala22denomelem = zeros(sizeenergy,sizetheta);
Integrala22denom = zeros(1,sizeenergy);

% Reflectivity at back surface with back surface as Substrate

for dummy = 1 : sizeenergy
    Rbacksub(dummy) = 0;
end

% Reflectivity at back surface with back surface as Mirror

for dummy = 1 : sizeenergy
    Rbackmir(dummy) = 1;
end

% Reflectivity at back surface with back surface as Texture

for dummy = 1 : sizeenergy
    Rbacktex(dummy) = 1;
end



% Getting Spectral Radiance value units in W/m2/nm wrt Wavelength in nm, AM
% comes from AMsourcefile
row_scan = 1;
temp_energy = Energymin;
var_energy = AM(row_scan,5);
row_input = 1;

while ((var_energy <= Energymax)&&(AM(row_scan,5) ~= AM(end,5)))
        if (var_energy >= temp_energy)
            spectralradiance(row_input) = AM(row_scan,4);
            row_input = row_input + 1;
            row_scan = row_scan + 1;
            var_energy = AM(row_scan,5);
            temp_energy = temp_energy + Energyresol;
        end

        if ((var_energy < temp_energy)&&(AM((row_scan),5) ~= AM(end,5)))
            row_scan = row_scan + 1;
            var_energy = AM(row_scan,5);
```

```
        end
end

[~,sizespectral] = size(spectralradiance);
for dummy = (sizespectral + 1):sizeenergy
    spectralradiance(dummy) = 0;
end

row_scan = 1;
temp_energy = Energymin;
var_energy = AM(row_scan,5);
row_input = 1;

while ((var_energy <= Energymax)&&(AM(row_scan,5) ~= AM(end,5)))
        if (var_energy >= temp_energy)
            spectralradiance(row_input) = AM(row_scan,6);
            row_input = row_input + 1;
            row_scan = row_scan + 1;
            var_energy = AM(row_scan,5);
            temp_energy = temp_energy + Energyresol;
        end

        if ((var_energy < temp_energy)&&(AM((row_scan),5) ~= AM(end,5)))
            row_scan = row_scan + 1;
            var_energy = AM(row_scan,5);
        end
end

[~,sizespectral] = size(spectralradiance);
for dummy = (sizespectral + 1):sizeenergy
    spectralradiance(dummy) = 0;
end

% Scanning Alpha values for InGaP
countenergyInGaP = (BandgapInGaP - Energymin)/Energyresol;

for dummy = 1 : countenergyInGaP
    AlphaInGaP(dummy) =0;
end

row_scan = 1;
temp_energy = BandgapInGaP;
var_energy = AlphaInGaPread(row_scan,15);
row_input = int16(countenergyInGaP + 1);

while ((var_energy <= Energymax)&&(row_input <= sizeenergy)&&(
    AlphaInGaPread((row_scan),15) ~= AlphaInGaPread(end,15)))
    if (var_energy >= temp_energy)
        if (abs(var_energy - temp_energy)<=Energyresol)

            test = AlphaInGaPread(row_scan,16);
            AlphaInGaP(row_input) = test;
            row_scan = row_scan + 1;

        elseif (abs(var_energy - temp_energy)>(Energyresol))
            AlphaInGaP(row_input) = 0;
        end

```

```
            row_input = row_input + 1;
            var_energy = AlphaInGaPread(row_scan,15);
            temp_energy = temp_energy + Energyresol;

    elseif (var_energy < temp_energy)
        row_scan = row_scan + 1;
        var_energy = AlphaInGaPread(row_scan,15);
    end

end

% Extrapolating values of AlphaInGaP

for dummy = 1:sizeenergy
    if (dummy >countenergyInGaP)
        if (AlphaInGaP(dummy)==0)
            base = AlphaInGaP(dummy -1);
            dummy2 = dummy;
            countinterpolation = 1;
            while ((AlphaInGaP(dummy2)==0) && (dummy2<sizeenergy))
                dummy2 = dummy2 +1;
                countinterpolation = countinterpolation +1;
            end

            Tail = AlphaInGaP(dummy2);

            if (dummy2 == sizeenergy)
                base = AlphaInGaP(dummy -2);
                Tail = AlphaInGaP(dummy -1);
            end

            valincr = (Tail - base)/countinterpolation;

            for dummy3 = dummy : (dummy2-1)
                AlphaInGaP(dummy3) = AlphaInGaP(dummy3 - 1) + valincr;
            end

            if (dummy2 == sizeenergy)
                AlphaInGaP(sizeenergy) = AlphaInGaP(sizeenergy - 1) +
    valincr;
            end
        end
    end
end

% Scanning Alpha values for GaAs

countenergyGaAs = (BandgapGaAs - Energymin)/Energyresol;
for dummy = 1 : countenergyGaAs
    AlphaGaAs(dummy) =0;
end

row_scan = 1;
temp_energy = BandgapGaAs;
var_energy = AlphaGaAsread(row_scan,15);
row_input = int16(countenergyGaAs + 1);

while ((var_energy <= Energymax)&&(row_input <= sizeenergy)&&(AlphaGaAsread
```

```
    ((row_scan),15) ~= AlphaGaAsread(end,15)))
    if (var_energy >= temp_energy)
        if (abs(var_energy - temp_energy)<=Energyresol)
            test = AlphaGaAsread(row_scan,16);
            AlphaGaAs(row_input) = test;
            row_scan = row_scan + 1;
        elseif (abs(var_energy - temp_energy)>(Energyresol)
            AlphaGaAs(row_input) = 0;
        end
            row_input = row_input + 1;
            var_energy = AlphaGaAsread(row_scan,15);
            temp_energy = temp_energy + Energyresol;
    elseif (var_energy < temp_energy)
        row_scan = row_scan + 1;
        var_energy = AlphaGaAsread(row_scan,15);
    end
end

% Extrapolating values of AlphaGaAs

for dummy = 1:sizeenergy
    if (dummy >countenergyGaAs)
        if (AlphaGaAs(dummy)==0)
            base = AlphaGaAs(dummy -1);
            dummy2 = dummy;
            countinterpolation = 1;
            while ((AlphaGaAs(dummy2)==0) && (dummy2<sizeenergy))
                dummy2 = dummy2 +1;
                countinterpolation = countinterpolation +1;
            end

            Tail = AlphaGaAs(dummy2);

            if (dummy2 == sizeenergy)
                base = AlphaGaAs(dummy -2);
                Tail = AlphaGaAs(dummy -1);
            end

            valincr = (Tail - base)/countinterpolation;

            for dummy3 = dummy : (dummy2-1)
                AlphaGaAs(dummy3) = AlphaGaAs(dummy3 - 1) + valincr;
            end

            if (dummy2 == sizeenergy)
                AlphaGaAs(sizeenergy) = AlphaGaAs(sizeenergy - 1) + valincr
    ;
            end
        end
    end
end


% Converting units into per m from per cm by multiplying by 100
AlphaInGaP = AlphaInGaP*100;
AlphaGaAs = AlphaGaAs*100;

% Scanning Reflectivity value without AR energywise
```

```
row_scan = 1;
temp_energy = Energymin;
var_energy = Reflect(row_scan,1);
row_input = 1;

while ((var_energy <= Energymax)&&(row_input <= sizeenergy)&&(Reflect((
    row_scan),1) ~= Reflect(end,1)))
    if (var_energy >= temp_energy)
        if (abs(var_energy - temp_energy)<Energyresol)
            Rfront(row_input) = Reflect(row_scan,2);
            row_scan = row_scan + 1;
        elseif (abs(var_energy - temp_energy)>=(Energyresol))
            Rfront(row_input) = 0;
        end
            row_input = row_input + 1;
            var_energy = Reflect(row_scan,1);
            temp_energy = temp_energy + Energyresol;
    end

    if ((var_energy < temp_energy)&&(Reflect((row_scan),1) ~= Reflect(end
    ,1)))
        row_scan = row_scan + 1;
        var_energy = Reflect(row_scan,1);
    end
end

% Extrapolating values of Rf without AR coating
% abbreviation for front-surface reflectance

for dummy = 1:sizeenergy
    if(Rfront(dummy) == 0)
        base = Rfront(dummy -1);
        dummy2 = dummy;
        countinterpolation = 1;
        while ((Rfront(dummy2)==0) && (dummy2<sizeenergy))
            dummy2 = dummy2 +1;
            countinterpolation = countinterpolation +1;
        end

        Tail = Rfront(dummy2);

        if (dummy2 == sizeenergy)
            base = Rfront(dummy -2);
            Tail = Rfront(dummy -1);
        end

        valincr = (Tail - base)/countinterpolation;

        for dummy3 = dummy : (dummy2-1)
            Rfront(dummy3) = Rfront(dummy3 - 1) + valincr;
        end

        if (dummy2 == sizeenergy)
            Rfront(sizeenergy) = Rfront(sizeenergy - 1) + valincr;
        end
    end
end

```

```
% Adjusting for Rf value / 100
Rfront = Rfront/100;

% Scanning Reflectivity value with AR energywise
row_scan = 1;
temp_energy = Energymin;
var_energy = Reflect(row_scan,1);
row_input = 1;

while ((var_energy <= Energymax)&&(row_input <= sizeenergy)&&(Reflect((
    row_scan),1) ~= Reflect(end,1)))
    if (var_energy >= temp_energy)
        if (abs(var_energy - temp_energy)<Energyresol)
            RfrontAR(row_input) = Reflect(row_scan,3);
            row_scan = row_scan + 1;
        elseif (abs(var_energy - temp_energy)>=(Energyresol))
            RfrontAR(row_input) = 0;
        end
            row_input = row_input + 1;
            var_energy = Reflect(row_scan,1);
            temp_energy = temp_energy + Energyresol;
    end

    if ((var_energy < temp_energy)&&(Reflect((row_scan),1) ~= Reflect(end
    ,1)))
        row_scan = row_scan + 1;
        var_energy = Reflect(row_scan,1);
    end
end

% Extrapolating values of Rf with AR coating

for dummy = 1:sizeenergy
    if(RfrontAR(dummy) == 0)
        base = RfrontAR(dummy -1);
        dummy2 = dummy;
        countinterpolation = 1;
            while ((RfrontAR(dummy2)==0) && (dummy2<sizeenergy))
                dummy2 = dummy2 +1;
                countinterpolation = countinterpolation +1;
            end

            Tail = RfrontAR(dummy2);

            if (dummy2 == sizeenergy)
                base = RfrontAR(dummy -2);
                Tail = RfrontAR(dummy -1);
            end

            valincr = (Tail - base)/countinterpolation;

            for dummy3 = dummy : (dummy2-1)
                RfrontAR(dummy3) = RfrontAR(dummy3 - 1) + valincr;
            end

            if (dummy2 == sizeenergy)
                RfrontAR(sizeenergy) = RfrontAR(sizeenergy - 1) + valincr;
            end
```

```
    end
end

% Adjusting for Rf value / 100
RfrontAR = RfrontAR/100;

var_len_InGaP = 300*(10^-9);%decide the thicknesses of InGaP when calculating absorptivity
var_len_GaAs = 200*(10^-9);%decide the thicknesses of GaAs when calculating absorptivity

% Calculating starting points for integration in the array of energy and
% start point in array
% It would be used to integrate discrret spectral radiance and absorptivity
num_iter_InGaP = sizeenergy - ((Energymax-BandgapInGaP)/Energyresol);
num_iter_GaAs = sizeenergy - ((Energymax-BandgapGaAs)/Energyresol);

%for substrate w/o AR
var_Energy = 1 ;
while (var_Energy <= sizeenergy)
    Transmission_InGaP(var_Energy) =    exp(((-1)*(var_len_InGaP)*(AlphaInGaP(var_Energy)))/cos(0));
    Transmission_GaAs(var_Energy) =     exp(((-1)*(var_len_GaAs)*(AlphaGaAs(var_Energy)))/cos(0));

    T1 = Transmission_InGaP;
    T2 = Transmission_GaAs;
    T3(var_Energy) = 1;
    Rb = Rbacksub;

    a11sub(var_Energy)   = (1-Rfront(var_Energy))*(1-T1(var_Energy));
    a11ARsub(var_Energy) = (1-RfrontAR(var_Energy))*(1-T1(var_Energy));

    a21sub(var_Energy)   = (1-Rfront(var_Energy))*T1(var_Energy)*(1-T2(var_Energy));
    a21ARsub(var_Energy) = (1-RfrontAR(var_Energy))*T1(var_Energy)*(1-T2(var_Energy));

    a22sub(var_Energy)   = (1-Rfront(var_Energy))*(1-T2(var_Energy));
    a22ARsub(var_Energy) = (1-RfrontAR(var_Energy))*(1-T2(var_Energy));

    var_Energy = var_Energy + 1 ;
end

BandgapInGaPcount  = (BandgapInGaP - Energymin)/Energyresol;
BandgapGaAscount   = (BandgapGaAs - Energymin)/Energyresol;

%for Mirror w/o AR
var_Energy = 1 ;
while (var_Energy <= sizeenergy)
    Transmission_InGaP(var_Energy) =    exp(((-1)*(var_len_InGaP)*(AlphaInGaP(var_Energy)))/cos(0));
    Transmission_GaAs(var_Energy) =     exp(((-1)*(var_len_GaAs)*(AlphaGaAs(var_Energy)))/cos(0));

    T1 = Transmission_InGaP;
    T2 = Transmission_GaAs;
    T3 (var_Energy) =1 ;
```

```
    Rb = Rbackmir;

    a11(var_Energy)   = Absorptivity11(Rfront(var_Energy),T1(var_Energy),T2(var_Energy),T3(var_Energy),Rb(var_Energy));
    a11AR(var_Energy) = Absorptivity11(RfrontAR(var_Energy),T1(var_Energy),T2(var_Energy),T3(var_Energy),Rb(var_Energy));

    a21(var_Energy)   = Absorptivity21(Rfront(var_Energy),T1(var_Energy),T2(var_Energy),T3(var_Energy),Rb(var_Energy));
    a21AR(var_Energy) = Absorptivity21(RfrontAR(var_Energy),T1(var_Energy),T2(var_Energy),T3(var_Energy),Rb(var_Energy));

    a22(var_Energy)   = Absorptivity22(Rfront(var_Energy),T1(var_Energy),T2(var_Energy),T3(var_Energy),Rb(var_Energy));
    a22AR(var_Energy) = Absorptivity22(RfrontAR(var_Energy),T1(var_Energy),T2(var_Energy),T3(var_Energy),Rb(var_Energy));

    var_Energy = var_Energy + 1 ;
end

% for textured mirror as back surface
 var_Energy = 1 ;
while (var_Energy <= sizeenergy)
    Transmission_InGaP(var_Energy)  =    exp(((-1)*(var_len_InGaP)*(AlphaInGaP(var_Energy)))/cos(0));
    Transmission_GaAs(var_Energy)   =    exp(((-1)*(var_len_GaAs)*(AlphaGaAs(var_Energy)))/cos(0));

    T1 = Transmission_InGaP;
    T2 = Transmission_GaAs;
    T3(var_Energy) = 1;
    Rb = Rbacktex;

    %calculation for texture Back Surface integral component
    % int the equation

    tempcount  = 1;

    while (tempcount <= sizetheta)
       Transmission_InGaPtemp(var_Energy,tempcount)    =    exp(((-1)*(var_len_InGaP)  *(AlphaInGaP(var_Energy))) /cos(Theta(tempcount)));
       Transmission_GaAstemp(var_Energy,tempcount)     =    exp(((-1)*(var_len_GaAs)    *(AlphaGaAs(var_Energy)))  /cos(Theta(tempcount)));

       T1temp = Transmission_InGaPtemp;
       T2temp = Transmission_GaAstemp;



        if (tempcount < Criticalanglecount)
            Integrala11num1elem(var_Energy,tempcount) = (cos(Theta(tempcount)) * ((1 - T1temp(var_Energy,tempcount)) * T2temp(var_Energy,tempcount)));
            Integrala11num2elem(var_Energy,tempcount) = 0;
            Integrala11denomelem(var_Energy,tempcount)= 0;

            Integrala21num1elem(var_Energy,tempcount) = (cos(Theta(tempcount)) * (1 - T2temp(var_Energy,tempcount)));
```

```
            Integrala21num2elem(var_Energy,tempcount) = 0;
            Integrala21denomelem(var_Energy,tempcount)= 0;
            Integrala22num2elem(var_Energy,tempcount) = 0;
            Integrala22denomelem(var_Energy,tempcount)= 0;
        end

        if (tempcount >= Criticalanglecount)
        % for a11
            Integrala11num1elem(var_Energy,tempcount)     = (cos(Theta(tempcount)) * ((1 - T1temp(var_Energy,tempcount)) * T2temp(var_Energy,tempcount)));
            Integrala11num2elem(var_Energy,tempcount)     = (cos(Theta(tempcount)) * (1 - T1temp(var_Energy,tempcount)) * T1temp(var_Energy,tempcount) * T2temp(var_Energy,tempcount));
            Integrala11denomelem(var_Energy,tempcount)    = (cos(Theta(tempcount)) * T1temp(var_Energy,tempcount) * T2temp(var_Energy,tempcount)* T1temp(var_Energy,tempcount) * T2temp(var_Energy,tempcount));

        %for a21
            Integrala21num1elem(var_Energy,tempcount)     = (cos(Theta(tempcount)) * (1 - T2temp(var_Energy,tempcount)));
            Integrala21num2elem(var_Energy,tempcount)     = (cos(Theta(tempcount)) * (1 - T2temp(var_Energy,tempcount)) * T1temp(var_Energy,tempcount) * T1temp(var_Energy,tempcount) * T2temp(var_Energy,tempcount));

        %for a22
            Integrala22num2elem(var_Energy,tempcount)     = (cos(Theta(tempcount)) * (1 - T2temp(var_Energy,tempcount)) * T2temp(var_Energy,tempcount));
            Integrala22denomelem(var_Energy,tempcount)    = (cos(Theta(tempcount)) * T2temp(var_Energy,tempcount) * T2temp(var_Energy,tempcount));
        end

        tempcount = tempcount + 1;
    end


    % Discreet Integration of theta terms
    Integrala11num1(var_Energy)=trapz(Theta,Integrala11num1elem(var_Energy,:));
    Integrala11num2(var_Energy)=trapz(Theta,Integrala11num2elem(var_Energy,:));
    Integrala11denom(var_Energy)=trapz(Theta,Integrala11denomelem(var_Energy,:));

    Integrala21num1(var_Energy)=trapz(Theta,Integrala21num1elem(var_Energy,:));
    Integrala21num2(var_Energy)=trapz(Theta,Integrala21num2elem(var_Energy,:));
    Integrala22num2(var_Energy)=trapz(Theta,Integrala22num2elem(var_Energy,:));
    Integrala22denom(var_Energy)=trapz(Theta,Integrala22denomelem(var_Energy,:));

    Integrala21denom=Integrala11denom;
    Integrala22num1=Integrala21num1;
```

```
    a11tex(var_Energy)=Absorptivity11tex(Rfront(var_Energy),T1(var_Energy),T2(var_Energy),T3(var_Energy),Integrala11num1(var_Energy),Integrala11num2(var_Energy),Integrala11denom(var_Energy),Rb(var_Energy));
    a11ARtex(var_Energy)=Absorptivity11tex(RfrontAR(var_Energy),T1(var_Energy),T2(var_Energy),T3(var_Energy),Integrala11num1(var_Energy),Integrala11num2(var_Energy),Integrala11denom(var_Energy),Rb(var_Energy))


    a21tex(var_Energy=Absorptivity21tex(Rfront(var_Energy),T1(var_Energy),T2(var_Energy),T3(var_Energy),Integrala21num1(var_Energy),Integrala21num2(var_Energy),Integrala21denom(var_Energy),Rb(var_Energy));
    a21ARtex(var_Energy)=Absorptivity21tex(RfrontAR(var_Energy),T1(var_Energy),T2(var_Energy),T3(var_Energy),Integrala21num1(var_Energy),Integrala21num2(var_Energy),Integrala21denom(var_Energy),Rb(var_Energy))
    a22tex(var_Energy)=Absorptivity22tex(Rfront(var_Energy),T1(var_Energy),T2(var_Energy),T3(var_Energy),Integrala22num1(var_Energy),Integrala22num2(var_Energy),Integrala22denom(var_Energy),Rb(var_Energy));
    a22ARtex(var_Energy)=Absorptivity22tex(RfrontAR(var_Energy),T1(var_Energy),T2(var_Energy),T3(var_Energy),Integrala22num1(var_Energy),Integrala22num2(var_Energy),Integrala22denom(var_Energy),Rb(var_Energy));
    var_Energy=var_Energy+1;
end

%% Calulating Current Generated in Each Subcell at varying lengths of
%InGaP and GaAs
% for Back as Substrate

for var_len_InGaP=1:sizelenInGaP
    for var_len_GaAs=1:sizelenGaAs
        var_Energy=1;
        while (var_Energy<=sizeenergy)
            Transmission_InGaP(var_Energy)=exp(((-1)*(LengthInGaP(var_len_InGaP))*(AlphaInGaP(var_Energy)))/cos(0));
            Transmission_GaAs(var_Energy)=exp(((-1)*(LengthGaAs(var_len_GaAs))*(AlphaGaAs(var_Energy)))/cos(0));

            T1=Transmission_InGaP;
            T2=Transmission_GaAs;
            T3(var_Energy)=1;
            Rb=Rbackmir;

            a11sub(var_Energy)=(1-Rfront(var_Energy))*(1-T1(var_Energy));
            a11ARsub(var_Energy)=(1-RfrontAR(var_Energy))*(1-T1(var_Energy));


            a21sub(var_Energy)=(1-Rfront(var_Energy))*T1(var_Energy)*(1-T2(var_Energy));
            a21ARsub(var_Energy)=(1-RfrontAR(var_Energy))*T1(var_Energy)*(1-T2(var_Energy));

            a22sub(var_Energy)=(1-Rfront(var_Energy))*(1-T2(var_Energy));
```

```
            a22ARsub(var_Energy)=(1-RfrontAR(var_Energy))*(1-T2(var_Energy)
    )
            if (var_Energy<num_iter_InGaP)
                 if (var_Energy<num_iter_GaAs)
                        Jsc1elemsub(var_Energy)=0;
                        Jsc1ARelemsub(var_Energy)=0;

                        Jsc2elemsub(var_Energy)=0;
                        Jsc2ARelemsub(var_Energy)=0;
                 else
                      Jsc2elemsub(var_Energy)=q*(a22sub(var_Energy)*
    photonfluxdensity(var_Energy));
                      Jsc2ARelemsub(var_Energy)=q*(a22ARsub(var_Energy)*
    photonfluxdensity(var_Energy));
                 end
             else
                 Jsc1elemsub(var_Energy)=q*(a11sub(var_Energy)*
    photonfluxdensity(var_Energy));
                 Jsc1ARelemsub(var_Energy)=q*(a11ARsub(var_Energy)*
    photonfluxdensity(var_Energy));

                 Jsc2elemsub(var_Energy)=q*(a21sub(var_Energy)*
    photonfluxdensity(var_Energy));
                 Jsc2ARelemsub(var_Energy)=q*(a21ARsub(var_Energy)*
    photonfluxdensity(var_Energy));
             end
            var_Energy=var_Energy+1;
        end
        Jsc1sub=trapz(Energy,Jsc1elemsub);
        Jsc2sub=trapz(Energy,Jsc2elemsub);

        Jsc1ARsub=trapz(Energy,Jsc1ARelemsub);
        Jsc2ARsub=trapz(Energy,Jsc2ARelemsub);


        Jsc1finsub(var_len_InGaP,var_len_GaAs)=Jsc1sub;
        Jsc2finsub(var_len_InGaP,var_len_GaAs)=Jsc2sub;

        Jsc1ARfinsub(var_len_InGaP,var_len_GaAs)=Jsc1ARsub;
        Jsc2ARfinsub(var_len_InGaP,var_len_GaAs)=Jsc2ARsub;
    end
end


save('Jsc1sub.mat','Jsc1sub');
save('Jsc2sub.mat','Jsc2sub');
save('Jsc1finsub.mat','Jsc1finsub');
save('Jsc2finsub.mat','Jsc2finsub');

% for  Mirror Rear Surface
% calculating absorptivity with varying length
% Solar incidence angle = 0

for var_len_InGaP=1:sizelenInGaP
    for var_len_GaAs=1:sizelenGaAs
        var_Energy=1;
        while (var_Energy<=sizeenergy)
            Transmission_InGaP(var_Energy)=exp(((-1)*(LengthInGaP(
```

```
var_len_InGaP))*(AlphaInGaP(var_Energy)))/cos(0));
        Transmission_GaAs(var_Energy)=exp(((-1)*(LengthGaAs(var_len_GaAs))*(AlphaGaAs(var_Energy)))/cos(0));

        T1=Transmission_InGaP;
        T2=Transmission_GaAs;
        T3(var_Energy)=1;
        Rb=Rbackmir;

        a11(var_Energy)=Absorptivity11(Rfront(var_Energy),T1(var_Energy),T2(var_Energy),T3(var_Energy),Rb(var_Energy));
        a11AR(var_Energy)=Absorptivity11(RfrontAR(var_Energy),T1(var_Energy),T2(var_Energy),T3(var_Energy),Rb(var_Energy));

        a21(var_Energy)=Absorptivity21(Rfront(var_Energy),T1(var_Energy),T2(var_Energy),T3(var_Energy),Rb(var_Energy));
        a21AR(var_Energy)=Absorptivity21(RfrontAR(var_Energy),T1(var_Energy),T2(var_Energy),T3(var_Energy),Rb(var_Energy));

        a22(var_Energy)=Absorptivity22(Rfront(var_Energy),T1(var_Energy),T2(var_Energy),T3(var_Energy),Rb(var_Energy));
        a22AR(var_Energy)=Absorptivity22(RfrontAR(var_Energy),T1(var_Energy),T2(var_Energy),T3(var_Energy),Rb(var_Energy));

         if (var_Energy<num_iter_InGaP)
             if (var_Energy<num_iter_GaAs)
                    Jsc1elem(var_Energy)=0;
                    Jsc1ARelem(var_Energy)=0;

                    Jsc2elem(var_Energy)=0;
                    Jsc2ARelem(var_Energy)=0;
             else
                  Jsc2elem(var_Energy)=q*(a22(var_Energy)*photonfluxdensity(var_Energy));
                  Jsc2ARelem(var_Energy)=q*(a22AR(var_Energy)*photonfluxdensity(var_Energy));
         else
             Jsc1elem(var_Energy)=q*(a11(var_Energy)*photonfluxdensity(var_Energy));
             Jsc1ARelem(var_Energy)=q*(a11AR(var_Energy)*photonfluxdensity(var_Energy));

             Jsc2elem(var_Energy)=q*(a21(var_Energy)*photonfluxdensity(var_Energy));
             Jsc2ARelem(var_Energy)=q*(a21AR(var_Energy)*photonfluxdensity(var_Energy));
            end
            var_Energy=var_Energy+1;
        end
    Jsc1=trapz(Energy,Jsc1elem);
    Jsc2=trapz(Energy,Jsc2elem);

    Jsc1AR=trapz(Energy,Jsc1ARelem);
    Jsc2AR=trapz(Energy,Jsc2ARelem);

    Jsc1fin(var_len_InGaP,var_len_GaAs)=Jsc1;
    Jsc2fin(var_len_InGaP,var_len_GaAs)=Jsc2;
```

```
        Jsc1ARfin(var_len_InGaP,var_len_GaAs)=Jsc1AR;
        Jsc2ARfin(var_len_InGaP,var_len_GaAs)=Jsc2AR;
    end
end

save('Jsc1.mat','Jsc1');
save('Jsc2.mat','Jsc2');
save('Jsc1fin.mat','Jsc1fin');
save('Jsc2fin.mat','Jsc2fin');

for var_len_InGaP=1:sizelenInGaP
    for var_len_GaAs=1:sizelenGaAs
        var_Energy=1;
        while (var_Energy <= sizeenergy)
            Transmission_InGaP(var_Energy)  =    exp(((-1)*(LengthInGaP(var_len_InGaP))*(AlphaInGaP(var_Energy)))/cos(0));
            Transmission_GaAs(var_Energy)   =    exp(((-1)*(LengthGaAs(var_len_GaAs))*(AlphaGaAs(var_Energy)))/cos(0));

            T1 = Transmission_InGaP;
            T2 = Transmission_GaAs;
            T3(var_Energy) = 1;
            Rb = Rbacktex;

            %calculation for texture Back Surface integral component
            % int the equation
            tempcount  = 1;

            while (tempcount <= sizetheta)
               Transmission_InGaPtemp(var_Energy,tempcount)    =    exp(((-1)*(LengthInGaP(var_len_InGaP))  *(AlphaInGaP(var_Energy))) /cos(Theta(tempcount)));
               Transmission_GaAstemp(var_Energy,tempcount)     =    exp(((-1)*(LengthGaAs(var_len_GaAs))    *(AlphaGaAs(var_Energy)))  /cos(Theta(tempcount)));

               T1temp = Transmission_InGaPtemp;
               T2temp = Transmission_GaAstemp;
               T3temp(var_Energy,tempcount) = 1;

                if (tempcount < Criticalanglecount)
                    Integrala11num1elem(var_Energy,tempcount) = (cos(Theta(tempcount)) * ((1 - T1temp(var_Energy,tempcount)) * T2temp(var_Energy,tempcount)));
                    Integrala11num2elem(var_Energy,tempcount) = 0;
                    Integrala11denomelem(var_Energy,tempcount)= 0;

                    Integrala21num1elem(var_Energy,tempcount) = (cos(Theta(tempcount)) * (1 - T2temp(var_Energy,tempcount)));
                    Integrala21num2elem(var_Energy,tempcount) = 0;
                    Integrala21denomelem(var_Energy,tempcount)= 0;
                    Integrala22num2elem(var_Energy,tempcount) = 0;
                    Integrala22denomelem(var_Energy,tempcount)= 0;
                end

                if (tempcount >= Criticalanglecount)
                % for a11
                    Integrala11num1elem(var_Energy,tempcount)     = (cos(
```

```
Theta(tempcount)) * ((1 - T1temp(var_Energy,tempcount)) * T2temp(var_Energy,tempcount)));
                    Integrala11num2elem(var_Energy,tempcount)     = (cos(Theta(tempcount)) * (1 - T1temp(var_Energy,tempcount)) * T1temp(var_Energy,tempcount) * T2temp(var_Energy,tempcount));
                    Integrala11denomelem(var_Energy,tempcount)    = (cos(Theta(tempcount)) * T1temp(var_Energy,tempcount) * T2temp(var_Energy,tempcount)* T1temp(var_Energy,tempcount) * T2temp(var_Energy,tempcount));

                %for a21
                    Integrala21num1elem(var_Energy,tempcount)     = (cos(Theta(tempcount)) * (1 - T2temp(var_Energy,tempcount)));
                    Integrala21num2elem(var_Energy,tempcount)     = (cos(Theta(tempcount)) * (1 - T2temp(var_Energy,tempcount)) * T1temp(var_Energy,tempcount) * T1temp(var_Energy,tempcount) * T2temp(var_Energy,tempcount));


                %for a22
                    Integrala22num2elem(var_Energy,tempcount)     = (cos(Theta(tempcount)) * (1 - T2temp(var_Energy,tempcount)) * T2temp(var_Energy,tempcount));
                    Integrala22denomelem(var_Energy,tempcount)    = (cos(Theta(tempcount)) * T2temp(var_Energy,tempcount)* T2temp(var_Energy,tempcount));
                end
                tempcount = tempcount + 1;
            end
            % Discreet Integration of theta terms
            Integrala11num1(var_Energy)  = trapz(Theta,Integrala11num1elem(var_Energy,:));
            Integrala11num2(var_Energy)  = trapz(Theta,Integrala11num2elem(var_Energy,:));
            Integrala11denom(var_Energy) = trapz(Theta,Integrala11denomelem(var_Energy,:));

            Integrala21num1(var_Energy)  = trapz(Theta,Integrala21num1elem(var_Energy,:));
            Integrala21num2(var_Energy)  = trapz(Theta,Integrala21num2elem(var_Energy,:));
            Integrala22num2(var_Energy)  = trapz(Theta,Integrala22num2elem(var_Energy,:));
            Integrala22denom(var_Energy) = trapz(Theta,Integrala22denomelem(var_Energy,:));

            Integrala21denom = Integrala11denom;
            Integrala22num1  = Integrala21num1;

            a11tex(var_Energy)     = Absorptivity11tex(Rfront(var_Energy),T1(var_Energy),T2(var_Energy),T3(var_Energy),Integrala11num1(var_Energy),Integrala11num2(var_Energy),Integrala11denom(var_Energy),Rb(var_Energy));
            a11ARtex(var_Energy)   = Absorptivity11tex(RfrontAR(var_Energy),T1(var_Energy),T2(var_Energy),T3(var_Energy),Integrala11num1(var_Energy),Integrala11num2(var_Energy),Integrala11denom(var_Energy),Rb(var_Energy))
            a21tex(var_Energy)     = Absorptivity21tex(Rfront(var_Energy),
```

```
T1(var_Energy),T2(var_Energy),T3(var_Energy),Integrala21num1(var_Energy),Integrala21num2(var_Energy),Integrala21denom(var_Energy),Rb(var_Energy));
            a21ARtex(var_Energy)   = Absorptivity21tex(RfrontAR(var_Energy),T1(var_Energy),T2(var_Energy),T3(var_Energy),Integrala21num1(var_Energy),Integrala21num2(var_Energy),Integrala21denom(var_Energy),Rb(var_Energy))
            a22tex(var_Energy)     = Absorptivity22tex(Rfront(var_Energy),T1(var_Energy),T2(var_Energy),T3(var_Energy),Integrala22num1(var_Energy),Integrala22num2(var_Energy),Integrala22denom(var_Energy),Rb(var_Energy));
            a22ARtex(var_Energy)   = Absorptivity22tex(RfrontAR(var_Energy),T1(var_Energy),T2(var_Energy),T3(var_Energy),Integrala22num1(var_Energy),Integrala22num2(var_Energy),Integrala22denom(var_Energy),Rb(var_Energy))
            %done till here
            if (var_Energy < num_iter_InGaP)
                 if (var_Energy >= num_iter_GaAs)
                    Jsc2elemtex(var_Energy)   = q*(a22tex(var_Energy)*photonfluxdensity(var_Energy));
                    Jsc2ARelemtex(var_Energy) = q*(a22ARtex(var_Energy)*photonfluxdensity(var_Energy));
                end
            else
                    Jsc1elemtex(var_Energy)   = q*(a11tex(var_Energy)*photonfluxdensity(var_Energy));
                    Jsc1ARelemtex(var_Energy) = q*(a11ARtex(var_Energy)*photonfluxdensity(var_Energy));

                    Jsc2elemtex(var_Energy)   = q*(a21tex(var_Energy)*photonfluxdensity(var_Energy));
                    Jsc2ARelemtex(var_Energy) = q*(a21ARtex(var_Energy)*photonfluxdensity(var_Energy));
            end


            var_Energy = var_Energy + 1 ;

        end
        Jsc1tex = trapz(Energy,Jsc1elemtex);
        Jsc2tex = trapz(Energy,Jsc2elemtex);

        Jsc1ARtex = trapz(Energy,Jsc1ARelemtex);
        Jsc2ARtex = trapz(Energy,Jsc2ARelemtex);

        Jsc1fintex(var_len_InGaP,var_len_GaAs) = Jsc1tex;
        Jsc2fintex(var_len_InGaP,var_len_GaAs) = Jsc2tex;

        Jsc1ARfintex(var_len_InGaP,var_len_GaAs) = Jsc1ARtex;
        Jsc2ARfintex(var_len_InGaP,var_len_GaAs) = Jsc2ARtex;
    end
end

save('Jsc1tex.mat','Jsc1tex');
save('Jsc2tex.mat','Jsc2tex');
save('Jsc1fintex.mat','Jsc1fintex');
save('Jsc2fintex.mat','Jsc2fintex');
```

```
Jm1sub = 0; Jm1ARsub = 0;
Jm2sub = 0; Jm2ARsub = 0;

Jm1    = 0; Jm1AR    = 0;
Jm2    = 0; Jm2AR    = 0;

Jm1tex = 0; Jm1ARtex = 0;
Jm2tex = 0; Jm2ARtex = 0;
% finding max subcell current generated in each case

for dummy1 = 1 : sizelenInGaP
    for dummy2 = 1 : sizelenGaAs
        % For Back as Substrate
        if (Jsc1finsub(dummy1,dummy2) > Jm1sub )
            Jm1sub = Jsc1finsub(dummy1,dummy2);
        end

        if (Jsc2finsub(dummy1,dummy2) > Jm2sub )
            Jm2sub = Jsc2finsub(dummy1,dummy2);
        end

        if (Jsc1ARfinsub(dummy1,dummy2) > Jm1ARsub )
            Jm1ARsub = Jsc1ARfinsub(dummy1,dummy2);
        end

        if (Jsc2ARfinsub(dummy1,dummy2) > Jm2ARsub )
            Jm2ARsub = Jsc2ARfinsub(dummy1,dummy2);
        end

        % For Back as Mirror

        if (Jsc1fin(dummy1,dummy2) > Jm1 )
            Jm1 = Jsc1fin(dummy1,dummy2);
        end

        if (Jsc2fin(dummy1,dummy2) > Jm2 )
            Jm2 = Jsc2fin(dummy1,dummy2);
        end

        if (Jsc1ARfin(dummy1,dummy2) > Jm1AR )
            Jm1AR = Jsc1ARfin(dummy1,dummy2);
        end

        if (Jsc2ARfin(dummy1,dummy2) > Jm2AR )
            Jm2AR = Jsc2ARfin(dummy1,dummy2);
        end

         % For Back as Textured Mirror
        if (Jsc1fintex(dummy1,dummy2) > Jm1tex )
            Jm1tex = Jsc1fintex(dummy1,dummy2);
        end

        if (Jsc2fintex(dummy1,dummy2) > Jm2tex )
            Jm2tex = Jsc2fintex(dummy1,dummy2);
        end

        if (Jsc1ARfintex(dummy1,dummy2) > Jm1ARtex )
            Jm1ARtex = Jsc1ARfintex(dummy1,dummy2);
```

```
        end

        if (Jsc2ARfintex(dummy1,dummy2) > Jm2ARtex )
            Jm2ARtex = Jsc2ARfintex(dummy1,dummy2);
        end
    end
end

save('Jm1sub.mat','Jm1sub');
save('Jm2sub.mat','Jm2sub');
save('Jm1.mat','Jm1');
save('Jm2.mat','Jm2');
save('Jm1tex.mat','Jm1tex');
save('Jm2tex.mat','Jm2tex');

% For Back as Substrate
Jrefsub = 0.1*min([Jm1sub Jm2sub]);
JrefARsub = 0.1*min([Jm1ARsub Jm2ARsub]);

% For Back as Mirror
Jref = 0.1*min([Jm1 Jm2]);
JrefAR = 0.1*min([Jm1AR Jm2AR]);

% For Back as Textured Mirror
Jreftex = 0.1*min([Jm1tex Jm2tex]);
JrefARtex = 0.1*min([Jm1ARtex Jm2ARtex]);
```